Joint Institute for Wood Products Innovation

Cellulose Nanocrystals as a Value-Based Additive for Low Carbon Footprint Concrete with Limestone

Final Report

Authors:

Krishna Siva Teja Chopperla, Postdoctoral Scholar, Oregon State University, Corvallis, OR
Sivakumar Ramanathan, Postdoctoral Scholar, Oregon State University, Corvallis, OR
Keshav Bharadwaj Ravi, Postdoctoral Scholar, Oregon State University, Corvallis, OR
Angel Mateos, Research Engineer, University of California Pavement Research Center, Berkeley, CA
John Harvey, Professor, University of California, Davis, CA
Somayeh Nassiri, Associate Professor, University of California, Davis, CA
Jeffrey Alan Buscheck, Lab Manager, University of California Pavement Research Center, Berkeley, CA
Sabbie Miller, Assistant Professor, University of California, Davis, CA
O. Burkan Isgor, PI, Oregon State University, Corvallis, OR
W. Jason Weiss, PI, Oregon State University, Corvallis, OR

March 8, 2023

Table of Contents

List of Tables

List of Figures

vi

1. Executive Summary

This project evaluated cellulose nanocrystals (CNCs) as an additive that can aid in concrete mixture modifications in an effort to reduce concrete's carbon footprint. This project explored the use of CNCs in cementitious materials containing various amounts of limestone (LS). The heat of hydration, porosity, flexural strength, and drying shrinkage were measured. The binders were also evaluated for their resistance to ion transport by measuring their electrical resistivity. The scope was extended to also study binders that include supplementary cementitious materials (SCMs) and CNCs. The SCM mixtures studied were (i) 50% slag, (ii) 25% fly ash and 25% slag, and (iii) 20% fly ash and 5% silica fume. In addition, full-scale field trials were done at the University of California at Davis to demonstrate CNCs use with Ordinary Portland Cement (OPC) and Portland-Limestone Cement (PLC) in the field. An embodied carbon calculator was used to evaluate the benefits of utilizing CNCs.

In general, the following observations were made from the evaluation of the performance of the mixtures with CNCs and limestone:

- Lower dosages of CNC (up to 0.5% CNCs) to OPC-LS mixtures resulted in an increased degree of hydration of binder at all ages. At early ages, the increase in the degree of hydration of cement clinker was attributed to the combined effect of LS and CNCs. At a later age, the increased degree of hydration of cement clinker was primarily attributed to the CNCs.
- CNCs addition did not have a significant impact on the overall porosity and flexural strength of the paste samples.
- CNCs addition did not have a statistically significant impact on the drying shrinkage of mortar samples with limestone.
- The addition of CNCs to OPC-LS mixtures resulted in up to 38% increase in the 28-day bulk resistivity mainly due to increase clinker hydration and reduction in pore connectivity. It was observed that a mixture for which 22% of the OPC was replaced with LS and containing 0.2% CNC had an equivalent performance in terms of transport properties compared to the 100% OPC system.
- The addition of 20% LS and 0.2% CNCs together resulted in mixtures with ~19% reduced GHG emissions with comparable mechanical and transport properties to the conventional 100% OPC mixture.

From the evaluation of the performance of the OPC-SCM and PLC-SCM mixtures with CNCs, the following observations were made:

- CNCs addition did not have a significant impact on the 7-day heat release values for most SCM mixtures. Future research includes understanding the mechanism of CNCs effect on the hydration of SCM mixtures.

1

37   •   CNCs addition did not have a significant impact on the overall porosity, and the B3B
38   flexural strengths of majority of the SCM mixtures with CNCs were within $\pm$15% of the
39   flexural strength of mixtures without CNCs.
40   •   CNCs addition to the SCM mixtures resulted in an increase in the overall pore connectivity
41   and a reduction in the bulk resistivity when measured at 28 and 56 days, however the bulk
42   resistivity of the SCM mixtures are significantly higher than the reference OPC mixture.
43   The observed trend may be due to the agglomeration of CNCs, changes in the pore structure
44   due to delayed early age hydration when CNCs are used, and adsorption of CNCs on SCMs
45   resulting in slightly altering the reaction kinetics of SCMs. Further research is needed to
46   understand the mechanisms behind the effect of CNCs on the pore structure characteristics
47   and transport properties of the SCM mixtures.

48 The use of CNC with PLC was successfully used in field trials in California. The PLC mixtures
49 with and without CNCs had similar fresh concrete properties including slump, air content, set time
50 and unit weight. Hardened properties such as strength, modulus of elasticity, resistivity, and
51 shrinkage were also similar for both mixtures.

2. CHAPTER 1: Background

Cellulose nanomaterials (CNMs) are non-toxic, non-petroleum-based materials that may be used as concrete additives [1-3]. CNMs are derived from bio-degradable carbon-neutral sources [1-5] and include cellulose nanofibers (CNFs) and cellulose nanocrystals (CNCs). CNFs are fibrillated and are typically ~500-2000 nm long and 4-20 nm wide. CNCs are rod shaped crystals that are typically made using acid hydrolysis (though different processing approaches may be used) and are 50-500 nm in length and 3-20 nm in width [1, 6]. CNCs have been used in cementitious mixtures and have shown potential to improve mechanical properties of concrete [2, 3, 7-13] Similarly, it was shown that the addition of CNFs could improve concrete performance by promoting crack bridging and improving the post peak behavior of concrete [3, 9, 14-16].

Past work showed that the addition of CNCs improve the hydration of cementitious mixtures containing ordinary portland cement (OPC) [17]. This was attributed to two mechanisms – steric stabilization and short circuit diffusion (SCD) [17, 18]. Steric stabilization[1] contribute to property improvement at lower CNC dosages (up to 0.3% by binder volume), presumably due to a dispersing effect on the particles [17, 19]. It was also hypothesized that the adsorption of CNCs on cement grains resulted in the formation of preferential pathways for water to ingress through the C-S-H layer around the cement grains (i.e., short circuit diffusion), which increased the hydration of cement. This observation of improved hydration was confirmed by other researchers for mixtures containing up to 0.5% CNCs [3, 17, 18, 20-22].

Moon et al. [2] showed that modifying the CNC production process and cellulose source produces CNCs with different surface charges and attached functional groups. To study the effect of CNC type, Fu et al. [23] evaluated Type I/II and Type V OPC mixtures with CNCs derived from different sources and produced using different processing methods. It was reported that in addition to the CNC type, the chemistry of the cement also plays a role in material performance. Fu et al. [23] observed that the aluminate phases might influence early age hydration due to their surface charge, which results in preferential adsorption of CNCs on C_3A rather than the C_3S clinker phases. The preferential adsorption of CNCs on C_3A implied that the degree of reaction of the clinker of Type V OPC was higher when compared to Type I/II OPC. The literature also reported that while early-age cement hydration may be retarded due to CNC addition (probably due to the CNC blocking the surface of the cement), this retardation generally occurs before 20 hours after mixing. After approximately 30-40 hours, the rate of hydration increases with CNC. This accelerated hydration also results in an increase in the ultimate degree of hydration (up to 8%) compared to a mixture with no added CNCs [17, 23]. (This 8% increase refers to the mixture with 1% CNCs which had a degree of hydration of ~63 % at 7 days compared to a mixture without CNCs which had a degree of hydration of ~55% at the same age).

---

[1] Dispersion of cement grains due to adsorption on CNCs on their surfaces

87   The addition of CNCs was shown to improve the mechanical properties of the cementitious
88   mixtures. Some of the previous studies on the addition of CNCs showed a 20-30% increase in
89   compressive strengths and 11-20% increase in flexural strengths [19-21]. On the other hand, there
90   are studies that also show that CNC addition did not have any statistically significant effect on
91   strength [16]. The increase in strength when it occurred was attributed to both the increase in the
92   degree of cement hydration and an increase in pore filling and refinement [14, 20-22, 24, 25]. In
93   addition, improvement in the elastic modulus of C-S-H due to CNC addition was reported [17, 19,
94   21, 23, 26].

95   CNCs were also reported to refine pores in cementitious mixtures by reducing the pore size
96   distribution, improving the transport properties of the hardened mixtures [22, 27, 28]. Various
97   researchers have reported a decrease in the porosity of cementitious mixtures containing CNCs.
98   The tortuosity of the cementitious matrix was also reported to increase with the addition of CNCs
99   [26]. It was shown in literature that the addition of CNCs resulted in the improvement of electrical
100   resistivity of the cementitious mixtures [3, 24, 26, 29]. The increase in bulk resistivity indicates
101   that the transport properties of mixtures could be improved by CNC addition [24, 30].

102   In addition to the research work done in the laboratory, CNCs have been used in the field for
103   construction of a parking lot pavement in Greenville, South Carolina in 2018. Also, CNCs have
104   recently been produced and placed commercially in a bridge in Yreka, California in 2020 [31, 32]
105   to demonstrate the feasibility of using CNCs in large-scale concrete structures in the field. It was
106   reported that the concrete with CNCs had similar or slightly better 28-day compressive strength
107   compared to concrete with no added CNCs.

108   While CNCs may improve the mechanical and transport properties of cementitious materials, steps
109   have not been taken to demonstrate potential reductions in clinker and greenhouse gas (GHG) or
110   CO_2 emissions. This project discusses the potential of using CNCs to reduce the clinker content in
111   the concrete and thus reducing GHG emissions [33-35]. In this work, CNCs were used in
112   conjunction with the use of limestone to replace OPC.

113   Portland limestone cements (PLCs) are a viable alternative to OPCs [36-41]. Mixtures made using
114   PLC (ASTM C595 cement) have similar performance to mixtures made using OPC [41, 42].
115   Similar studies were performed using added limestone [36, 38, 43-45]. It was shown that the size
116   of the limestone can play a critical role due nucleation, particle packing, and dilution [38, 42, 44-
117   46]. PLCs could reduce up to 15% of the emissions associated with the production phase of cement
118   [47]. Therefore, this research was conducted to determine whether LS and CNCs can be used
119   synergistically to lower GHG emissions while not compromising on performance.

120   ## 2.1. Computational Modeling Framework

121   A thermodynamic and pore partitioning model for concrete (PPMC) modeling framework is used
122   in this study to predict the performance of concrete [48-51]. The details of this modeling

4

123 framework will not be repeated here for brevity and interested readers are pointed to reading the
124 cited documents. Briefly, the chemical composition of the OPC and SCM, and the maximum
125 degree of reactivity (DOR*; measured using the Pozzolanic Reactivity Test [52-54]) of the SCM
126 are used as inputs to a kinetic [55] model and thermodynamic modeling [56] framework. The
127 GEMS3K software [57, 58] in conjunction with the CemData v18.01 thermodynamic database
128 [59] is used to perform thermodynamic calculations to predict the reaction products that form when
129 OPC and OPC+SCM binders react [56, 59-66]. The volumes of gel pores (<5nm in size) and
130 capillary pores (>5nm) in the hydrated cementitious paste is calculated from the reaction products
131 using a Pore Partitioning Model [67, 68]. The pore volumes are scaled to concrete using the PPMC,
132 which is then used to predict the performance of concrete [49, 50]. This modeling framework has
133 been shown to accurately predict the porosity, formation factor, and compressive strength of
134 concrete made with OPCs, PLCs, and SCMs [48-50, 69-71].

2.2. Organization and Contents of the Report

136 This report is composed of five chapters. The first chapter (section 2) consists of background on
137 CNCs research, introduction of the work performed, and the list of main research objectives. It
138 also briefs the computational modeling framework used in the study to predict the performance of
139 the mixtures such as porosity. The background section of this chapter gives a brief description of
140 CNCs and literature review of CNCs use in cementitious materials. The authors of this chapter are
141 S. Ramanathan, K.S.T. Chopperla, K. Bharadwaj, O.B. Isgor, and W.J. Weiss.

142 The second chapter (section 3) presents the research findings observed from evaluating the OPC-
143 LS-CNC mixtures performance. Chapter 2 briefs material characterization and the experimental
144 procedures used. Chapter 2 also includes the discussion on the results of the mixtures tested for
145 heat of hydration, non-evaporable water content, flexural strength, porosity, pore connectivity,
146 electrical resistivity, and drying shrinkage. The majority of the results and findings in the chapter
147 are published in ACI Materials Journal [72]. The authors of this chapter are S. Ramanathan, K.S.T.
148 Chopperla, O.B. Isgor, and W.J. Weiss.

149 The third chapter (section 4) presents the research findings from evaluating the performance of the
150 mixtures with SCMs and CNCs. The extended goal of this project is to evaluate the performance
151 of CNCs in mixtures with SCMs as using SCMs can enable further reducing the GHG emissions.
152 Chapter 3 includes the discussion of the results of the mixtures tested for heat of hydration, flexural
153 strength, porosity, pore connectivity, and electrical resistivity. Ongoing work is evaluating the
154 interactions between CNCs and SCMs, and the role of CNCs in improving the performance of the
155 mixtures with SCMs. The authors of this chapter are K.S.T. Chopperla, S. Ramanathan, O.B. Isgor,
156 and W.J. Weiss.

157 The fourth chapter (section 5) includes the details of the full-scale field trials done in California
158 using mixtures with OPC, PLC, and CNCs. The chapter includes details of the test sections

5

159 preparation and construction, fresh and hardened concrete properties, and hydrothermal
160 deformation of the slabs. Chapter 4 is authored by A. Mateos, J. Harvey, S. Nassiri, J.A. Buscheck,
161 and S. Miller. The final chapter (section 6) summarizes the studies and their findings and includes
162 the overall conclusions. The report also includes an appendix (section 8) that contains the estimate
163 of the amount of CNCs required in construction of a lane mile of concrete pavement and the mill
164 certificates of the materials used in the field trials.

165 2.3. Research Objectives

166 The main objectives of the project are:

167 - To evaluate whether an OPC-LS-CNC can be designed to have a similar performance to
168   the conventional OPC mixture to lower GHG emissions
169 - To calculate the GHG emissions of the mixtures used and determine the optimum CNC
170   dosage needed to lower carbon footprint
171 - To demonstrate the use of LS and CNCs in full scale field trails in slabs and to monitor
172   their performance

173

3. CHAPTER 2: Reducing GHG Emissions using CNCs, OPC, and Limestone

This chapter focuses on the objective of examining whether OPC in a concrete mixture can be replaced with LS and CNC to create a system with similar performance and a lower embodied carbon content (greenhouse gas emissions).

3.1. Constituent Materials and Characterization Procedures

Commercially available Type II OPC and LS (96% purity) were used in this study. Four LS replacement levels were used (0%, 10%, 20%, and 30% by mass of OPC). This is in addition to the LS already present in OPC. CNCs that were obtained in the form of suspension with 11% w/w CNC solids were used. The CNCs were manufactured by Forest Products Laboratory using sulfuric acid hydrolysis process. Four CNC concentrations used were 0%, 0.2%, 0.5%, and 1.0% solid volume by volume of binder (i.e., OPC+LS). CNC concentration was measured in terms of the volume of binder to be consistent with the previous studies [3, 17].

The CNC suspension and ASTM type II deionized (DI) water were chilled to 5 °C before the dispersion process. Chilled water (5°C) was used for dispersion to compensate the heat generated from dispersion [73], The CNC suspension was batched in the bowl of a high shear blender (Waring Commercial CB15VP blender) along with chilled DI water based on the procedure adapted from specification 10A of the American Petroleum Institute (API). Shear mixing was carried out for a total of 60 seconds at 4000 rpm in two sessions. After the first 30 seconds, the sides and bottom of the mixing bowl were scraped using a silicone spatula to release any adhered / agglomerated CNCs for about 15 seconds. The temperature of the solution was approximately 23 °C after the dispersion at the time of mixing. The water was adjusted to maintain a constant water-to-binder ratio (w/b) was 0.40. Shear blending using a high shear mixer was chosen for CNC dispersion as mechanical methods have been effective in dispersing agglomerates of nanomaterials [73, 74].

The chemical composition and physical properties of the OPC and LS are shown in Table 1. The chemical composition was determined using X-ray fluorescence (XRF) from which the oxide composition was determined using the fused bead process according to ASTM C114-18 [41, 75, 76]. The loss on ignition (LOI) of the cementitious powders was determined by igniting approximately 5 g of material in a ceramic crucible up to 1000 °C for three hours and measuring the mass after ignition. The fused beads were prepared by combining 1 g of the ignited powder with 5 g flux (for OPC) and 0.55 g powder with 5.5 g flux (for LS). The flux composed of 49.75% lithium metaborate, 49.75% lithium tetraborate, and 0.50% lithium iodide was mixed gently in a platinum crucible and fused in a furnace (Claisse LeNeo fluxer) for approximately 25 minutes at 1450 °C.

7

208 Table 1. Chemical composition (in wt%) and physical properties of the OPC and LS

Material	Na_2O	MgO	Al_2O_3	SiO_2	SO_3	K_2O	CaO	Fe_2O_3	LOI	d_{50} (μm)	G
OPC	0.21	1.43	3.95	19.95	2.55	0.48	63.32	2.28	2.71	13.9	3.15
Limestone	0.14	5.74	0.79	2.93	0.13	0.12	86.50	0.41	42.27	15.2	2.71

209

210 Particle size distribution was obtained using laser diffraction (Horiba LA-920) [41]. The powder
211 was dispersed in isopropyl alcohol in front of a laser lamp assembly. Approximately 3-5 g of
212 material was added slowly in 0.5 g increments, and the solution was sonicated and circulated to
213 prevent the agglomeration of particles. Median particle size (d50) and specific gravity (G) values
214 of the SCMs are presented in Table 1 and are measured as an average of five runs. The specific
215 gravity of OPC and LS powder are also presented in Table 1. No other chemical admixture was
216 added to the mixture to avoid conflicting influences of CNCs and chemical admixtures.

217 A locally sources fine aggregate was used for making drying shrinkage samples. The oven dry
218 specific gravity of the fine aggregate was 2.39 and absorption capacity was 2.59%.

219 3.2. Mixing Procedures

220 3.2.1. Paste mixing

221 The cementitious materials were dry mixed for 90 s using a vacuum mixer at 400 rpm and 70%
222 vacuum. The CNC dispersed mix water was placed in a mixing bowl, and the dry mixed
223 cementitious materials were added, and mixed using a vacuum mixer (Renfert Inc. model
224 18281000) for 90 s at 400 rpm and a 70% vacuum level. The mixing cup was scraped using a
225 silicone spatula for 15 s, and vacuum mixing was carried out for an additional 90 s. A similar
226 mixing procedure was followed for cementitious paste mixing in literature [42].

227 3.2.2. Mortar mixing

228 Mortar samples having 0.40 water to binder ratio were prepared for drying shrinkage testing. The
229 prepared mortar samples consisted of 50% by volume of fine aggregate. Mortar was mixed in a
230 Hobart mixer as per ASTM C305-20. All the mixing water was placed in the bowl. The
231 cementitious material was added to water and then it was mixed at the slow speed (140 r/min) for
232 30 s. Over the next 30 s, the fine aggregate was added. The speed was changed to medium speed
233 (285 r/min) and mixed the mortar for 30 s. The mixer was stopped for 90 s, in this duration the
234 bowl and the paddle were scrapped down. Then the mixing was finished by mixing it for 60 s at
235 medium speed.

8

3.3. Tests on Cementitious Pastes

3.3.1. Isothermal calorimetry

Heat release was measured using isothermal calorimetry (TAM Air, TA Instruments) according to ASTM C1679-17. Cementitious pastes were mixed using a vacuum mixer as described in the mixing procedure. After mixing, 6-7 g of the cementitious paste was transferred to a glass ampoule and sealed. The glass ampoules were then lowered into the isothermal calorimeter which was pre-conditioned at 23 ± 0.05 °C. Data was not collected for the first 45 minutes. Heat flow and heat release were measured, and the data was collected for 7 days. Two replicates of all mixtures were tested for each mixture, and the average of the two replicates was reported [41, 77]. Replicate testing for all mixtures showed variability of less than 2% between the replicates.

3.3.2. Ball-on-three-ball (B3B) flexural strength

The cementitious paste mixture prepared was placed in 50 mm (diameter) × 100 mm (length) cylindrical molds in two layers and each layer was vibrated to ensure adequate compaction of the material. The molds were sealed, and the samples were placed on a roller for 24 hours to minimize the potential effect of bleeding. After 24 hours, the samples were removed from the roller and cured under sealed conditions at 23 ± 1 °C until sample preparation began for flexural strength testing.

Flexural strength testing was performed using the B3B test at 7 and 28 days according to ASTM C1904-20 [78]. A detailed procedure for B3B flexural strength testing can be found in the literature [78, 79]. At the age of testing, the cylinder was demolded, and the top and bottom of the cylinder were discarded to avoid end effects (approximately 20 mm from each end). The central portion of the cylinder was cut into disks that were 2.65 ± 0.15 mm thick. These samples were tested on a B3B testing frame [79]. The flexural strength was calculated based on the equation described in literature [79, 80]. The testing was carried out within 15 minutes of cutting the sample. At least six replicates were tested for all mixtures at each age of testing, and the coefficient of variation (COV) was less than 10% except in one mixture, whose COV was 12%.

3.3.3. Thermogravimetric analysis (TGA)

Immediately after flexural strength testing at 28 days, the central portion of each disk was obtained and ground into a fine powder using a mortar and pestle. The powdered sample was then sieved using a 75 μm sieve (#200 sieve). The samples were then immediately double sealed in plastic bags to minimize carbonation.

Calcium hydroxide and non-evaporable water content for the cementitious powders were obtained using thermogravimetric analysis (TGA). The testing consisted of placing approximately 30-50 mg of samples on a platinum pan, and the sample was then loaded into the TGA (TGA 5500, TA

9

270 Instruments). The TGA chamber was heated at the rate of 10°C/minute to 1000°C in a nitrogen
271 atmosphere. Calcium hydroxide content (normalized to per g of binder) and non-evaporable water
272 content (per g of binder) were calculated using equations 1 and 2a, respectively. The onset and end
273 temperatures were obtained using the tangential method described in Kim and Olek [81]. Replicate
274 testing for the mixtures showed that the variability was less than 2%.

$$m_{CH} = 4.11.\frac{m_{CH,start} - m_{CH,end}}{m_{init,anhyd}} + 0.74.\left(2.27.\frac{m_{Cc,start} - m_{Cc,end}}{m_{init}} - m_{Cc,init}\right) \qquad \text{(Eq. 1)}$$

276 where, m_{CH} is the mass of calcium hydroxide, $m_{CH,start}$ is the onset temperature of calcium
277 hydroxide mass decomposition, $m_{CH,end}$ is the end point of calcium hydroxide decomposition,
278 $m_{Cc,start}$ and $m_{Cc,end}$ are the onset and end points of calcium carbonate decomposition, $m_{Cc,init}$ is the
279 calcium carbonate present in the binder, $m_{init,anhyd}$ is the anhydrous sample mass in the TGA.

$$w_{ne} = \frac{A.m_{105} - B.\,m_{1000}}{m_{1000}} \qquad \text{(Eq. 2a)}$$

281 where, w_{ne} is the non-evaporable water content, m_{105} and m_{1000} are the sample masses at 105
282 °C and 1000 °C respectively obtained from the TGA, A and B are constants calculated from
283 equations 2b and 2c, respectively to account for the loss on ignition.

$$A = \left[(1 - r_{LS})(1 - LOI_{cem}) + \left(r_{SCM}.(1 - LOI_{LS})\right) + \left(D_{CNC}.\rho_{CNC}.k_{CNC}.\left(\frac{1 - r_{LS}}{\rho_{cem}} - \frac{r_{LS}}{\rho_{LS}}\right)\right)\right]$$

285 (Eq. 2b)

$$B = \left[1 + D_{CNC}.\rho_{CNC}.k_{CNC}.\left(\frac{1 - r_{LS}}{\rho_{cem}} + \frac{r_{LS}}{\rho_{LS}}\right)\right] \qquad \text{(Eq. 2c)}$$

287 LOI_{OPC} and LOI_{LS} are the loss on ignition for OPC and LS used in the study, r_{LS} is the LS
288 replacement level, D_{CNC} is the CNC suspension dosage by volume percentage of binder, ρ_{CNC}, ρ_{cem},
289 and ρ_{LS} are the specific gravities of CNCs, OPC, and LS respectively. k_{CNC} is the weight percentage
290 of the CNC solids (11% solids by weight).

291 3.3.4. Porosity and bulk resistivity of cementitious pastes

292 Porosity and bulk resistivity were measured using 50 mm × 100 mm cylinders at 7 and 28 days.
293 The cylinders were cured in sealed condition after casting until testing. The bulk resistivity was
294 measured on vacuum saturated samples in accordance with AASHTO TP 119-20 [82].

295   The demolded samples were placed under vacuum at 7 ± 2 Torr for 3 hours. After this, a simulated
296   pore solution containing 7.6 g/L of sodium hydroxide, 10.64 g/L of potassium hydroxide, and 2
297   g/L of calcium hydroxide was allowed to saturate the samples under vacuum for one hour.
298   Simulated pore solution was utilized to vacuum saturate the samples to maintain uniform pore
299   solution resistivity across all samples for formation factor calculations. After vacuum saturation,
300   the samples were stored in the simulated pore solution for 24 ± 4 hours at 23°C. The samples were
301   then measured for electrical impedance to calculate resistivity value. The bulk resistivity was
302   calculated according to equations 3a and 3b. Appropriate corrections for temperature and sample
303   geometry were applied as detailed in Ref. [83]. Two replicates of each mixture were tested and the
304   average data was reported.

305
$$\rho_{sat} = R_{sat} \frac{A}{L} \qquad\qquad\qquad \text{(Eq. 3a)}$$

306
$$\rho_{sat-corrected} = \rho_{sat} \cdot e^{\left[\frac{E_{A-cond}}{R} \left(\frac{1}{T} - \frac{1}{T_0} \right) \right]} \qquad\qquad \text{(Eq. 3b)}$$

307   where, $\rho_{sat-corrected}$ is the temperature corrected saturated bulk resistivity, ρ_{sat} is the saturated bulk
308   resistivity (in Ω-m), R_{sat} is the vacuum saturated resistance (in Ω), A is the cross-sectional area of
309   the sample (in m^2), L is the length of the sample, E_{A-cond} is the activation energy of conduction
310   (considered as 15 kJ/mol based on [84]), R is the universal gas constant (8.314 kJ/mol-K), T is
311   the sample temperature at the time of measurement (in K), and T_0 is the reference temperature
312   (298.15 K).

313   For the same cylinders, the saturated weight and the apparent weight were obtained immediately
314   after the bulk resistivity measurement. The cylinders were then dried at 105 °C until a constant
315   mass was achieved (i.e., the difference between two successive mass measurements is less than
316   0.1%) [85]. The porosity of the cylinders (in accordance with AASHTO TP 135) was calculated
317   according to equation 4 and reported as an average of two samples for all the mixtures.

318
$$\Phi_{paste} = \frac{w_{sat} - w_{dry}}{w_{sat} - w_{app}} \qquad\qquad\qquad \text{(Eq. 4)}$$

319   where, Φ_{paste} is the porosity of the cementitious paste, w_{sat} is the vacuum saturated sample mass,
320   w_{dry} is the constant mass obtained after drying the samples at 105 °C, w_{app} is the apparent mass of
321   the samples.

322   The saturated formation factor (F_{sat}) of the mixtures was calculated according to equation 5

323
$$F_{sat} = \frac{\rho_{sat-corrected}}{\rho_{ps}} \qquad\qquad\qquad \text{(Eq. 5)}$$

11

where, $\rho_{sat-corrected}$ is the temperature corrected saturated bulk resistivity and ρ_{ps} is the resistivity of the simulated pore solution (0.127 Ω-m). Since the samples were vacuum saturated and stored in simulated pore solution, it is assumed that the pore solution resistivity is uniform for all samples.

The pore connectivity (a combination of tortuosity and constriction), β of the paste samples is calculated from equation 6.

$$\beta = \frac{\rho_{ps}}{\phi_{paste} \cdot \rho_{sat-corrected}} \quad \text{(Eq. 6)}$$

where, ρ_{ps} is the resistivity of the simulated pore solution (0.127 Ω-m).

3.3.5. Dynamic vapor sorption (DVS)

Dynamic vapor sorption (DVS) measurements were made on two samples (LS20-CNC0.0 and LS20-CNC0.2) that were seal cured for 28 days to determine if CNCs have an effect on the pore size distribution of paste samples. The samples were demolded at 28 days, broken into small chunks that weigh ~70-80 mg. These chunks were vacuum saturated with limewater. They were placed under vacuum for 3 hours, and saturated calcium hydroxide solution for an hour under vacuum. The samples were then placed under the solution for three days in a 23 °C chamber to allow for the sample chunks to get completely saturated. At three days, an assumption of full saturation (i.e. degree of saturation of 100%) is made due to the small sample size.

DVS measurements were carried out using a Q5000 vapor sorption equipment (TA Instruments) in an inert nitrogen atmosphere. The steps for ramping down the relative humidity to 0% is as follows:

1. The saturated sample was equilibrated at 23.00 °C
2. The relative humidity was set to 97.50 % and held for 2880 minutes
3. The relative humidity was ramped down to 90%, 80%, 50%, 11%, and 0% in consecutive steps over a duration of 5880 minutes for each step.
4. Each step was maintained until the mass change recorded was <0.001% for 15 minutes.
5. After reaching 0% RH, the sample was held at isothermal condition for 1440.00 min to equilibrate

The pore radius at each RH was calculated using equation 7 and 8. The pore radius is assumed to be the sum of Kelvin radius and thickness of water adsorbed film [86]. Kelvin radius can be determined using equation 7 and t-curve can be determined using equation 8 [87, 88].

$$r_k = -\frac{2\gamma V_m}{RT ln(RH)} \quad \text{(Eq. 7)}$$

$$t = \left(\frac{A V_m}{6\pi RT(RH)}\right)^{1/3} \quad \text{(Eq. 8)}$$

12

where, r_k is Kelvin radius (m), t is thickness of water adsorbed film, γ is surface tension of the pore solution ($= 72\times10^{-3}$ N/m), Vm is the molar volume of the pore solution, R is the ideal gas constant with a value of 8.314 J/(mol.K), T is the absolute temperature (K), and A is Hamaker constant for the interaction of solid-liquid-gas (considered to be -19×10^{-20} J). The degree of saturation (DOS) at each RH is calculated using equation 9.

$$DOS_{RH,x} = (M_{RH,x} - M_{RH,0})/(M_{RH,100}-M_{RH,0}) \qquad\qquad (Eq.\ 9)$$

where, $DOS_{RH,x}$ is the degree of saturation at x% RH, $M_{RH,x}$ is mass of the sample at x% RH, $M_{RH,0}$ is mass of the sample at 0% RH, and $M_{RH,100}$ is mass of the sample at 100% RH.

3.4. Tests on Cementitious Mortars

3.4.1. Drying shrinkage

Mortar samples of dimensions 25 mm (width) x 25 mm (height) x 285 mm (length) were prepared for four different mixtures (OPC, OPC-0.2%CNC, LS30, LS30-0.2%CNC). The curing and drying shrinkage measurement procedures for the mortar specimens were followed according to ASTM C596-18. Three specimens were cast for each mixture, and the average and standard deviation of the drying shrinkage strain measured over the drying period were reported.

3.5. Experimental Results and Discussion

3.5.1. Heat release

Figure 1 shows the variation of heat flow (the derivative of the heat release) for the first 24 hours with a change in CNC dosage. At all LS replacement levels, the heat release was retarded by approximately 2-3 hours (indicated by the curve shifting to the right) with the addition of CNCs. This retardation causes a delay in the onset of the acceleration period, which was approximately similar for 0.2% and 0.5% CNC dosages and higher for 1.0% CNC dosage in all cases. This trend of retardation due to increased CNC dosage is consistent with literature. Based on the Parrot-Killoh (PK) model [89], the heat flow curve can be divided into three phases, namely, the nucleation and growth phase, the diffusion in three dimensions, and the reduction in transport of ionic species at later ages, which was discussed in detail in [89, 90]. For mixtures with CNCs, the rate of reaction of OPC-LS mixtures in the nucleation and growth phase (~6 hours) was slower compared to the mixtures without CNCs. However, the diffusion phase occurs for a longer duration in mixtures containing CNCs compared to the mixtures without added CNCs. This was evident from the higher heat flow for mixtures with CNCs at all LS replacement levels. A similar trend of retardation with CNC addition was observed by Fu et al. [23] and Cao et al. [17]. Cao et al. [17] attributed this retardation to the adsorption of CNCs on the cement grains, resulting in fewer surfaces undergoing hydration. A similar retardation effect was explained in the literature for superplasticizers and other chemical admixtures interacting with cementitious mixtures [6, 17, 91].

13

389

390   (a)

391

392   (b)

14
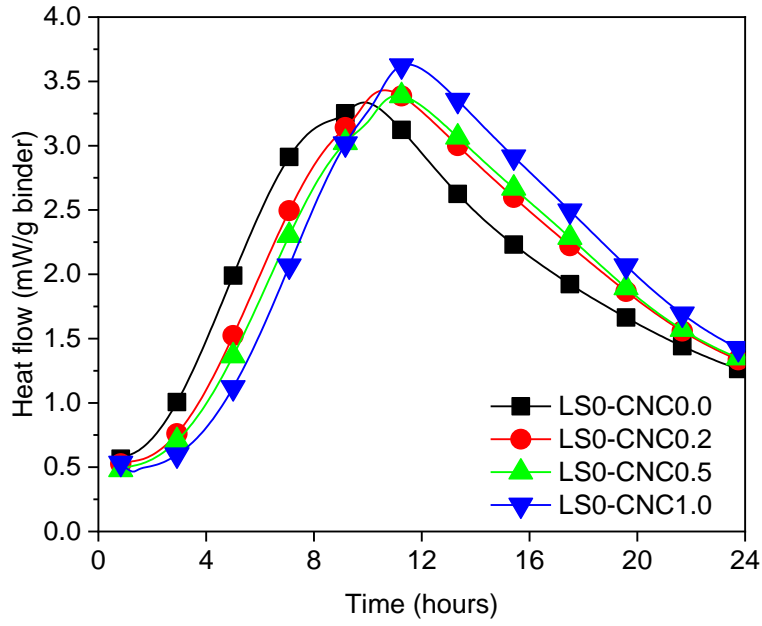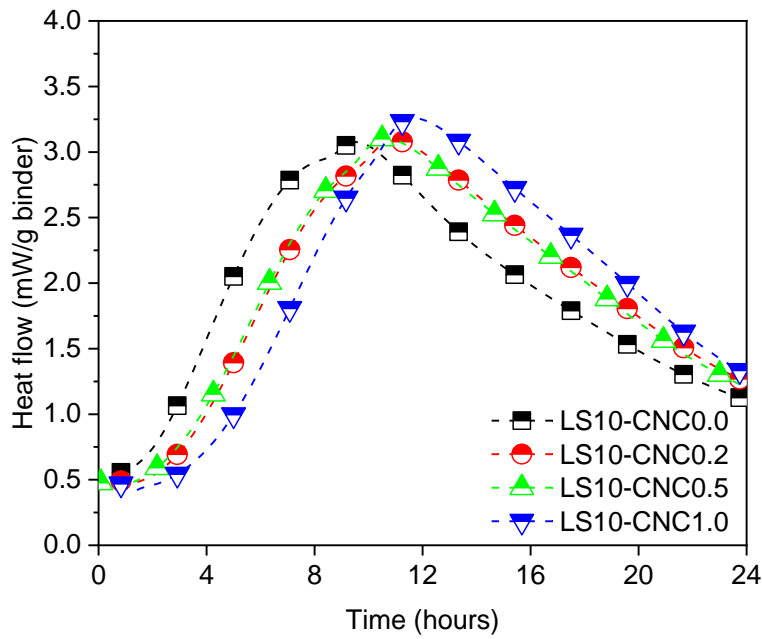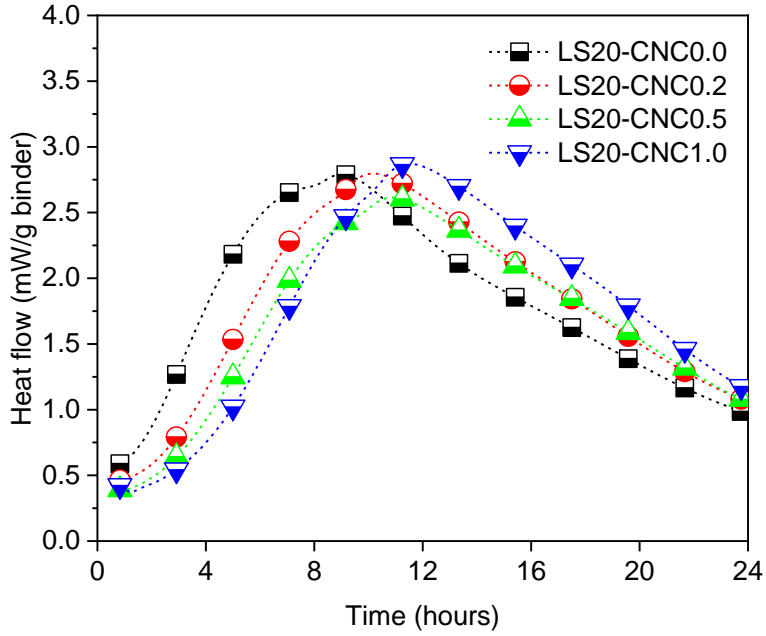
393

394 (c)

395
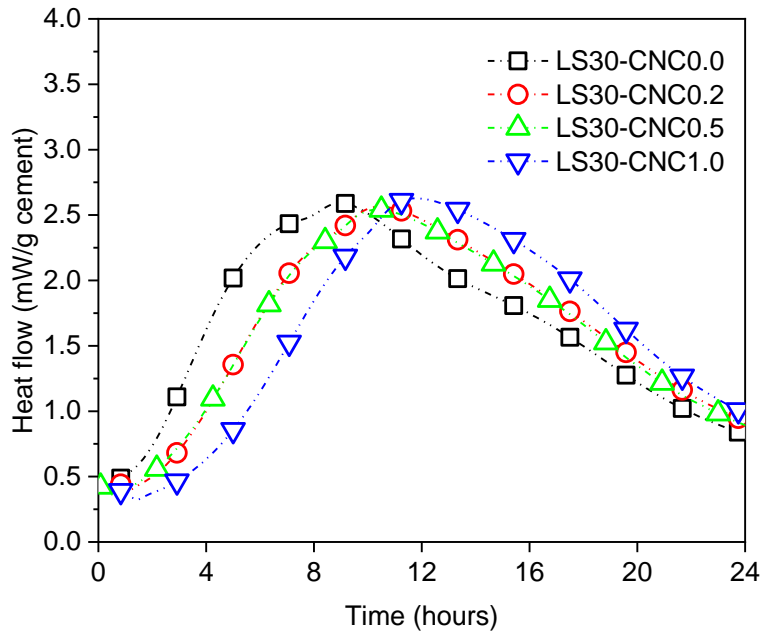
396 (d)

397 Figure 1. Change in heat flow with varying CNC dosage – (a) LS0 (b) LS10 (c) LS20 (d)
398 LS30

15

399 CNCs addition appeared to affect the heat flow peak associated with silicate hydration in the
400 mixture as well as the aluminate peak (or sulfate depletion peak), as shown in Figure 1. The heat
401 flow in the mixtures without CNCs (shown in black and square markers) was characterized by two
402 distinct peaks occurring at approximately 7 (LS30) to 8.25 (LS0) hours and approximately 8.5
403 (LS20) to 10 (LS0) hours, respectively for silicate and aluminate peaks. However, for the mixtures
404 containing CNCs, these peaks mostly overlap. The overlapping peaks likely correspond to silicate
405 and aluminate reactions occurring at approximately the same time, and as a result, the peak heat
406 flow rate appeared to be higher with added CNCs. Similar observations in peak overlap were made
407 by others in literature for cementitious mixtures containing fly ash [92, 93]. It was reported that
408 the optimal sulfate level in OPC-fly ash mixtures caused an offset between the C_3S hydration peak
409 and the aluminate peak [93]. In this case, the addition of CNCs to OPC-LS mixtures could have
410 an influence on the sulfate balance. The change in sulfate balance may be due to the adsorption of
411 sulfate ester end groups of CNCs on C_3A phase of OPC. However, additional studies are needed
412 to examine this. The higher rate of heat flow in the deceleration phase is likely due to short circuit
413 diffusion [17].

414 Figure 2 shows the 7-day heat release for the mixtures studied here. The heat release values ranged
415 from 302 J – 311 J/g binder (LS0), 285 J – 293 J/g of binder (LS10), 261 J – 274 J/g binder (LS20),
416 and 247 J – 252 J/g binder (LS30) for the various mixtures as in Fig. 2a-d. Up to the first 24 hours,
417 the heat release of the mixtures with CNCs lagged behind the mixtures without CNCs, indicating
418 the retardation due to CNC addition. After approximately 24 hours, there was a cross-over in the
419 heat release curves, indicating an increased rate of hydration for mixtures with CNCs due to short
420 circuit diffusion. For mixtures with no CNCs, dilution and filler effects can explain the results
421 [94]. However, with the addition of CNCs, there was a slight increase in the 7-day heat release.
422 For a given LS replacement level, the addition of CNCs resulted in 2-3% increase in heat release
423 per g of binder compared to mixtures with no added CNCs.

16

424

425

(a)

426

427

(b)

FULL 6(c)(i)

428

429   (c)

430
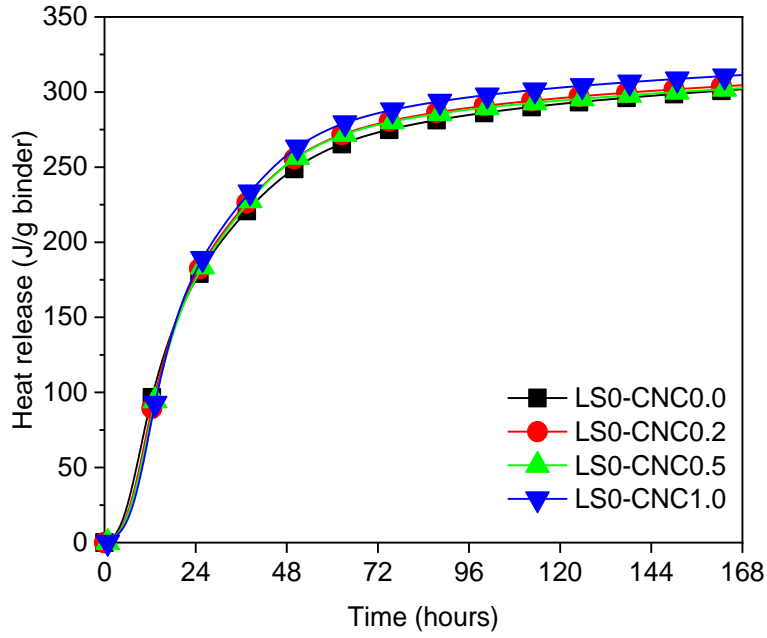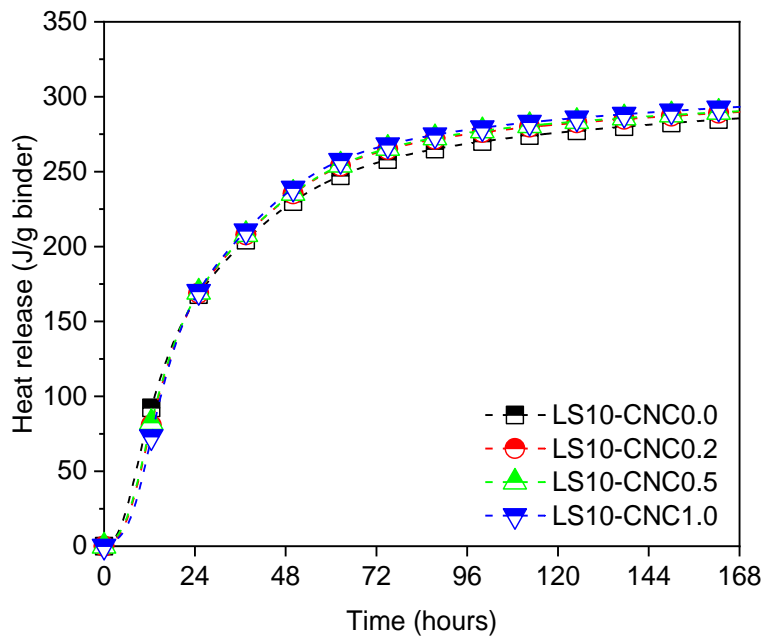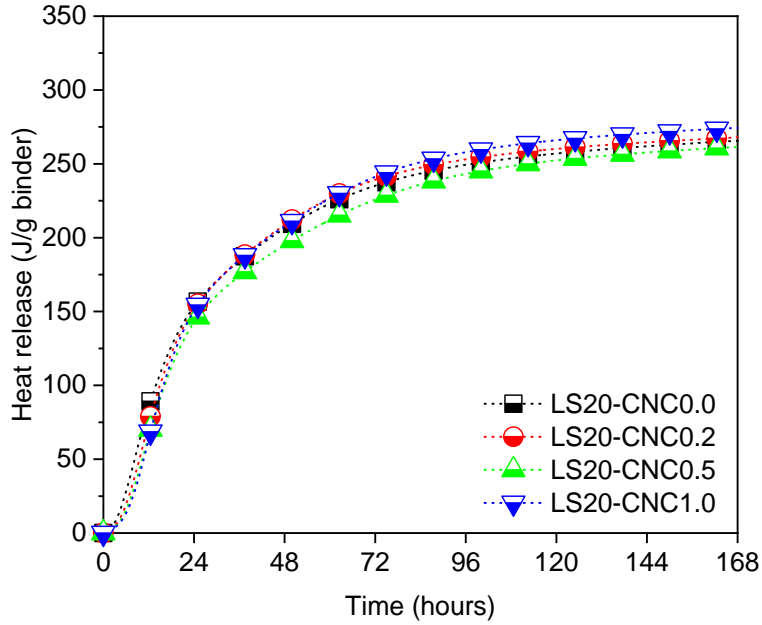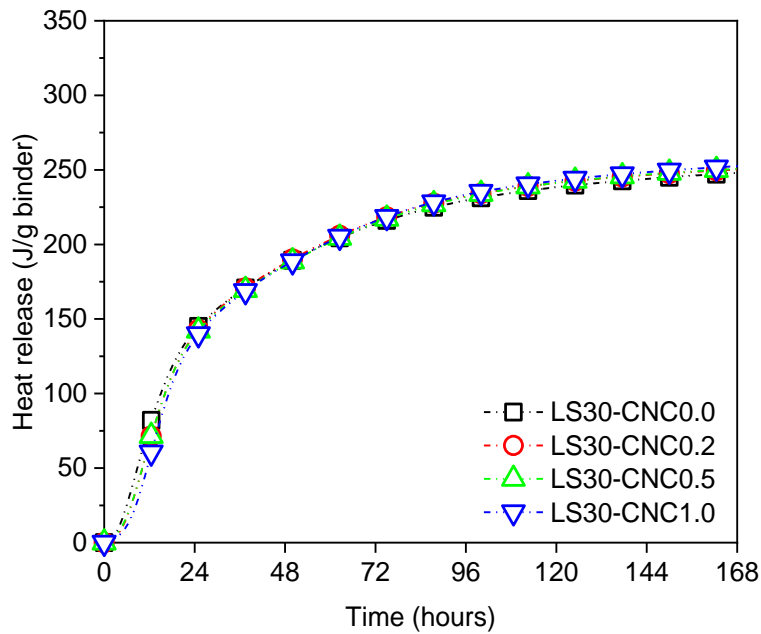
431   (d)

Figure 2. Representative 7-day heat release of mixtures at different CNC dosages for
LS30 mixtures

The replacement of OPC with LS in the mixtures causes a proportional decrease in the 7-day heat
release values due to the dilution effect. The dilution effects are offset by addition of LS and CNCs.

436 The combined effect of LS and CNCs was evident from Figure 3, where it was observed that the
437 7-day heat release of the mixtures with added CNCs and LS lie above the dilution line. This
438 increase in heat release was likely due to enhanced hydration of the cement clinker resulting from
439 a combination of short circuit diffusion (SCD) and nucleation effect due to the presence of CNCs
440 and LS, respectively [17, 44, 45]. This increase in hydration may also be due to other factors.
441 Some have speculated that this may be due to changes in pore solution chemistry; however, studies
442 [95] have evaluated the changes in pore solution chemistry and reported little change in ions during
443 the first 12 hours, and changes on the order of 20% or less after that (CNC having a slightly higher
444 Na^+, OH^- concentration and a slightly lower K^+, SO_3 concentration). Similar improvements in the
445 heat of hydration were observed in literature for OPC pastes with CNC addition. Fu et al. [23]
446 observed an approximately 5% increase in the degree of hydration of Type I/II clinker up to 7
447 days. It is likely that the use of clinkers with low C_3A contents could result in further enhancement
448 in the clinker hydration [6, 29, 96]. The formation of carboaluminate phases due to the added LS
449 [97] could also contribute to the increase in the heat release.
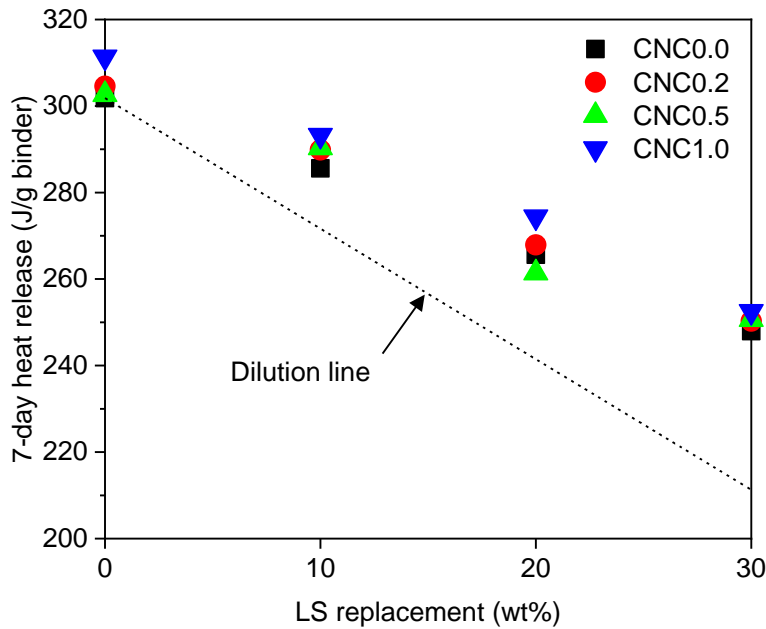
451 Figure 3. Effect of CNC dosage on 7-day heat release

452 3.5.2. Thermogravimetric analysis – calcium hydroxide and non-evaporable water content

453 The 28-day calcium hydroxide content of the mixtures is shown in Figure 4. The 28-day calcium
454 hydroxide content of the mixtures varied from 9.9 g - 11.7 g /100 g binder for CNC0.0 mixtures,
455 11.7 g – 13.7 g/100g binder for CNC0.2 mixtures, 11.9 g – 13.5 g/100g binder for CNC0.5
456 mixtures, and 10.3 g – 13.5 g / 100g binder for CNC1.0 mixtures. When CNCs were added (up to
457 0.5% by binder volume) to the mixture, there was an increase in the 28-day calcium hydroxide
458 content of the mixtures that can be explained by the increase in the clinker hydration. The average

19

459   increase in calcium hydroxide content at low CNC dosage (0.5% CNCs by volume) was ~36%
460   (LS0), ~17% (LS10), and ~1% (LS30). The increase in calcium hydroxide content on the addition
461   of low doses of CNCs is consistent with reported data in the literature [6, 15]. At lower CNC
462   dosages, steric stabilization may allow for greater diffusion of water through the matrix to the
463   cement grains, resulting in enhanced hydration of the clinker [6]. At 1.0% CNC dosages, however,
464   there was no significant influence of CNCs on the calcium hydroxide content of the OPC-LS
465   mixtures. This is probably due to the reduced impact of CNCs on cement hydration as CNCs tend
466   to agglomerate at higher CNC dosages [17, 19].
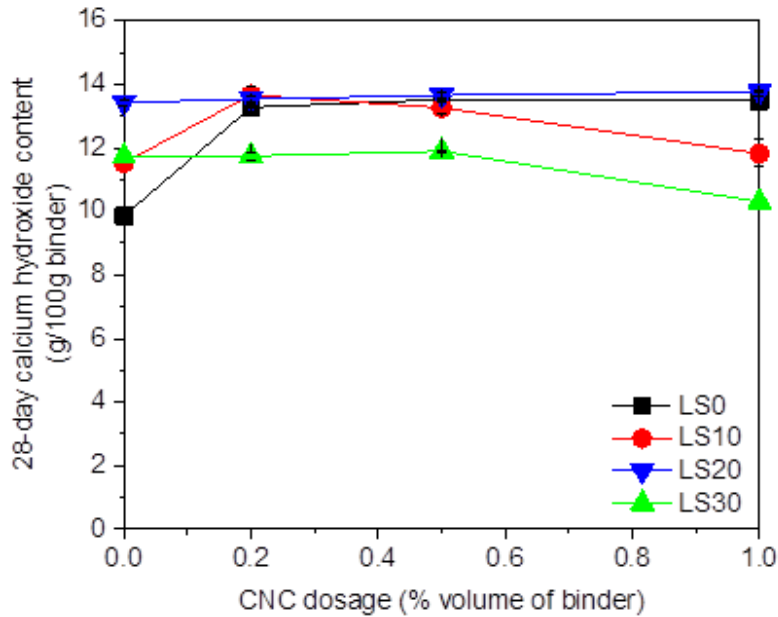
467

468   Figure 4. 28-day calcium hydroxide content of different mixtures

469   The later-age degree of hydration can be computed by calculating the non-evaporable water
470   content (w_n). It was observed that the increase in w_n from 7 to 28 days was generally higher for
471   mixtures containing CNCs compared to those without. Figure 5 shows the 28-day non-evaporable
472   water content of the different mixtures at different CNC dosages.

20

473
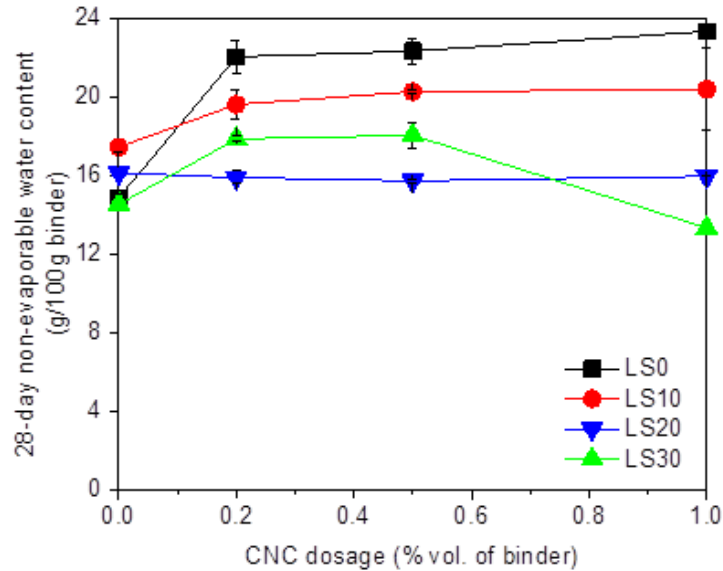
Figure 5. 28-day non-evaporable water content of the mixtures

It was evident that the addition of small amounts of CNCs (up to 0.5% by volume of binder) resulted in an increase in the non-evaporable water content when compared to the mixtures with no CNCs. The increase in w_n ranged from 14% (LS10) – 47% (LS0) and 16% (LS10) – 48% (LS0) with 0.2% and 0.5% CNC addition, respectively. LS10-CNC0.0 was observed to be an exception as the w_n was higher than LS0-CNC0.0 mixture. Increased bound water content for high LS mixtures up to 0.5% CNC dosage indicated a more "effective" clinker usage i.e., more cement participates in the hydration reaction. This indicated that CNCs could be added to OPC-LS mixtures to improve clinker efficiency while reducing the clinker content. Cao et al. [17, 18] reported similar increases in the non-evaporable water content of mixtures containing CNCs.

3.5.3. B3B flexural strength

Figure 6 shows a parity plot for the 7-day and 28-day B3B flexural strengths for the mixtures with and without CNCs. The 7-day B3B flexural strengths of mixtures range from 20.2 MPa (LS30) – 21.1 MPa (LS0), 15.9 MPa (LS30) – 21.2 MPa (LS0), and 16 MPa (LS30) – 20.6 MPa (LS10) at 0.2%, 0.5%, and 1.0% CNC dosage, respectively. It should be noted that the B3B flexural strengths indicate characteristic strength of the mixtures, and they are higher than flexural strength determined using conventional flexural strength testing due to the size effect. A detailed discussion of the size effect of samples on B3B flexural strength can be found in literature [79].

21

492

493
(a)

494

495
(b)
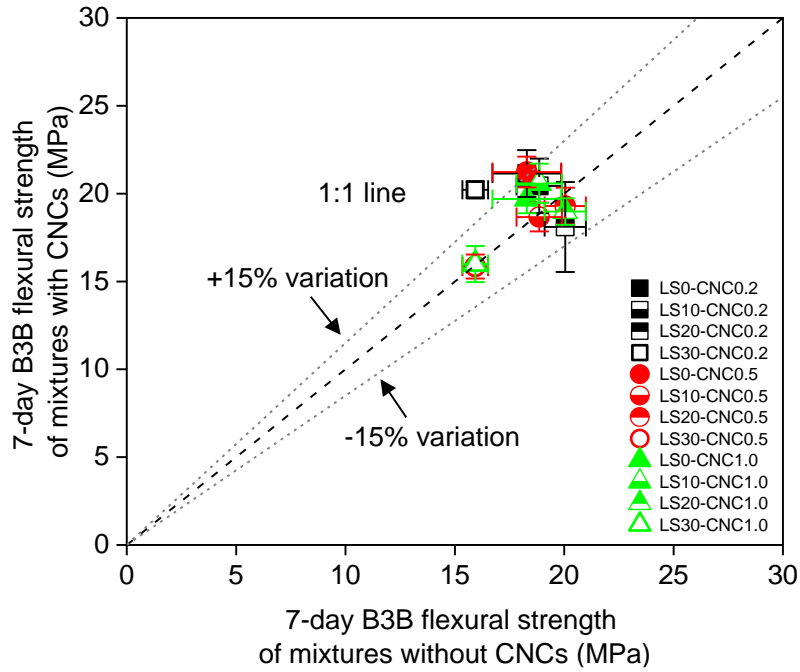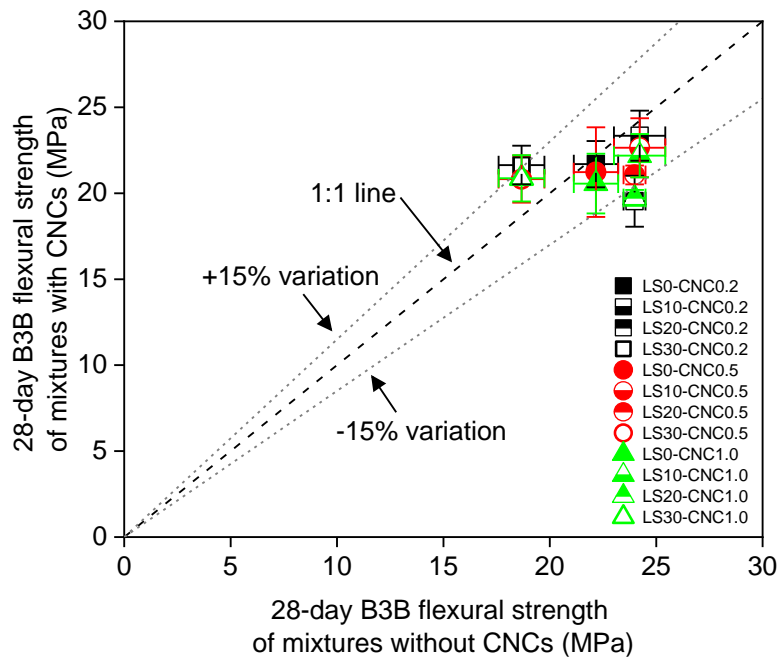
Figure 6. Effect of CNC dosage on B3B flexural strength – (a) 7 days (b) 28 days. A data point
on the 1:1 line indicates similar performance, and a data point above the 1:1 line indicates better
performance for mixtures with added CNCs (i.e., the measurement on the Y-axis). 1 MPa =
145.04 psi.

22

500	Comparing the mixtures with and without CNCs at 7 days, it was observed that CNCs do not have
501	adverse effects on early-age strength development. Clear effects of dilution due to high LS
502	replacement was seen in the early age flexural strength for mixtures without CNCs consistent with
503	the literature, where reduction in early age mechanical properties was seen with an increase in LS
504	replacement [46]. However, the addition of CNCs compensates for this dilution effect (along with
505	the nucleation effect of LS) and the increase in strength was generally within 15% of the mixtures
506	without CNCs with the exception of LS30-CNC0.2, which showed a 27% increase. A similar trend
507	was observed for 28-day B3B flexural strength; there were no adverse effects on the strength
508	development of mixtures due to CNC addition. The 28-day flexural strength of the mixtures with
509	CNCs was within 15% of the mixtures without CNCs.

510	3.5.4. Bulk resistivity and pore structure characteristics

511	The 7-day and 28-day bulk resistivity and saturated formation factor values of the mixtures with
512	different LS replacement levels is shown in Figure 7 and Figure 8 respectively. CNCs did not
513	substantially impact the 7-day bulk resistivity (and saturated formation factor) of the mixtures,
514	seen from Figure 7a and Figure 8a. Only dilution and filler effects on account of LS replacement
515	predominated at this age, which was consistent with literature for OPC-LS mixtures [46].
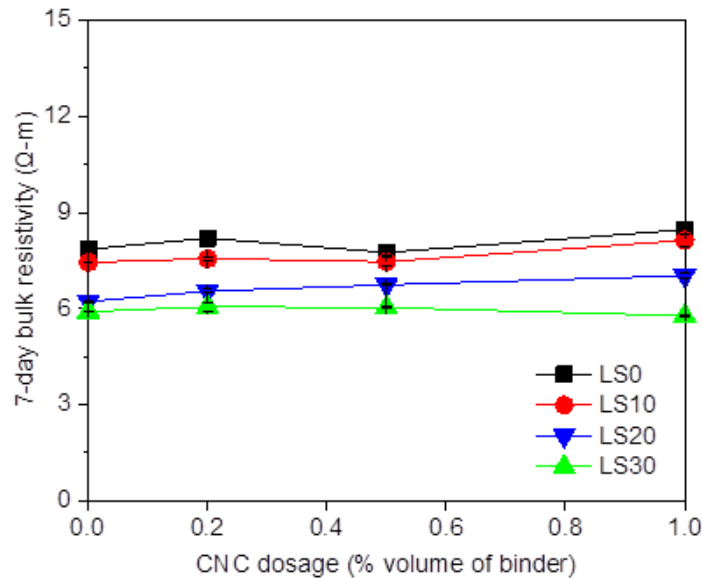
516

517	(a)
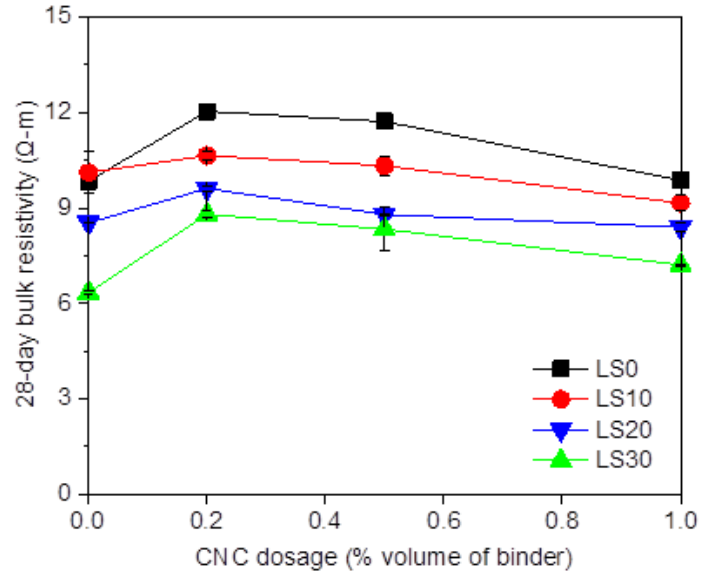
518

519 (b)

520 Figure 7. Effect of CNC dosage on saturated bulk resistivity (a) 7-days (b) 28-days

521

522

523 (a)

FULL 6(c)(i)
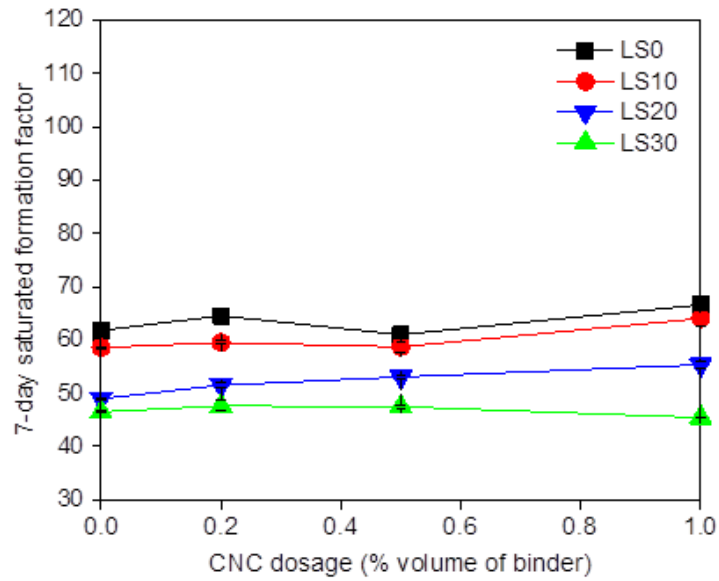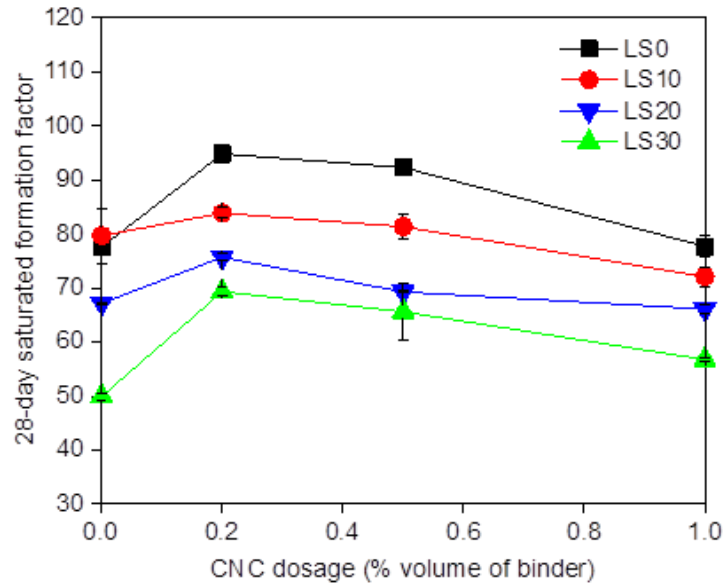
524

525   (b)

526   Figure 8. Effect of CNC dosage on saturated formation factor (a) 7-days (b) 28-days

527   The effect of CNC addition on the bulk resistivity (and saturated formation factor) of the different
528   mixtures was seen at 28 days (Figure 7b and Figure 8b). CNC dosages of up to 0.5% by binder
529   volume resulted in an increase in the 28-day saturated bulk resistivity compared to the mixtures
530   without CNCs for a given LS replacement level. The increase in bulk resistivity values ranged
531   from 5% (LS10) - 38% (LS30) and 2% (LS10) - 31% (LS30) at 0.2% and 0.5% CNC dosage by
532   binder volume, respectively. The dilution effect due to LS addition was compensated by a
533   combination of LS and CNC dosages up to 0.5% by binder volume. However, no such
534   compensation was observed at higher CNC dosage. When the CNC dosage was 1.0% by binder
535   volume, the effect was pure dilution, and the 28-day bulk resistivity was similar to mixtures with
536   no added CNCs.

537   The 28-day porosity data for the different mixtures with and without CNCs is shown in Figure 9.
538   A thermodynamic modeling approach [98] (briefed in Chapter 1) was used to provide an idea of
539   how porosity of mixtures varies with LS replacement. The porosity of CNC0.0 mixtures
540   determined from thermodynamic modeling [98] is shown in Figure 9 as a baseline to compare the
541   porosity of mixtures with and without CNCs. The experimental results were in good agreement
542   with the modeling results for CNC0.0 mixtures. At all CNC dosages, the porosity of the mixtures
543   was the lowest for LS0 mixtures and increased with increase in LS content. This was consistent
544   with literature for mixtures without CNCs [98, 99], where the porosity of mixtures decreased first
545   (up to 2% LS addition) and then increased with an increase in LS replacement. No significant
546   changes in total porosity of the samples were observed when CNCs were added and the variation
547   was less than 1% when compared to the corresponding mixtures without CNCs.

25
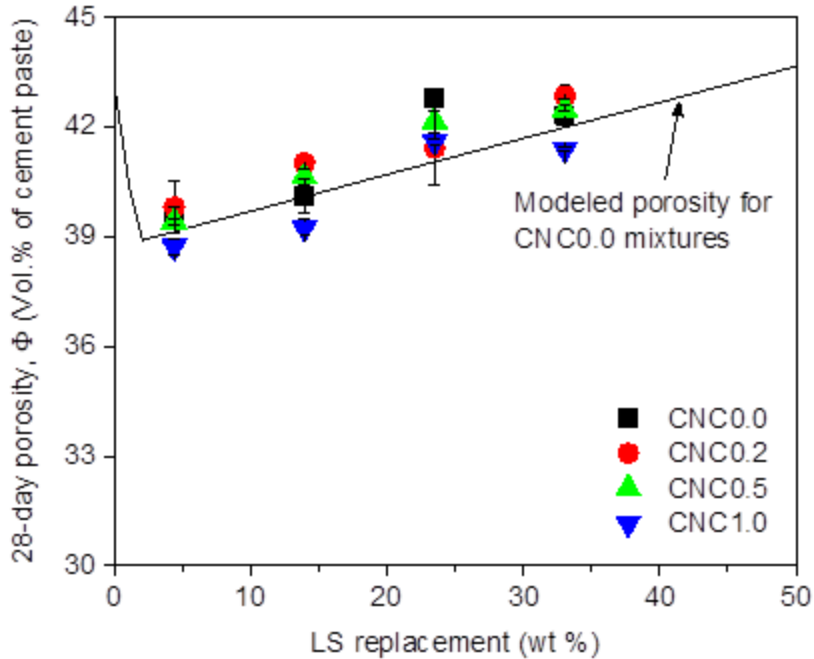
Figure 9. 28-day porosity of mixtures with and without CNCs. The ends of the error bars shown here represent the measured values and the markers show the average value of the two samples. The limestone replacement percentages also account for the limestone present in the cement clinker (4.1% for this cement).

While the porosity of the mixtures did not significantly vary, differences were observed in the pore connectivity (β) of the mixtures (shown in Figure 10). The pore connectivity of the mixtures without CNCs generally increased with an increase in LS replacement level and ranged from 0.03 (LS0 and LS10) - 0.05 (LS30), consistent with literature [98]. It was seen that low dosages of CNCs up to 0.5% by volume of binder caused a decrease in pore connectivity (indicating increased performance), and the lowest pore connectivity was observed for mixtures with 0.2% CNCs by volume of binder. For CNC0.2 and CNC0.5 mixtures, the decrease in pore connectivity ranged from 7% (LS10) - 29% (LS30) and 3% (LS10) – 24% (LS30) respectively compared to the CNC0.0 mixtures with the same LS replacement levels. At 1.0% CNC dosage, only LS30 showed decreased pore connectivity (compared to its 0% CNC counterpart i.e., LS30CNC0.0), whereas LS0, LS10, and LS20 mixtures did not follow the trend (compared to LS0CNC0.0, LS10CNC0.0, and LS20CNC0.0 respectively). This could be due to agglomeration of CNCs at higher CNC dosages as discussed in the previous section on B3B flexural strength. This decrease in pore connectivity with CNC addition was likely due to increased cement hydration resulting in pore filling and consequently increasing the bulk resistivity of the mixtures [14, 17, 21, 100].

26

568
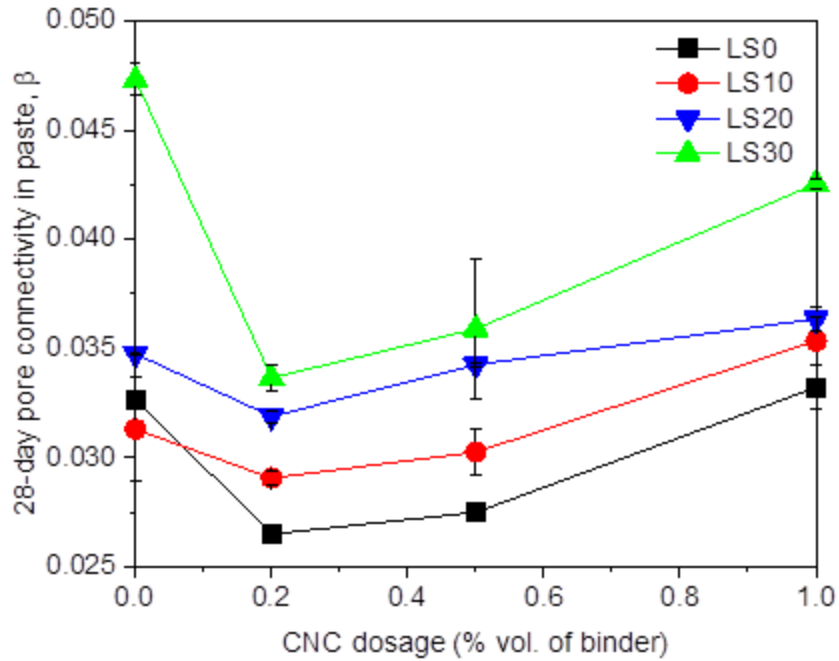
Figure 10. Pore connectivity in mixtures with and without CNCs at 28 days. The ends of the error bars shown here represent the measured values and the markers show the average value of the two samples.

3.5.5. Drying shrinkage

The drying shrinkage test results of the mixtures LS0-CNC0.0, LS0-CNC0.2, LS30-CNC0.0, and LS30-CNC0.2 are shown in Figure 11.

FULL 6(c)(i)
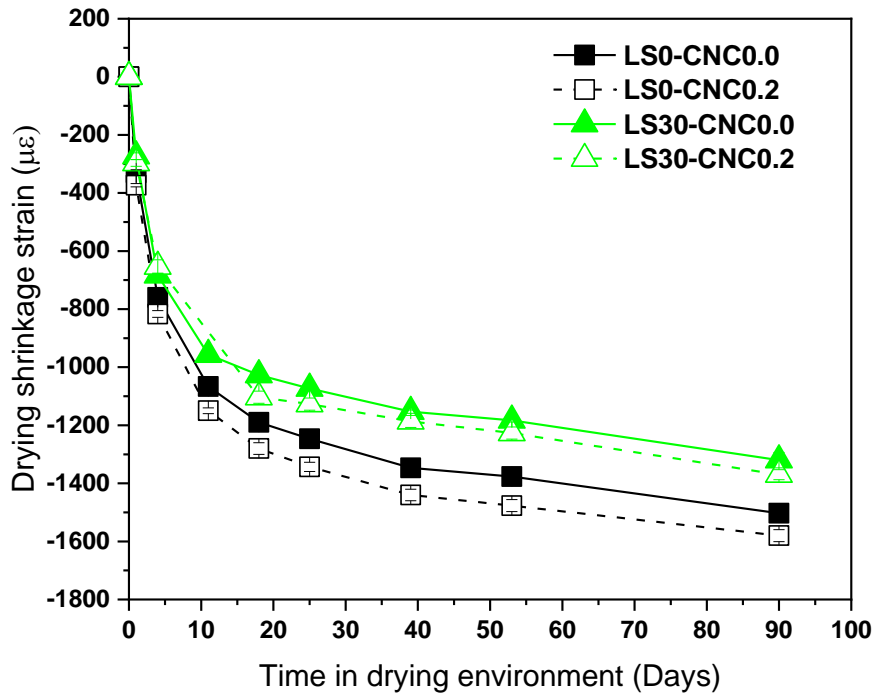
Figure 11. Drying shrinkage results of the mortar specimens

It was observed that LS0 mixtures with CNC had a slightly higher shrinkage strain than the mixture without CNC. After 90 days of exposure to the drying environment, a maximum difference of 5% of average shrinkage strain was observed between the LS0 mixtures with and without CNCs. The observed slightly higher shrinkage strain could probably be due to higher clinker hydration with the CNCs addition. For LS30 mixtures, there was no statistically significant difference in drying shrinkage strain between the mixtures with and without CNCs.

3.5.6. Dynamic vapor sorption

Figure 12 shows the cumulative pore volume determined for the LS20 paste samples with and without CNC. It was observed that the cumulative pore volumes are similar for the LS20 samples and not affected by the CNC addition. Figure 13 shows the pore size distribution of LS20 samples with and without CNC.

28

588
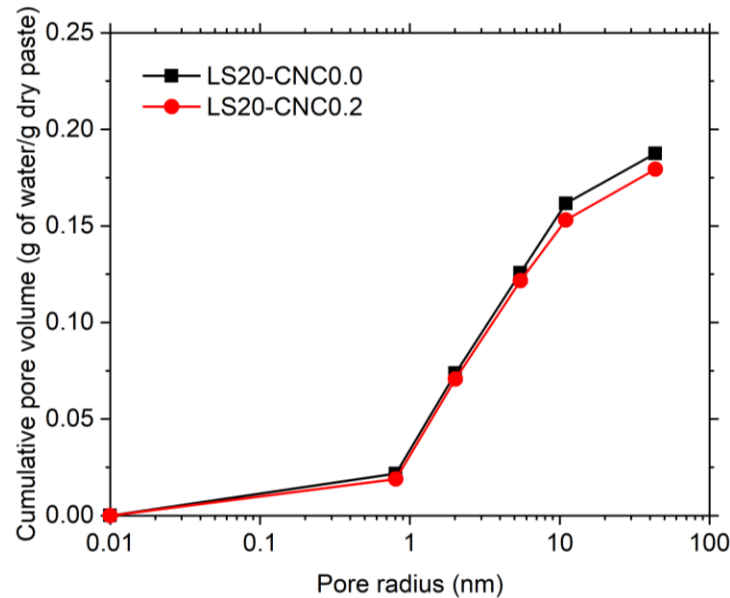
589

590   Figure 12. Cumulative pore volume of LS20 paste samples with and without CNC
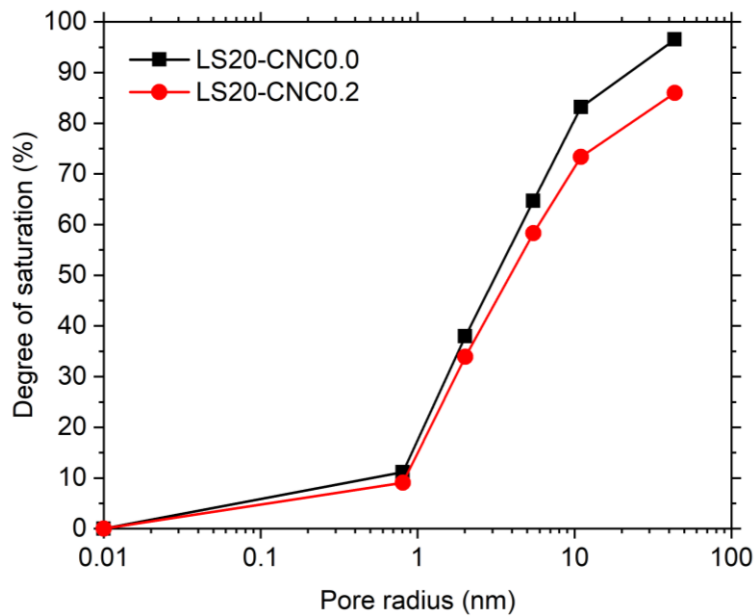
591

592   Figure 13. Pore size distribution of LS20 paste samples with and without CNC

593   The pores in the sample can be classified as capillary pores (with pore radius ≥ 5 nm) and gel pores
594   (with pore radius < 5 nm) [86]. From Figure 13, it was observed that the degree of saturation of
595   LS20-CNC0.2 mixture is slightly lower than LS20-CNC0.0 mixture indicating higher fraction of
596   capillary pores (and any entrapped air voids) in the LS20-CNC0.2 mixture. Despite the higher

29

597 fraction of capillary pores in LS20-CNC0.2 when compared to LS20-CNC0.0, it should be noted
598 that the pore connectivity (β) in LS20-CNC0.2 mixture was 8% lower than LS20-CNC0.0 mixture.

599 3.5.7. Thoughts on developing "greener" mixtures with CNCs

600 The approach studied here has two components with respect to making concrete greener. The first
601 component is to replace a part of OPC in the mixture by LS as it would reduce the GHG emissions.
602 The second component is to add CNCs to the mixture to augment the properties of mixtures with
603 LS. Replacing OPC with LS (>15%) can result in a decrease in bulk resistivity at high replacement
604 levels due to dilution effects (45). However, with CNC addition, an increase in bulk resistivity was
605 observed and compensated for the dilution effects. The following assumptions are made to
606 calculate the GHG emissions using the life cycle inventory (LCI) calculation tool developed by
607 Miller et al [41, 101]:

608 • The transportation distances for ingredients were assumed based on previous research
609 conducted [41, 101].
610 • All mixtures contain the same quantities of aggregates and chemical admixtures.
611 • A cradle-to-gate option (A1 to A3) was considered for evaluating emissions associated.
612 Only the emissions associated with raw material transport, manufacturing, batching, and
613 end of life were included here. In terms of life cycle assessment (LCA) modules, for the
614 raw materials and concrete production stage, LCA modules A1-A3 were considered.
615 Batching raw materials for concrete was considered the boundary for this phase.
616 Additionally, for end-of-life emissions associated, LCA modules C1-C4 was considered.
617 The emissions associated with the "in use" phase of concrete (i.e. B1-B7) and recycling
618 (i.e. LCA module D) was not considered here. LCA modules A4 and A5, associated with
619 the use phase of concrete were not considered here.
620 • Since CNCs are derived from carbon neutral sources, it was assumed that CNCs have
621 negligible CO_2 emissions. It is acknowledged that CNC manufacturing and CNC
622 dispersion in the construction phase (LCA modules A4 and A5) contributes to minor CO_2
623 emissions. The emissions associated with CNCs in a full-scale production environment
624 will depend on the distance of the plant from the raw materials, type of raw materials, and
625 the processing used to manufacture the CNC [102]. Additional research is needed on the
626 LCA of CNC when commercially produced. Work is in progress to evaluate the full LCA
627 of CNCs; however, it is anticipated as lab and pilot plants move to full scale the full LCA
628 of these materials will become more clearly understood. It should be noted that in this paper
629 refrigeration is used to limit fungal growth in the CNCs over the duration of the research
630 project. However, refrigeration is not necessary for full scale applications.
631

632 Figure 14 shows the plot of 28-day bulk resistivity as a function of GHG emissions. A general
633 form of the linear equation is shown in equation 10 and the parameters m and b for the different
634 CNC dosages is shown in Table 2.

$$\rho_{28-day} = m_i(f, CNC).GHG + b_i(f, CNC) \qquad \text{(Eq. 10)}$$

636 where, $\rho_{28\text{-day}}$ is the saturated bulk resistivity at 28 days, m is the slope, GHG is the % GHG
637 emissions reduced, and b is the intercept on the Y-axis.

638
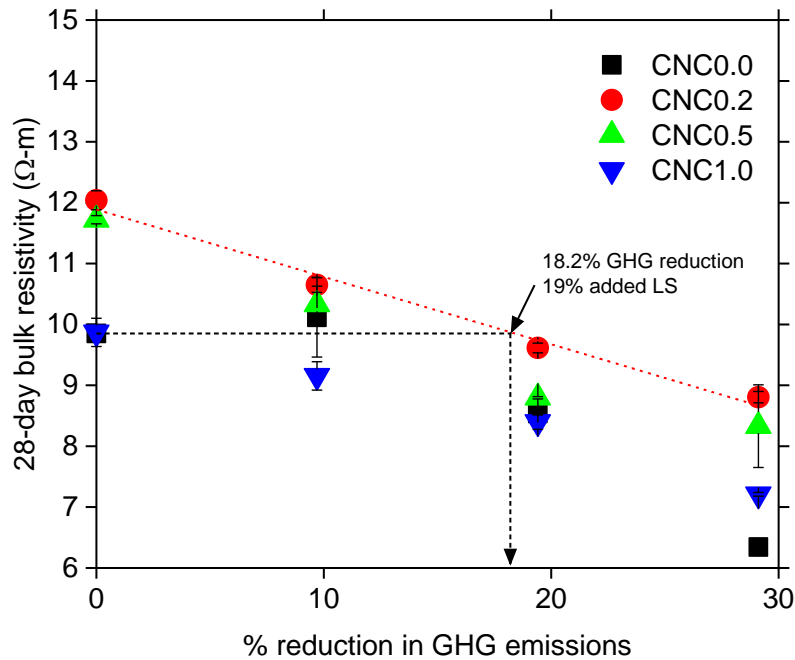
640 Figure 14. 28-day saturated bulk resistivity versus GHG emissions for OPC-LS mixtures with
641 and without CNCs. The ends of the error bars shown here represent the measured values and the
642 markers show the average value of the two samples.

643 Maximum reduction in GHG emissions possible with optimal LS and CNC contents was calculated
644 based on m and b from Table 2. It was found that equivalent performance (in terms of resistivity)
645 could be achieved by 19% LS addition (22% total LS) with 0.2% dosage of CNCs and this
646 corresponded to 18.2% reduction in GHG emissions compared to the LS0-CNC0.0 mixture.
647 Therefore, 20% LS addition with 0.2% CNC dosage was considered, which corresponded to a
648 19.4% decrease in GHG emissions. A comparison of the other cementitious paste properties is
649 shown in Table 3, where it was seen that LS20 mixtures with 0.2% CNC addition had similar
650 performance compared to a 100% OPC mixture with no added CNCs. Further reduction in GHG
651 emissions (~29%) can be achieved by adding 30% LS and 0.2% CNCs with similar 28-day B3B
652 flexural strength and slightly lower (~10.6%) 28-day saturated bulk resistivity compared to 100%
653 OPC mixture. It should be noted that single-operator variability of bulk resistivity measurement

654 according to ASTM C1876-19 should be within 12%, implying that the reduction in bulk resistivity
655 due to 30% LS and 0.2% CNC addition is not significant compared to 100% OPC mixture.

656   Table 2. Slope (m_i) and intercept (b_i) values for best fit lines

i	CNC dosage (% volume of binder)	m_i	b_i
1	0.0	-0.12	10.53
2	0.2	-0.11	11.89
3	0.5	-0.12	11.55
4	1.0	-0.09	9.97

657   Table 3. Comparison of properties between LS20-CNC0.2 and LS0-CNC0.0 mixtures

Property evaluated	Testing age	LS0-CNC0.0	LS20-CNC0.2	% change
Heat of hydration of clinker (J/g cement)	7 days	301.84	334.86	+10.9%
Non-evaporable water content (g/100g binder)	28 days	14.87 ± 0.00	15.79 ± 0.32	+6.2%
B3B flexural strength (MPa)	28 days	22.17 ± 1.04	19.56 ± 1.48	-11.7%
Saturated formation factor, F_{sat}	28 days	77.57 ± 0.00	75.70 ± 0.63	-2.4%
Overall porosity, Φ	28 days	39.45 ± 0.36%	43.30 ± 0.00%	+3.8%
Pore connectivity, β	28 days	0.0327	0.0305	-6.7%

658

659 Past research showed that the performance of PLCs (confirming to ASTM C595) was similar to
660 OPC [37, 38, 42, 98] in terms of mechanical properties and durability and hence is an acceptable
661 substitute in the push towards sustainability in the concrete industry. The use of PLCs could result
662 in reducing the GHG emissions by ~10%. Any further LS replacement without added reactive
663 SCMs would result in a significant reduction in mechanical and transport properties rendering the
664 possibility of using high LS dosages unfeasible. The addition of CNCs to OPC-LS mixtures
665 resulted in improved transport properties (which would result in reduced diffusion of deleterious
666 species) without compromising mechanical properties. The increased degree of hydration at 28
667 days in OPC-LS mixtures with CNCs indicated that the OPC clinker is utilized more effectively.
668 Therefore, the addition of CNCs to mixtures containing higher amounts of LS (up to 22%,
669 including the LS content in OPC) could push this envelope further and pave way for ternary blends
670 and result in "greener" mixtures without compromising on the performance.

32

3.6. Conclusions

OPC-LS-CNC mixtures were studied as a possible method to reduce GHG emissions. The addition of up to 0.5% CNCs to OPC-LS mixtures resulted in an increased degree of hydration of binder at all ages. At early ages, the increase in degree of hydration was attributed to the combined effect of LS and CNCs. At later age, the increased degree of hydration was due to the CNCs.

The addition of low dosages of CNCs up to 0.5% resulted in a decrease in pore connectivity of the mixtures and an increase in bulk resistivity of up to 38%. CNCs addition did not have a significant impact on the overall porosity and B3B flexural strength of the mixtures at both 7 and 28 days. Also, the addition of CNCs did not have a significant impact on the drying shrinkage strain of the mortar specimens made with limestone. There was slightly higher (~5%) drying shrinkage strain after 90 days in drying environment for the mixture with OPC and CNC when compared to mixture without CNC, probably due to higher clinker reaction in the presence of CNCs.

The addition of 20% LS and 0.2% CNCs together resulted in mixtures with ~19% reduced GHG emissions with comparable mechanical and transport properties to the conventional 100% OPC mixture. Higher GHG emission reductions up to ~29% can be achieved by adding 30% LS and 0.2% CNCs resulting in mixtures with similar mechanical properties and slightly lower (~11%) bulk resistivity. These findings pave way to explore the use of CNCs to achieve further lower GHG emissions and develop "greener" mixtures.

4. CHAPTER 3: Performance of Mixtures with SCMs and CNCs

As shown in Chapter 2, CNCs can be used to improve the performance of mixtures with limestone by increasing the degree of hydration and providing a way to reduce GHG emissions. To further reduce the GHG emissions, this research also evaluated the use of SCMs to replace the cement along with using CNCs. Therefore, the extended goal of this project, and the objective of this chapter, is to evaluate the performance of CNCs in mixtures with SCMs.

4.1. Constituent Materials and Characterization Procedures

4.1.1. Materials

Commercially available Type II OPC and a PLC made using the same clinker as OPC were used for this study. SCMs considered in this study were fly ash (FA), slag (SL), and silica fume (SF). The chemical composition and particle size parameters of the OPC, PLC, and the SCMs are shown in Table 4. X-ray fluorescence was used to determine the chemical composition of the materials, LOI was determined using a furnace, and particle size parameters were determined using laser diffraction technique. The detailed procedures for the material characterization and testing were described in Chapter 2. CNCs that were obtained in the form of suspension with 11% w/w CNC solids were used. The CNCs were manufactured by Forest Products Laboratory using sulfuric acid hydrolysis process. Four CNC concentrations used were 0%, 0.2%, 0.5%, and 1.0% solid volume by volume of binder.

Table 4. Chemical composition and particle size parameters of the OPC, PLC, and SCMs (NA: not applicable)

%	Cement		SCMs		
	OPC	PLC	Fly Ash (FA)	Slag (SL)	Silica Fume (SF)
SiO_2	19.95	18.38	51.86	31.58	95.88
Al_2O_3	3.95	3.62	21.70	12.13	0.69
Fe_2O_3	2.28	2.07	5.04	0.55	0.12
CaO	63.32	61.69	8.61	41.34	0.70
MgO	1.43	1.33	2.58	6.97	0.26
SO_3	2.55	2.48	0.78	3.75	0.15
LOI	2.71	6.42	1.42	0.00	4.30
Na_2O	0.21	0.22	2.58	0.24	0.16
K_2O	0.48	0.44	1.45	0.28	0.49
TiO_2	0.19	0.18	1.19	0.47	0.01
P_2O_5	0.10	0.10	0.23	0.00	0.05
ZnO	0.01	0.01	0.02	0.00	0.06
Mn_2O_3	0.07	0.07	0.03	0.19	0.04
Cl	0.003	0.003	0.01	0.00	0.01
Limestone	4.31	13.32	NA	NA	NA
d_{50} (μm)	10.52	15.70	13.01	29.08	4.96
d_{90} (μm)	27.89	59.18	44.62	87.81	11.28

Several binder combinations that are currently accepted by CALTRANS were used in this study. The OPC and PLC were used with 50% SL, 20% FA + 5% SF, and 25% FA + 25% SL. All the considered binder combinations were evaluated with and without CNCs.

4.1.2. Paste mixing and sample preparation

The cementitious materials were dry mixed for 90 s using a vacuum mixer at 400 rpm and 70% vacuum. The CNC dispersed mix water was placed in a mixing bowl, and the dry mixed cementitious materials were added, and mixed using a vacuum mixer (Renfert Inc. model 18281000) for 90 s at 400 rpm and a 70% vacuum level. The mixing cup was scraped using a silicone spatula for 15 s, and vacuum mixing was carried out for an additional 90 s. Pastes were prepared at a water to binder ratio of 0.40. The prepared pastes were cast in 50 mm diameter and 100 mm length cylinder molds. The cylinder molds with the fresh pastes were rotated on a roller at 60 rpm for 12 hours to prevent any bleeding and they were kept sealed until testing.

35

723 **4.1.3. Tests on cementitious pastes**

724 All the paste mixtures were tested for heat release (and heat flow), B3B flexural strength, porosity,
725 and saturated bulk resistivity. Heat release (and heat flow) were measured using isothermal
726 calorimetry for seven days. The samples were tested for B3B flexural strength at 28 and 56 days.
727 Samples were tested for porosity and bulk resistivity at 28 and 56 days. All samples were sealed
728 after casting until the age of testing. The detailed procedures for testing the samples were reported
729 in Chapter 2 and not repeated here for brevity.

730 ## 4.2. Experimental Results and Discussion

731 **4.2.1. Heat flow**

732 Figure 15a-f shows the heat flow (rate of heat release) for the OPC-SCM and PLC-SCM mixtures
733 up to first 40 hours. For all the SCM mixtures, CNC addition resulted in a slight retardation
734 (indicated by the curve shifting to the right) compared to mixtures without CNC. This retardation
735 causes a delay in the set time and the onset of the acceleration period. A higher CNC dosage
736 caused a longer retardation. Similar observation was made in Chapter 2 where CNCs were used
737 along with OPC and limestone. The heat flow peak intensity of the PLC-SCM mixtures is lower
738 compared to OPC-SCM mixtures because of additional reduction of clinker from LS replacement.
739 A secondary peak after approximately 24 hours was observed that requires further study.

740

741

742 (a)

(b)

(c)

743

744

745

746

FULL 6(c)(i)

(d)

(e)

747

748

749

750

751

38

(f)
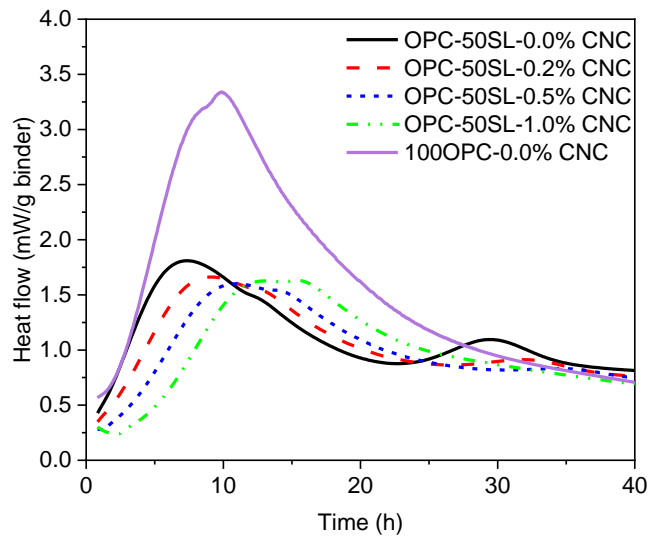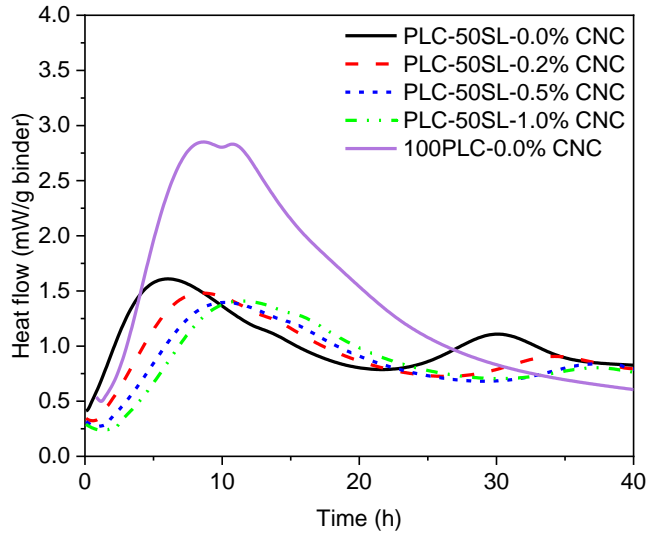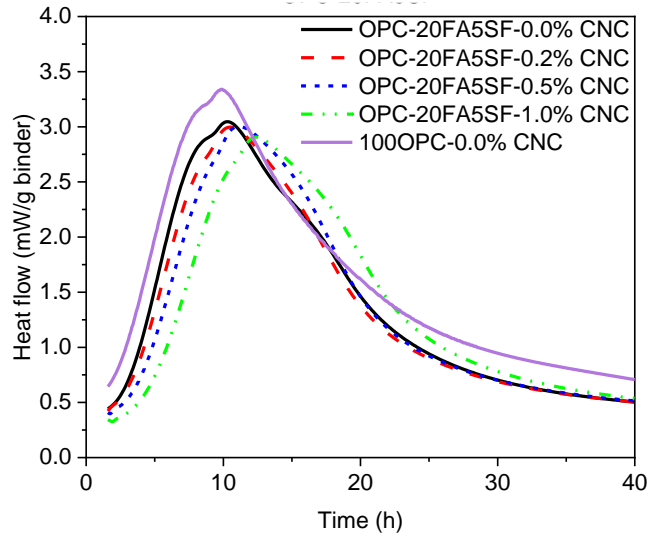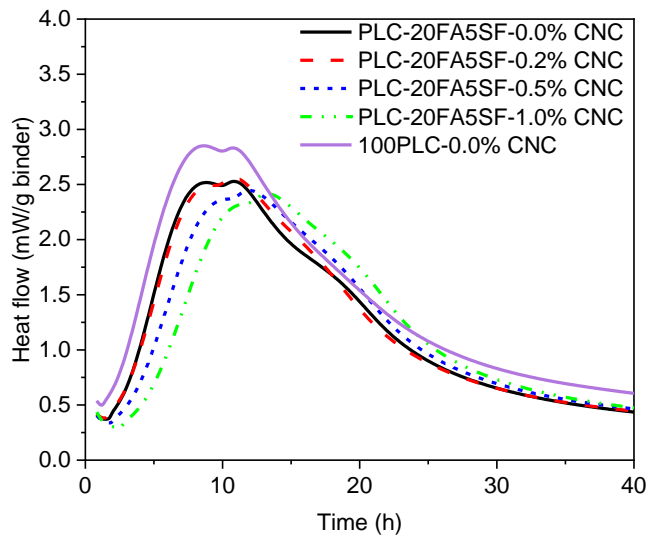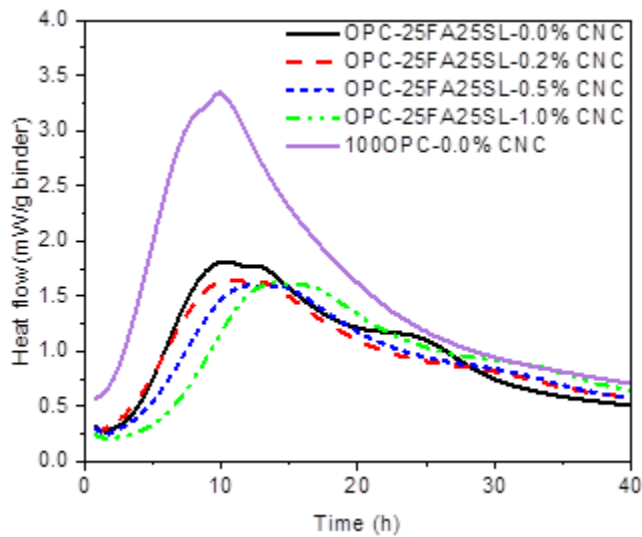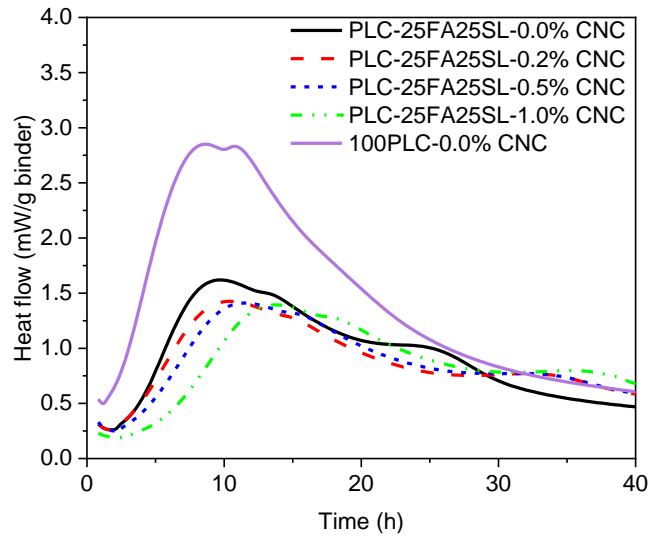
Figure 15. Change in heat flow with varying CNC dosage – (a) OPC-50SL (b) PLC-50SL (c) OPC-20FA5SF (d) PLC-20FA5SF (e) OPC-25FA25SL (f) PLC-25FA25SL

In case of OPC-SL50 mixture (Figure 15a), the shift in the silicate peak ranged from 1.5 hours (0% CNC) to 6.5 hours (1% CNC). In case of PLC-SL50 mixtures (Figure 15b), the filler effect of LS in the PLC caused an acceleration in the 0% CNC mixture (compared to the 100OPC-CNC0.0 mixture), but with increase in CNC dosage, the peak shifted with CNC content to later ages (i.e., from 2 hours (0% CNC) to 5 hours (1% CNC)). In both OPC-SL50 and PLC-SL50 mixtures, the slag hydration peak, characterized by the third peak (after approximately 24 hours) had lower intensity with CNC addition. For instance, in OPC-SL50-0.0% CNC mixture the slag hydration peak intensity was 1.2 mW/g binder occurring at 30 hours, whereas for the mixtures with CNC, the peak was shifted to 35 hours with a lower heat flow intensity of 1 mW/g binder. A similar trend was observed for PLC-SL50. It appears that addition of CNCs to OPC/PLC-SL mixtures resulted in retardation of slag hydration.

For OPC-20FA-5SF (Figure 15c) and PLC-20FA-5SF (Figure 15d) mixtures, the observed trends are similar. Any retardation in the pastes due to the presence of fly ash is compensated by the presence of SF in 0% CNC mixtures. In case of mixtures with CNC, there appears to be a retardation by 3 hours (OPC mixtures) and 5 hours (PLC mixtures). For mixtures with OPC-25FA-25SL (Figure 29e) and PLC-25FA-25SL (Figure 29f), similar trends are observed; with increase in CNC dosage, there is a shift in the silicate hydration peak to the right by a maximum of three hours. However, a much longer retardation (as long as 10 hours) of the peak associated with the slag hydration was observed at higher CNC dosage.

In all cases, the aluminate peak (or the sulfate depletion peak) for the mixtures with CNC had a higher intensity compared to mixtures without CNCs. In case of FA mixtures, the silicate and the

39

777   aluminate peaks overlapped, indicating that CNC addition may be close to causing a sulfate
778   imbalance like conditions, similar to the observations made for mixtures with LS and CNCs.

779   Figure 16 shows the 7-day heat release for the mixtures studied here. The 7-day heat release values
780   for OPC-SCM ranged from 302 – 311 J/g binder for OPC mixtures, 268 – 275 J/g binder for OPC-
781   50SL mixtures, 251 – 259 J/g binder for OPC-25FA25SL mixtures, and 268 – 274 J/g binder for
782   OPC-20FA5SF mixtures when CNC dosages were varied from 0 – 1% by volume of binder. The
783   7-day heat release values for the PLC-SCM mixtures ranged from 285 – 287 J/g binder for PLC
784   mixtures, 247 – 258 J/g binder for PLC-50SL mixtures, 233 – 241 J/g binder for PLC-25FA25SL
785   mixtures, and 248 – 251 J/g binder for PLC-20FA5SF mixtures when CNC dosages varied from 0
786   – 1% by volume of binder.

787

788

789   (a)

790

791

40

(b)
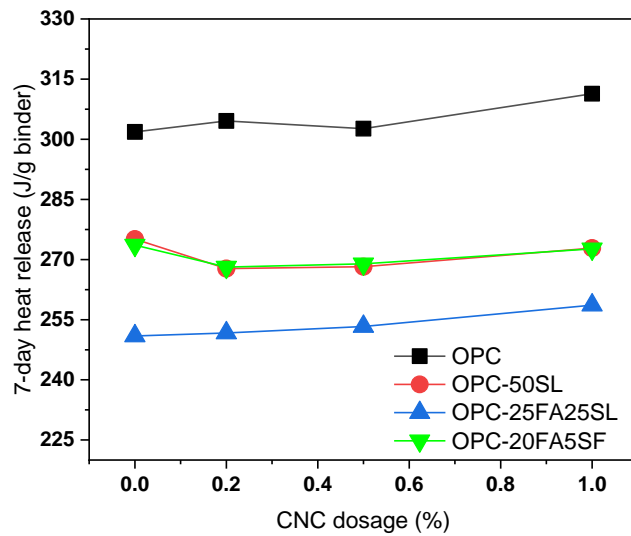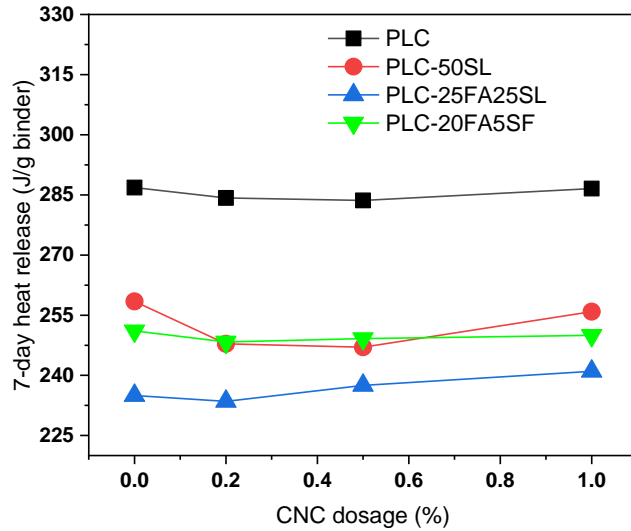
794   Figure 16. Effect of CNC dosage on 7-heat release (a) OPC mixtures (b) PLC mixtures

795   It was observed that overall, the CNCs addition did not significantly affect the 7-day heat release
796   value of the mixtures with SCMs. The 7-day heat release values of the mixtures with CNCs were
797   usually within $\pm 2\%$ of the 7-day heat release values of the respective mixtures without CNCs.
798   When CNCs were added at low dosages of 0.2 and 0.5% to PLC-50SL mixture, it was observed
799   that the 7-day heat release was reduced by 4.1 and 4.4%, respectively, and this needs to be further
800   investigated. When CNCs were added at 1.0% dosage to OPC-25FA25SL and PLC-25FA25SL
801   mixture, the 7-day heat release values were increased by 3.1 and 2.6%, respectively. The
802   adsorption behavior of CNCs on SCMs is not known, and it could be playing an important role in
803   terms of reaction rate of SCMs. More research work is needed to explain possible mechanisms for
804   the role of CNCs in hydration of SCM mixtures.

805   **4.2.2. B3B flexural strength**

806   Figure 17 shows a parity plot for the 28-day and 56-day B3B flexural strength for the mixtures
807   with and without CNCs. It should be noted that the B3B flexural strengths indicate characteristic
808   strength of the mixtures, and they are higher than flexural strength determined using conventional
809   flexural strength testing due to the size effect.

41

810

811

812

(a)

813

814

(b)
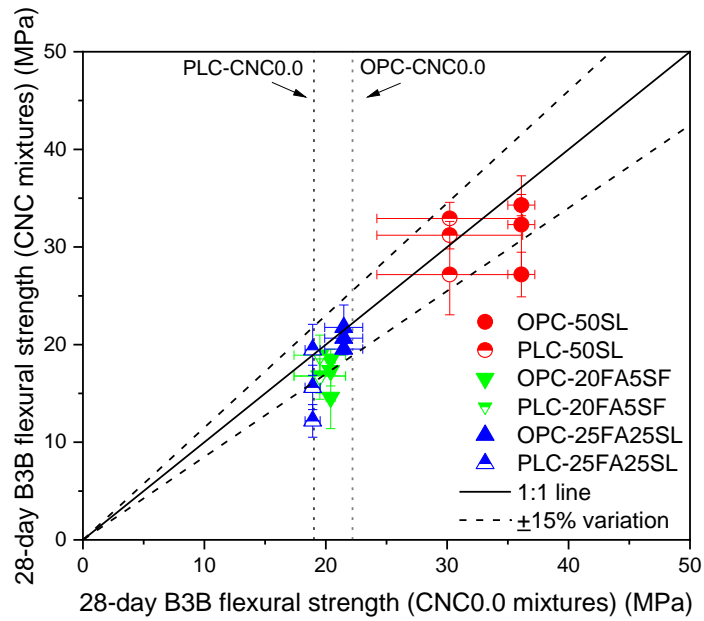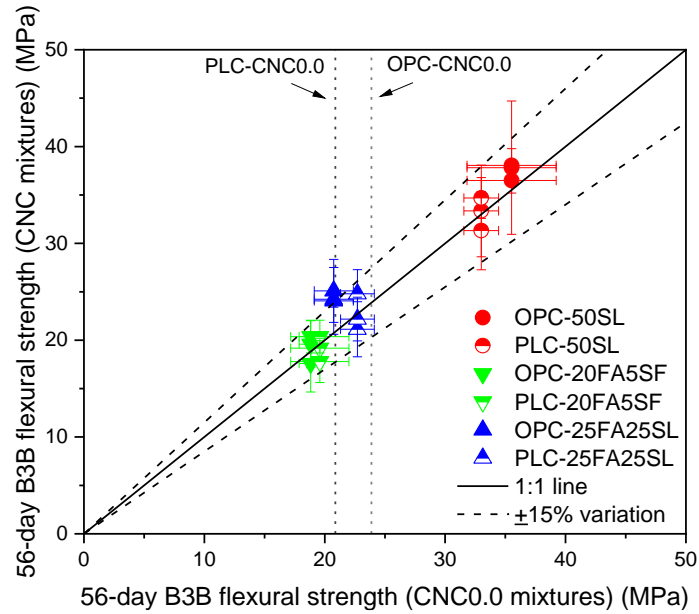
Figure 17. Effect of CNC dosage on B3B flexural strength – (a) 28 days (b) 56 days. A data point on the 1:1 line indicates similar performance, and a data point above the 1:1 line indicates better performance for mixtures with added CNCs (i.e., the measurement on the Y-axis).

42

818   With CNC addition, B3B flexural strength of the most mixtures were within 15% of the flexural
819   strength of the mixtures without CNC. The 28-day B3B flexural strengths of the mixtures that had
820   lower than 15% of the B3B flexural strengths of the mixtures without CNC were OPC-50SL-
821   CNC1.0, OPC-20FA5SF-CNC0.5, and PLC-25FA25SF-CNC0.5. With the exception of the three
822   mixtures, it can be said that the addition of CNCs did not have an adverse effect on the 28-day
823   flexural strengths of the mixtures with SCMs.

824   It was observed that the mixtures with PLC and SL, PLC-50SL and PLC-25FA25SL, had
825   improved strength from 28 days to 56 days. No adverse effects of adding CNCs in terms of flexural
826   strength was seen at 56 days, as none of the mixtures with CNCs had lower than 15% of the flexural
827   strength of the mixtures without CNCs. It was observed that 56-day B3B flexural strength of OPC-
828   25FA25SL mixtures with CNC had slightly higher (by 1 to 6%) than 15% of the B3B flexural
829   strength of the OPC-25FA25SL-CNC0.0.

830   **4.2.3. Bulk resistivity and pore structure characteristics**

831   The 28-day and 56-day saturated bulk resistivity values of the mixtures with OPC, PLC, and
832   different SCMs are shown in Figure 18. Bulk resistivities of the SCM mixtures with and without
833   CNCs were significantly higher than the OPC-CNC0.0 mixtures at both 28 and 56 days as seen in
834   Figure 18. Overall, the mixtures with 20FA5SF had the highest bulk resistivity among the mixtures
835   tested, likely due to the inclusion of finer material like silica fume that contributed to a reduction
836   in pore connectivity. At 28 days, the bulk resistivity of the SCM mixtures, except OPC-50SL,
837   decreased with the addition of CNCs at low dosages (0.2 and 0.5%) and increased at higher dosage
838   of 1.0% CNC. Only OPC-50SL and PLC-50SL had slightly higher 28-day resistivities (4.6 and
839   11.8%, respectively) at 1.0% CNC dosage when compared to the respective mixtures without
840   CNC. For OPC-50SL, the 28-day bulk resistivity of the mixtures were between 40.2 ohm.m and
841   47.4 ohm.m with varying CNC dosage.

842

843

(a)

(b)
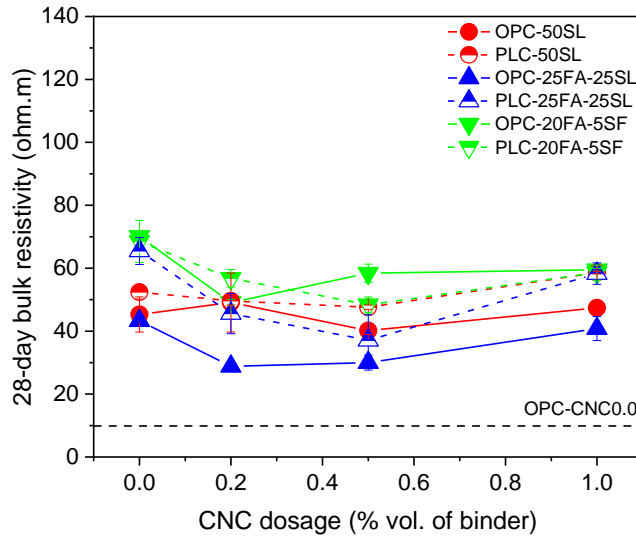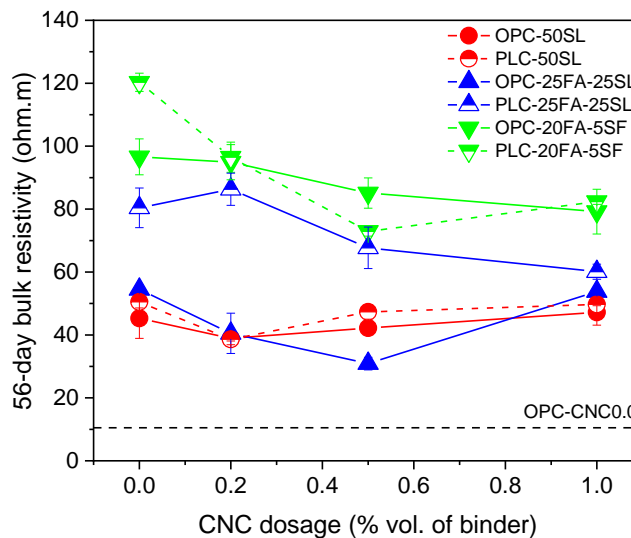
Figure 18. Effect of CNC addition on saturated bulk resistivity of the mixtures with SCMs (a) 28 days (b) 56 days.

At 56 days, it was observed that with the addition of CNCs, the bulk resistivities were decreased for most of the mixtures. The decrease in bulk resistivity with CNC addition ranged from 1.3% to 43.3%. The two mixtures that had higher bulk resistivity compared to their respective mixtures without CNC were OPC-50SL-CNC1.0 (higher by 4.2%) and PLC-25FA25SL-CNC0.2 (higher by 7.3%). The possible reasons for the overall trend of reduction in bulk resistivities with the addition of CNCs to the SCM mixtures include agglomeration of CNCs when SCMs are present and possible adsorption of CNCs on SCMs resulting in slower reaction of SCMs. A comparison

44

857 study is underway evaluating the long-term resistivity and chloride transport properties. The 28-
858 day and 56-day porosity data for the different mixtures with and without CNCs is shown in Figure
859 19. A thermodynamic modeling approach was used to provide an idea of how much porosity of
860 the samples would vary with different SCMs and SCM contents.
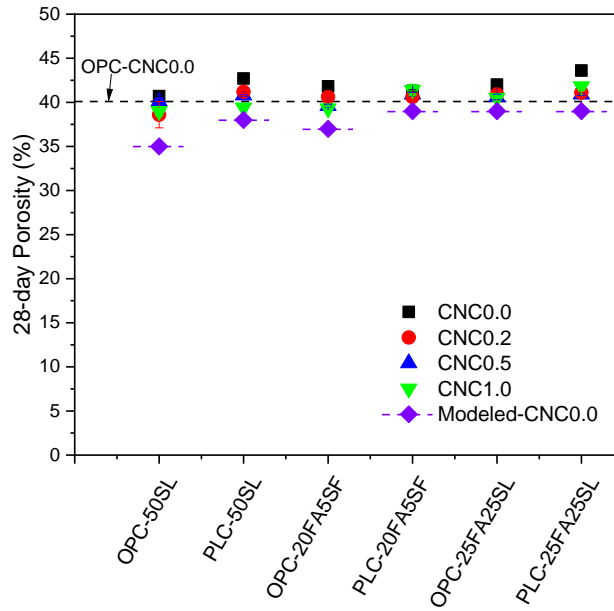
861

862   (a)
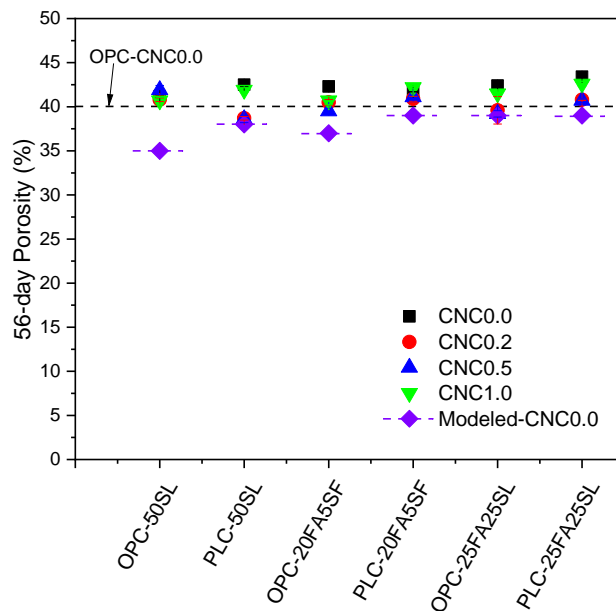
863

864   (b)

865   Figure 19. Porosity of the paste samples at (a) 28 days (b) 56 days

45

866 The porosity of CNC0.0 mixtures determined from thermodynamic modeling is shown in Figure
867 19 as a baseline to compare the porosity of mixtures with and without CNCs. The porosity of the
868 mixture OPC-CNC0.0 is also shown in Figure 19 as a reference. Minimal changes in total porosity
869 of the samples were observed when CNCs were added, and the variation was less than 3% for the
870 most mixtures and less than 4% for all the mixtures when compared to the corresponding mixtures
871 without CNCs. The mixtures that had more than 3% difference in porosity between the mixtures
872 with CNC and without CNC were PLC-50SL (CNC1.0 mixture at 28 days with 3.3% difference
873 and 56 days with 3.9% difference) and OPC-25FA25SL (CNC0.5 mixture at 56 days with 3.2%
874 difference).

875 The pore connectivity (β) of the mixtures determined at 28 days and 56 days are shown in Figure
876 20. It was observed that the pore connectivity of the SCM mixtures was significantly lower than
877 the OPC-CNC0.0 mixture as SCMs are known to improve the pore refinement. With the addition
878 of CNCs to the SCM mixtures, differences in the determined pore connectivity values were
879 observed. It was observed that the pore connectivity of the mixtures with CNCs were generally
880 higher than the respective mixtures without CNCs. Again, it is important to remember that SCMs
881 are even more effective at later ages so longer-term testing is still needed.

882
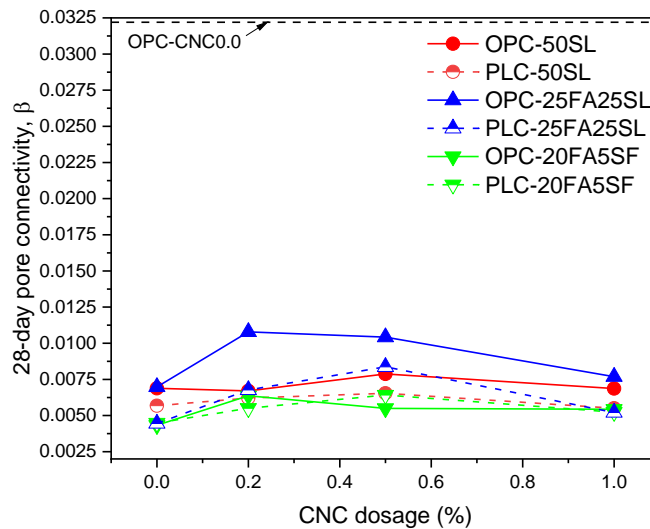
883

884   (a)
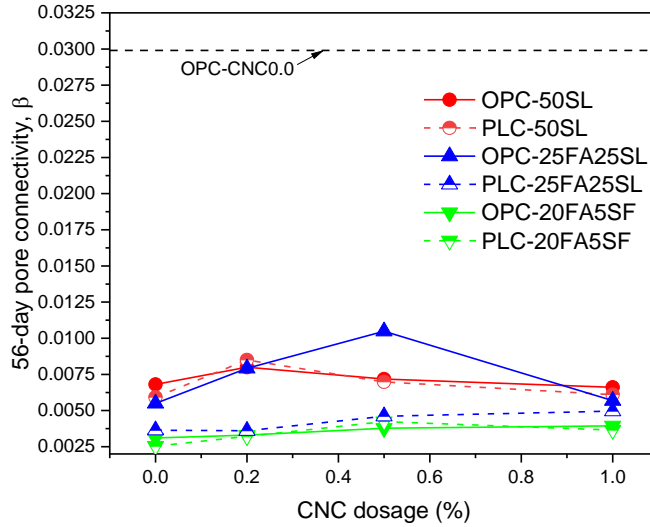
885

886   (b)

887   Figure 20. Effect of CNC dosage on pore connectivity (β) in the pastes (a) 28 days (b) 56 days

888   At 28 days, except the OPC-50SL mixture, the pore connectivity values peak at 0.2 or 0.5% CNC
889   dosage and reduce at 1.0% CNC dosage. In the case of OPC-50SL mixture, the 28-day pore
890   connectivity values were very similar at all CNC dosages except at 0.5% CNC dosage. Similar
891   trend was observed with 56-day pore connectivity values where it peaks at either 0.2 or 0.5% CNC
892   dosage and slightly reduces at 1.0% CNC dosage, with the exception of OPC-20FA5SF and PLC-
893   25FA25SL mixtures where the pore connectivity increased with increase in CNC dosage. The 28-
894   day pore connectivity values of the SCM mixtures ranged from 0.0045 to 0.0108, which are
895   significantly lower (by 66 - 86%) when compared to pore connectivity value (0.0322) of OPC-
896   CNC0.0 mixture. The 56-day pore connectivity values of the SCM mixtures ranged from 0.0025
897   to 0.0105, which are significantly lower (by 65 - 92%) when compared to pore connectivity value
898   (0.0299) of OPC-CNC0.0 mixture. The general increase in pore connectivity values with the CNC
899   dosage can explain the general decrease in saturated bulk resistivity of the SCM mixtures with
900   CNCs as the porosity did not significantly change with the CNC addition.

901   4.3. Conclusions

902   OPC-SCM-CNC and PLC-SCM-CNC mixtures were evaluated for CNCs use in the mixtures with
903   SCMs. Overall, CNCs addition to the SCM mixtures did not significantly affect the 7-day heat
904   release values, except the 25FA25SL mixtures where a reduction of up to 4.4% in 7-day heat
905   release at low CNC dosages. In the mixtures with 25FA25SL, there was up to 3.1% increase in 7-
906   day heat release at 1.0% CNC dosage. The interaction between CNCs and SCMs need to be
907   understood to clearly explain the effect of CNCs on the degree of hydration of the SCM mixtures,
908   and ongoing work is currently underway.

47

909 The 28- and 56-day B3B flexural strength of the majority of the SCM mixtures with CNC were
910 within $\pm$15% of the flexural strength of the respective mixtures without CNC. At 56 days, the
911 addition of CNCs improved the flexural strength of OPC-25FA25SL mixtures by 16 (at 1.0%
912 CNC) – 21% (at 0.5% CNC).

913 The addition of low dosages of CNCs up to 0.5% resulted in an overall increase in pore
914 connectivity of the SCM mixtures and reduction in bulk resistivity measured at 28 and 56 days. It
915 was noted that the 28-day pore connectivity values of the SCM mixtures ranged from 0.045 to
916 0.0108, which were significantly lower than the 28-day pore connectivity value of 0.0322 for OPC-
917 CNC0.0 mixture. The 56-day pore connectivity values of the SCM mixtures ranged from 0.025 to
918 0.0104, which were again significantly lower than the 56-day pore connectivity value of 0.0299
919 for OPC-CNC0.0 mixture. The 56-day saturated bulk resistivity values ranged from 30.9 to 120.3
920 ohm.m for the mixtures with SCMs depending on type of SCM and CNC dosage, which were
921 significantly higher than the 56-day bulk resistivity value of 10.5 ohm.m for OPC-CNC0.0
922 mixture.

923 The overall trend of reduction in bulk resistivities and increase in pore connectivity with the
924 addition of CNCs to the SCM mixtures could be due to the agglomeration of CNCs, alteration of
925 the pore structure due to delayed early hydration, and possible adsorption of CNCs on SCMs
926 resulting in lower reaction of SCMs. Further research is needed to understand the adsorption
927 behavior of CNCs on SCMs and evaluate the resulting effect on the performance of the SCM-CNC
928 mixtures. Future research shall also include studying the effect of reduction in pH of the pore
929 solution in the SCM mixtures on CNCs performance in the mixtures.

5. CHAPTER 4: Full Scale Field Trials of Slabs Placement using Mixtures with Limestone and CNCs at UC Davis Pavement Research Center

This chapter of the report summarizes the results of the implementation of the use of cellulose nanocrystals (CNC) in portland cement concrete (PCC) pavement. In this experiment, the use of CNC is evaluated in combination with portland-limestone cement (PLC) and compared with ordinary portland cement (OPC) concrete in a set of pilot slabs built on the research site of the University of California Pavement Research Center (UCPRC) in Davis, California.

5.1. Test Sections Preparation

Three test sections were built for three mixtures. The three mixtures were i) OPC mixture with 30% slag (labelled as OPC), ii) PLC mixture with 30% slag (labelled as PLC), and iii) PLC mixture with 30% slag and 0.1% CNC (labelled as CNC). The location of the test sections is shown in Figure 21 (picture taken after the application of the curing compound on the lean concrete base) and Figure 22 (picture taken after the construction of the concrete slabs).

Figure 21. Location of test sections (white path at the bottom of the picture; picture taken after the application of the curing compound on the lean concrete base).

49

946

947   Figure 22. Test sections (from picture bottom to top: PLC, CNC, and OPC)

948   **5.1.1. Test sections configuration**

949   The test sections were designed to study mixture constructability and mid-term (less than a year)
950   ambient environmental response. While mechanical and durability characteristics of the mixtures
951   are important as well, they do not constitute the main focus of the test sections experiment.
952   Mechanical properties were evaluated based on laboratory testing of specimens prepared from
953   mixtures sampled during the test sections construction. Limited durability laboratory testing was
954   conducted on specimens also prepared from the construction mixtures.

955   One of the goals of the experiment is to evaluate the ambient environmental response, focused on
956   moisture-related shrinkage and thermal deformations. To maximize those deformations, the
957   concrete slab thickness was set to a low value, 4 inches and slab width was set to 8 feet, rather than
958   the conventional 12 feet, so that the consolidation could be achieved with a vibrating rolling screed
959   while maintaining the 4-inch slump of the mixtures.

960   The location of the test sections was selected to build a walking path at the UCPRC site in Davis.
961   The total length of the walking path is approximately 70 feet, with an approximately 45 feet useful
962   length that is not affected by shading from nearby buildings so that uniform solar exposure could
963   be obtained. The three test sections, one per mixture type, were built along the useful length. Each
964   section consists of three 5 feet long slabs as shown in Figure 23.

50

PLC CNC OPC

5×8 ft ⊗ ⊗ ⊗

45 ft

⊗ Instrumented slabs | Full-depth joints (metal form)
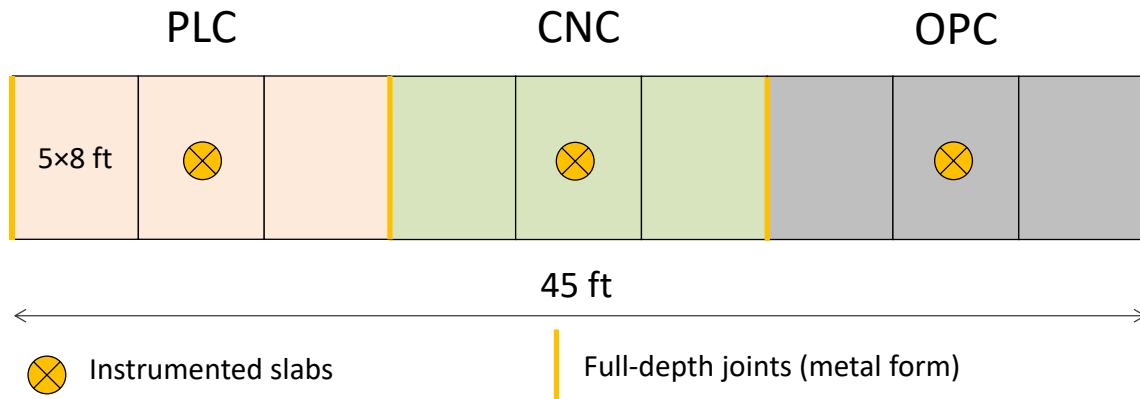
965

966   Figure 23. Test sections layout

967   Beneath the 5×8 ft (length × width) and 4 inch thick slabs is a lean concrete base that is 4 inch
968   thick, which in turn was placed on a 3 to 4 inch thick aggregate subbase (Figure 24). The subgrade
969   is clay. The shoulder was backfilled with loose aggregates after the construction of the concrete
970   slabs.

5×8 ft   10 ft

Sawcut (1.3 in.)   *Curing compound interlayer*

4 in.

4 in.   Lean Concrete Base
3-4 in.   Aggregate subbase
                             Clay subgrade
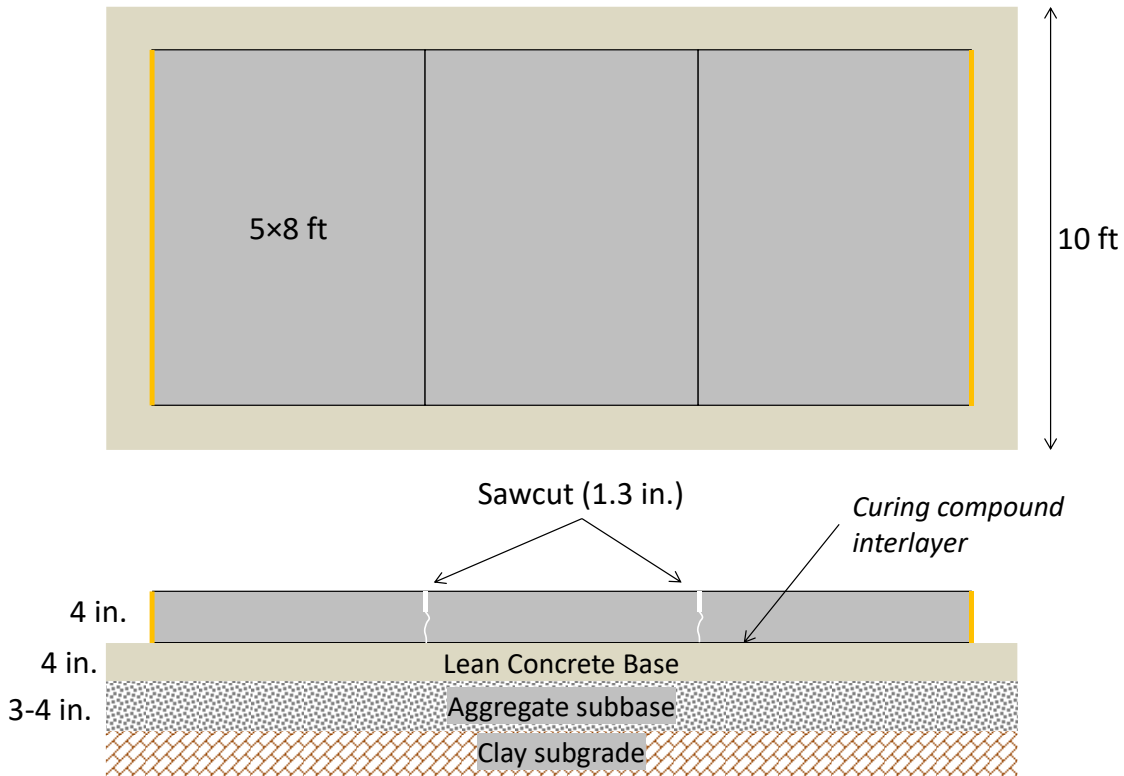
971

972   Figure 24. Test section configuration

51

5.1.2. Test section instrumentation

The instrumentation installed in each of the sections, shown in Figure 25, focuses on measuring the response to the ambient environment loading. The instrumentation of each section includes:

- Two thermocouples on rods for measuring temperature profile in the slabs and base.
- Two relative humidity (RH) sensors. The RH sensors are Sensirion SHT85, housed in a porous plastic tube.
- Two pairs of GeoKon 4200 vibrating wire strain gages (VWSGs), located at two of the slab corners, 10 in. from the shoulder edge of the slabs. Each pair includes a VWSG close to the top of the slab (0.8 in. from top) and another VWSG close to the bottom of the slab (0.8 in. from bottom).
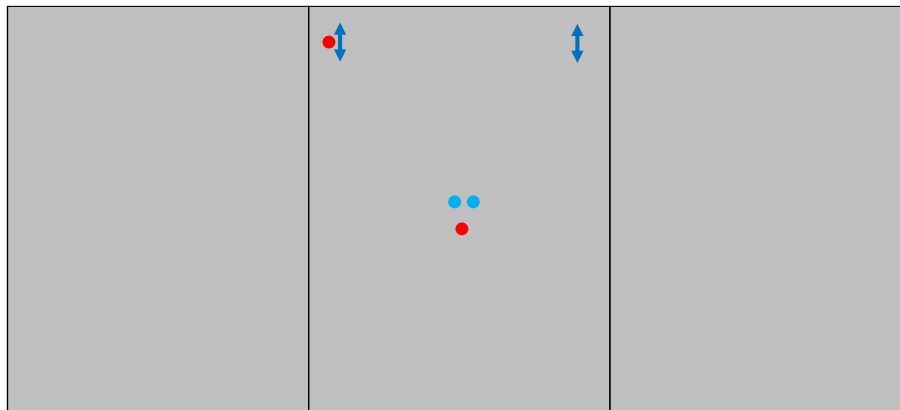
- ● Thermocouples rod; five depths: 0.2 in. / 0.8 in. / 2 in. / 4 in. (slab bottom) / 6 in. (lean concrete base)
- ● RH sensor (0.8 in. Depth)
- ↔ VWSGs; two depths: 0.8 in. / 3.2 in. (0.8 in. above slab bottom)

Figure 25. Test section instrumentation (Not to scale)

In addition to the instrumentation embedded in the test sections, three prisms per concrete mixture were fabricated and instrumented with a VWSG each (Figure 26 left). The prisms are 20×6×1.6 in. in size and they are referred as unrestrained shrinkage prisms (USP) in this report. The concrete for the prisms' fabrication was the same used for the construction of the slabs (sampled from the ready-mix trucks) although screened through 3/4 in. sieve to remove the largest aggregates. These prisms were cured the same as the slabs and left outdoors by the test sections so that they were subjected to the same ambient environmental conditions (Figure 26 right). These prisms measure the unrestrained deformations of the concrete as they are not bonded to any support.

FULL 6(c)(i)

993

994 Figure 26. Unrestrained shrinkage prisms

5.2. Materials and Mixtures

996 The chemical composition and fineness of OPC, PLC, and Ground granulated blast furnace slag
997 used are shown in Table 5. As expected, the PLC has higher fineness than OPC [38]. The mill
998 certificates of the cementitious materials are attached in the Appendix section. The three mixtures
999 were i) OPC mixture with 30% slag (OPC), ii) PLC mixture with 30% slag (PLC), and iii) PLC
1000 mixture with 30% slag and 0.1% CNC (CNC).

1001 Table 5. Chemical composition and fineness of OPC, PLC, and Slag used (NA: not available)

%	OPC	PLC	GGBFS
SiO_2	20.3	18.4	NA
Al_2O_3	4.1	3.5	17.5
Fe_2O_3	3.9	3.0	NA
CaO	62.4	58.4	NA
MgO	4.9	4.2	NA
SO_3	3.1	3.0	2.5
LOI	2.6	10	NA
Na_2O	0.19	0.24	0.45
K_2O	0.41	0.30	(Na_2O_e)
Limestone	3.4	14	NA
Blaine Fineness, cm^2/gm	4184	5470	4780

1002

1003 **5.2.1. OPC mixture**

1004 The OPC mixture design and materials were supplied by Cemex (Perkins plant, in Sacramento
1005 area). This mixture is used for concrete paving in regular applications where high early strength is

53

1006 not required. The mixture is designed to achieve the strength needed to open to traffic (550 psi
1007 flexural strength) in 10 days. The mixture design is shown in Table 6.

1008 Table 6. OPC mixture design (1 cy)

Material	Description	Design quantity
Coarse Aggregate	Gravel	1900 lb
Fine Aggregate	Sand	1313 lb
Cement	Type II/V ordinary portland cement (OPC), ASTM C150	413 lb
Ground granulated blast furnace slag (GGBFS)	Slag, Grade 120, ASTM C989	177 lb
Water reducer	Master Glenium 7500	4 oz/cwt
Water	-	34.0 gal

1009

1010 The Type II/V cement was produced by the Cemex Victorville plant (California). The slag was
1011 produced in Rizhao (China); slag content is 30% of total cementitious materials.

1012 For water-reducing admixture, the Master Glenium 7500 was selected after showing acceptable
1013 compatibility with the CNC suspension. The Master Glenium 7500 is a high-range water-reducing
1014 admixture, based on polycarboxylate technology, meeting ASTM C494 Types A and F
1015 specifications. The water-reducer content was based on trial batching conducted with the PLC
1016 mixture by UCPRC. All three mixtures were batched with 4 oz/cwt of Master Glenium 7500
1017 following the mix design.

1018 The water-reducer typically used by the supplier for this mixture, based on lignosulphonate
1019 technology, was assumed to be incompatible with a CNC slurry produced by sulfuric hydrolysis
1020 evaluated in the preliminary phase of this experiment.

1021 Some other properties of the OPC mixture are listed below:

1022 • Crushed alluvial aggregates, mainly siliceous
1023 • Water/total cementitious ratio is 0.481
1024 • Non-air-entrained concrete
1025 • Design slump: 4 inches

1026 **5.2.2. PLC mixture**

1027 The PLC mixture is the same as the OPC mixture except for replacement of the Type II/V cement
1028 with portland-limestone cement (Type IL, ASTM C595), on a one-to-one basis. The Type IL
1029 cement was produced by the Cemex Victorville plant (California). All other materials and
1030 quantities in Table 1 remain the same in the PLC mix

54

5.2.3. CNC mixture

The CNC mixture is the same as the PLC mixture except for the addition of the cellulose nanocrystals. The added CNC content is 0.1% (CNC solids by weight of total cementitious materials); this is 0.590 lb of CNC solids per cy of concrete.

The CNC was supplied by Forest Products Laboratory (FPL) and produced by sulfuric acid digestion (product name: 2022-FPL-CNC-213). According to FPL, from this production method, CNC has sulfuric half-esters on the surface. The CNC solids are rigid rods typically about 5 nm wide by 100-150 nm long. The product was supplied as a suspension with 10.4% CNC solids content.

5.3. Test Sections Construction

The subbase was prepared by the UCPRC team in April 2022. The lean concrete base (LCB) was supplied by Elite ready mix and placed and consolidated by Vanguard on May-6, 2022. The concrete was supplied by Cemex ready mix plant in Perkins, close to Sacramento, and placed, consolidated, and cured by UC Davis Facilities Construction team with support from UCPRC on June-27, 2022. The fresh concrete QC and specimen preparation were conducted by Twining with support from UCPRC team.

The timing of the construction of the slabs (June-27, 2022) is summarized below:
- Ready mix truck 1, CNC mixture: 12:50-12:55
- Ready mix truck 2, PLC mixture: 13:55-14:00
- Ready mix truck 3, OPC mixture: 14:45-14:50

The weather conditions during paving were dry and warm, with air maximum temperature and minimum relative humidity (RH) approximately 105°F (40°C) and 15%, respectively. Wind speed was below 2 mph and the sky was clear. Air minimum temperature and maximum RH, during the first nights after construction, were approximately 60°F (15°C) and 80%, respectively. Days following construction had similar weather conditions, typical of Davis during summer.

The concrete was consolidated with a vibrating rolling screed and finished with trowel. No surface texturing was applied. The curing was conducted with white pigmented, resign based, curing compound meeting ASTM C309 Type 2B specifications, applied at a nominal rate of 150 ft²/gal.

A few construction pictures are shown in Figure 27 - Figure 29. Figure 28a shows the test section after the preparation and before the concrete placement. Figure 28b shows the placement of PLC mixture. Figure 28c shows the use of vibrating rolling screed for the CNC mixture and Figure 28d shows finishing of OPC mixture.

FULL 6(c)(i)

1064 Figure 27. Test section instrumentation; left: thermocouple rod and pair of VWSFs; right:
1065 thermocouple rod and two RH sensors

(a)

(b)

FULL 6(c)(i)

(c)   (d)

Figure 28. Slabs construction pictures; (a) before concrete pouring; (b) placing PLC concrete; (c) consolidating CNC concrete; (d) finishing OPC concrete section

Figure 29. Trowel finishing of PLC section (bottom of photograph); CNC section already sprayed with curing compound (middle of photograph; note that white covering is from the curing compound and not the CNC effect); rolling screed consolidation of OPC concrete (middle-top of photograph).

57

5.3.1. Control of water content

The three mixtures (OPC, PLC, and CNC) all have a design water to cementitious materials ratio of 0.481, equivalent to 34.0 gal of water per cubic yard of concrete. The following steps were followed to ensure that the three mixtures would be produced with the same amount of mixing water:

- The three mixtures were batched at the plant with a target of 31.0 gal of water/cy.
- The actual amount of water added at the plant (batch water plus any water added by the truck driver) was noted in the truck dispatch.
- The remaining water (to match exactly 34.0 gal/cy) was added at the construction site either directly from the truck tank or as part of the CNC suspension.

The water content of the fresh concrete was measured following AASHTO T 318. Three specimens were tested per mixture type. The results are shown in Figure 30. The PLC and the CNC mixtures had similar measured water contents. For the three mixtures, the measured water contents were over the 8.9% theoretical water content (the theoretical water content is the same for the three mixtures).
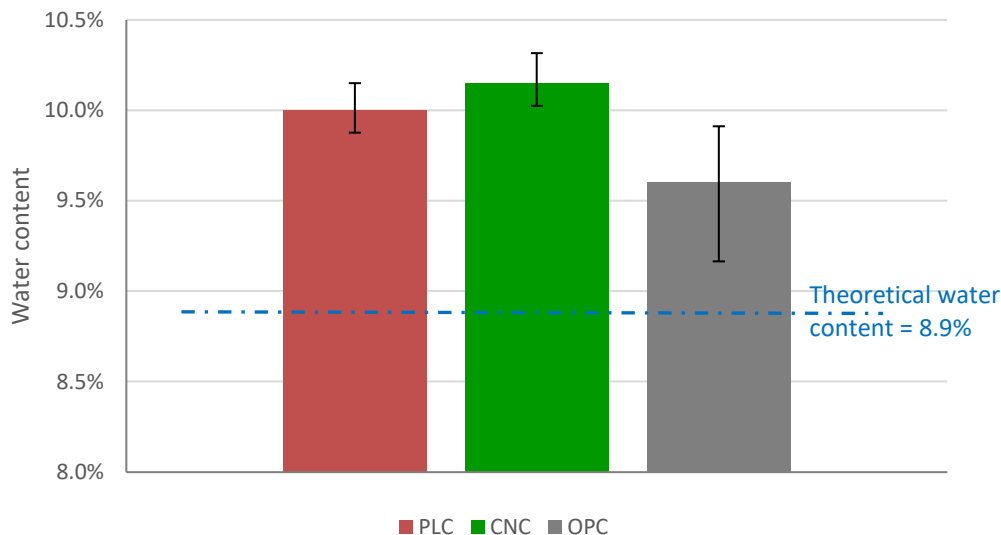
Figure 30. Measured water content (evaporable water / dry weight of mixture, AASHTO T 318) (Note: The theoretical water content includes the design batch water plus the water absorbed by the aggregates in the saturated surface-dry (SSD) condition.)

5.3.2. CNC addition

The CNC were dispersed in their water suspension 4-5 hours before mixing into concrete (CNC solids content of the suspension was 3.33%). A high-shear blender (Waring CB15 Commercial

58

1095 Blender) was used for this purpose. The CNC suspension was blended at 4000 rpm for 60 seconds
1096 twice. When the concrete truck arrived at the construction site, the CNC suspension was added to
1097 the concrete ready-mix truck from the hopper (Figure 31). The concrete was then mixed at the
1098 maximum speed (14-16 rpm) for five minutes.

1099

1100   Figure 31. Addition of the CNC suspension to the ready-mix truck at the construction site

1101 5.4. Experimental Methods

1102 Fresh concrete mixtures were tested for consistency by measuring slump following ASTM
1103 C143/C143M-20, temperature following ASTM C1064/C1064M-17, air content using the
1104 pressure method following ASTM C231/C231M-17, and unit weight following ASTM
1105 C138/C138M-17. In addition, setting time of the concrete was measured following ASTM C403.
1106 Three specimens per mixture were tested for the setting time measurement.

1107 The concrete specimens were prepared with mixture sampled from the corresponding read-mix
1108 truck during the slabs construction. The specimens were cured in wooden boxes or covered with
1109 wet burlap, in the either case inside a room, until 24 hours (Figure 32). Then they were demolded
1110 and stored in lime water at 23°C until testing. The laboratory testing included several properties
1111 evaluated at different times as shown in Table 7. Three specimens were tested for each property
1112 measurement.

FULL 6(c)(i)
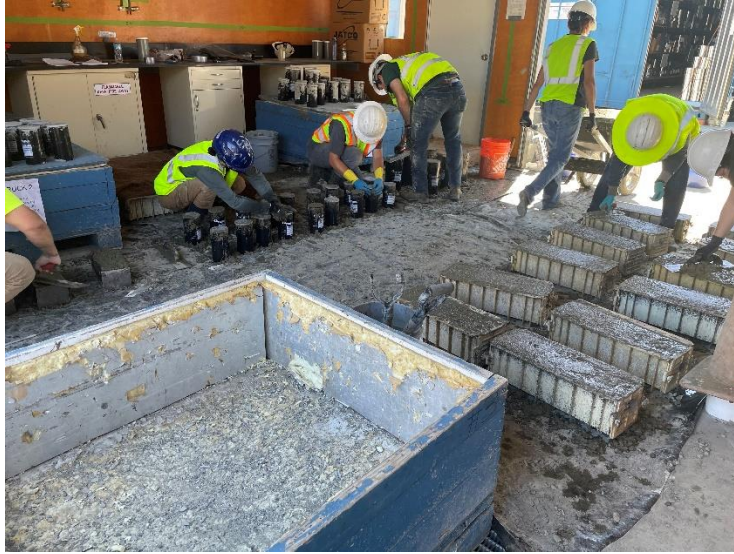
1113

1114   Figure 32. Specimen preparation and wooden boxes

1115   Table 7. List of hardened properties tested

Property	Standard	Specimen size (in.)	Testing times [1]
Flexural strength	ASTM C78	6×6×20 beams	10 days, 28 days, and 4 months
Compressive strength	ASTM C39	4×8 cylinders	10 days, 28 days, and 4 months
Modulus of elasticity	ASTM C469	6×12 cylinders	10 days, 28 days, and 4 months
Bulk electrical resistivity	ASTM C1876	4×8 cylinders	10 days, 28 days, and 4 months
Coefficient of thermal expansion (CTE)	AASHTO T 336	4×7 cylinders	42 days
Drying shrinkage	ASTM C157 [2]	4×4×11 prims	Up to 4 months

1116   [1] A fourth set of specimens was prepared for testing at 1 year age. Testing results not included in this report.
1117   [2] Except for the water immersion period; in this research, the specimens were subjected to drying at 7-day
1118   age.

5.5. Experimental Results

5.5.1. Fresh properties

1121   Fresh concrete testing results are presented in Table 8.

60

1122   Table 8. Fresh concrete testing results

Mixture	Slump (in.)	Temp	Air Content (%)	Unit Weight (lb/ft³)
PLC	6.50	88.2 °F (31.2 °C)	2.2	146.6
CNC	5.75	85.5 °F (29.7 °C)	1.9	147.8
OPC	7.75	88.9 °F (31.6 °C)	1.9	149.8

1123

1124   The slump of the mixtures with Type IL cement (PLC and CNC) was slightly lower than the slump
1125   of the mixture with Type II/V cement (OPC) with similar water content, indicating a higher water
1126   demand of the Type IL cement versus the Type II/V, for the same consistency. Most likely, this
1127   outcome is due to the higher fineness of the Type IL cement (Blaine 5470 cm²/g) compared to the
1128   Type II/V cement (Blaine 4184 cm²/g) used in this experiment (Blaine fineness from Cemex
1129   cement mill test reports).

1130   The small temperature differences between mixtures are most likely due to the different time of
1131   the day when each mixture was placed (CNC at approximately 1:00 pm, PLC at approximately
1132   2:00 pm, and finally OPC at approximately 3:00 pm).

1133   The construction workers and industry experts present at the construction site commented on the
1134   "creamy" consistency of the two mixtures with Type IL cement (CNC and PLC) compared to the
1135   mixture with Type II/V (OPC). The creamy consistency, based on construction workers and
1136   industry experts' opinion, would improve the constructability and reduce the segregation of the
1137   mixture. Most likely, this outcome is also due to the higher fineness of Type IL compared to the
1138   Type II/V cement used in this experiment.

1139   Construction workers and industry experts did not observe consistency or workability differences
1140   between the two mixtures with Type IL cement (CNC versus PLC).

1141   **5.5.2. Setting time**

1142   The setting time of the concrete was measured following ASTM C403. Three specimens were
1143   tested per mixture type. Penetration resistance evolution and set times are shown in Figure 33 and
1144   Table 9, respectively.
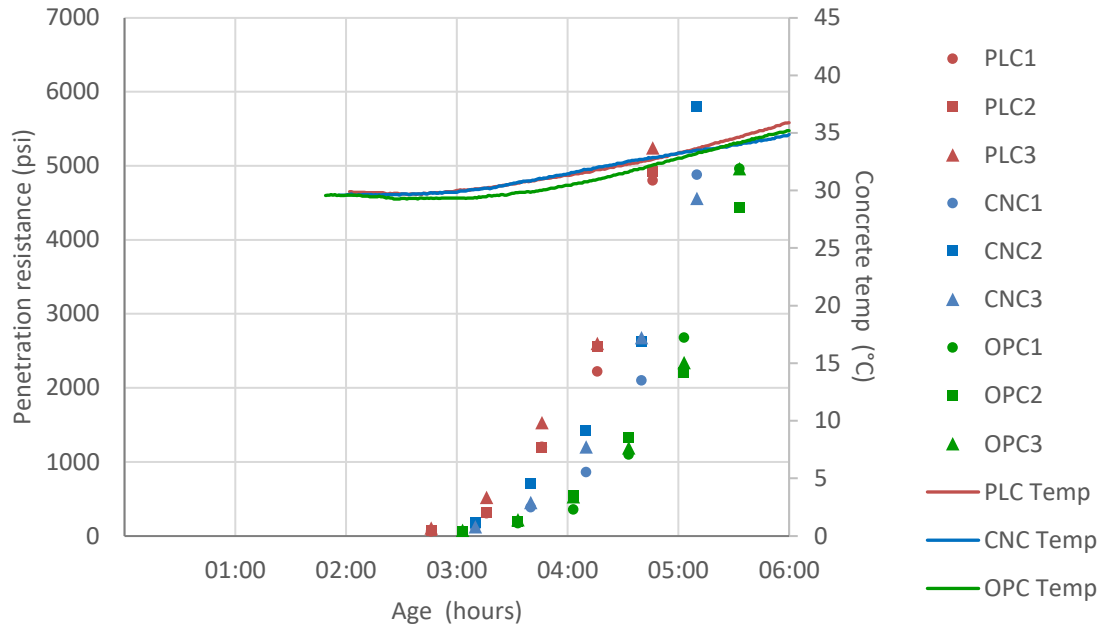
Figure 33. Penetration resistance (ASTM C403); temperature in the plot is measured in a dummy penetration resistance specimen

Table 9. Setting time results (ASTM C403)

Mixture	Initial Set (∗) (500 psi)	Final Set (∗) (4000 psi)
PLC	3:25	4:30
CNC	3:45	4:55
OPC	4:05	5:25

(∗) Set time is measured from the ready-mix truck batching time. For example, 4:30 means 4.5 hours after the ready-mix truck batching.

The OPC mixture's initial and final setting times were longer than the setting times of the two mixtures with Type IL, most like due to the lower fineness of the Type II/V compared to the Type IL. The setting time of the mixture with CNC was slightly delayed compared to the PLC mixture without CNC. It has been shown previously that CNC delays the set time of the cement, most likely by electrostatic dispersion of the cement [103] or the coating of clinker (primarily aluminate phases with CNC [6].

5.5.3. Hardened properties

The testing results are included in Figure 34 to Figure 39. Overall, the two mixtures with Type IL cement (CNC and PLC) were similar to each other for all properties (strength, modulus of

62

1160 elasticity, electrical resistivity, CTE, and shrinkage), with differences being either approximately
1161 10% or less (flexural and compressive strength) or not statistically significant at the 5%
1162 significance level (modulus of elasticity, electrical resistivity, CTE, and drying shrinkage).

1163 The two mixtures with Type IL (CNC and PLC) presented approximately 10-15% higher strength
1164 than the mixture with Type II/V (OPC). The resistivity of these two mixtures was also considerably
1165 better (higher) than the resistivity of the mixture with Type II/V. On the contrary, the mixtures
1166 with Type IL presented higher CTE than the mixture with Type II/V. Regarding drying shrinkage,
1167 the Type IL resulted higher strains in the short term (6 days drying) which is consistent with a
1168 more rapid hydration but lower strains after 4 months of drying, compared to the mixture with
1169 Type II/V. Overall, the differences between the two mixtures with Type IL versus the mixture with
1170 Type II/V were statistically significant.
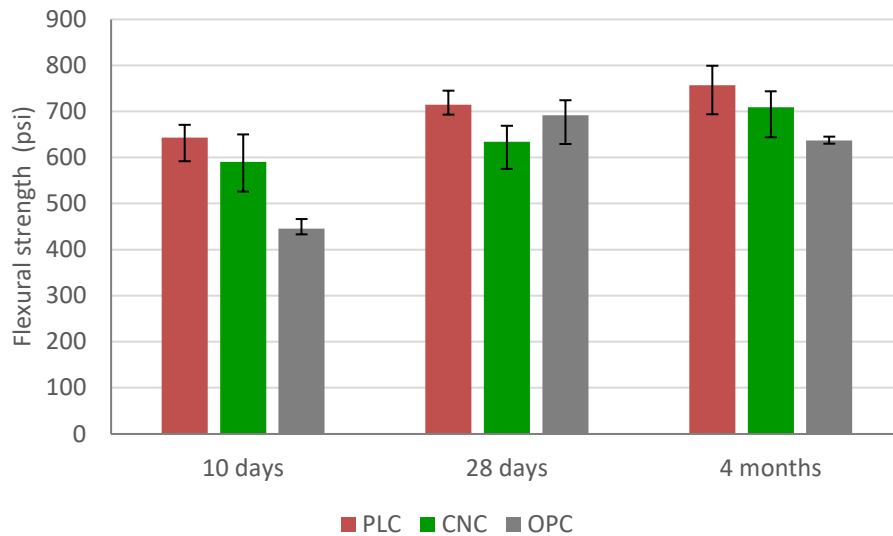
1171

1172   Figure 34. Flexural strength of the different mixtures
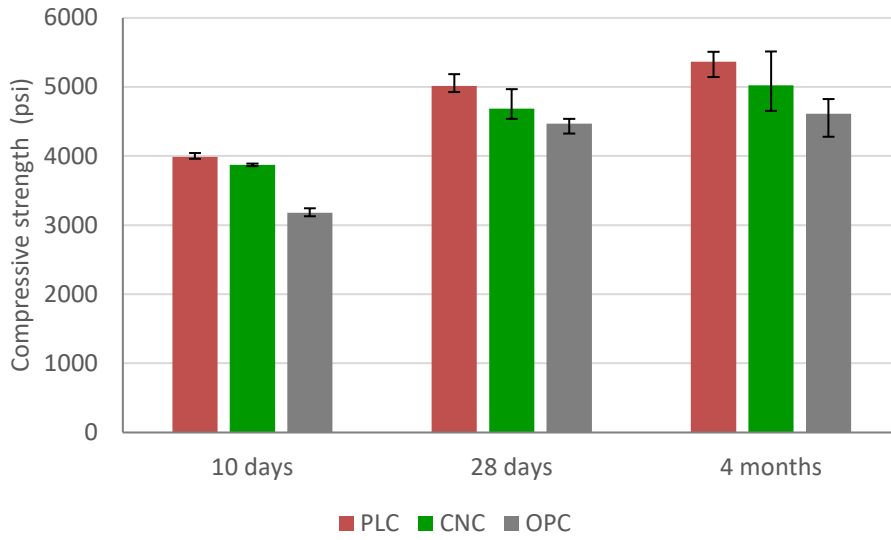
1173

1174   Figure 35. Compressive strength of the different mixtures.

1175
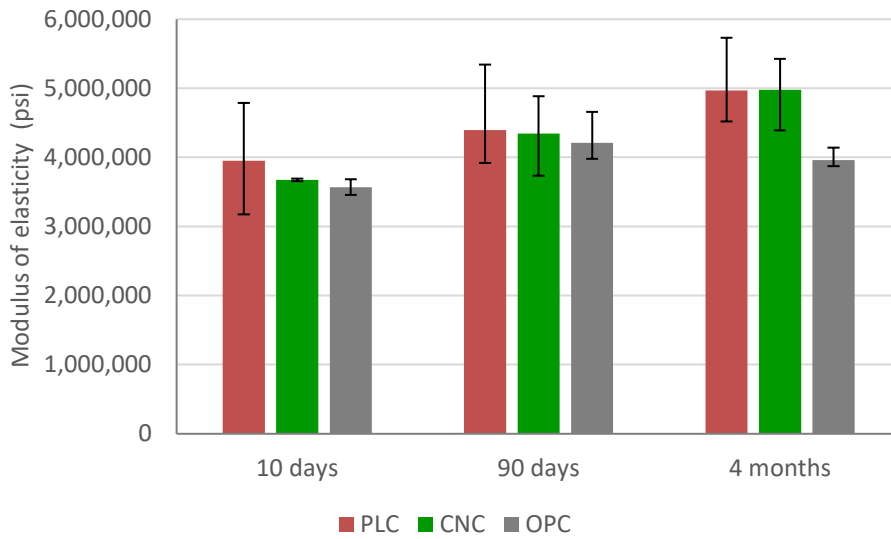
1176

1177   Figure 36. Modulus of elasticity of the different mixtures.

1178

FULL 6(c)(i)
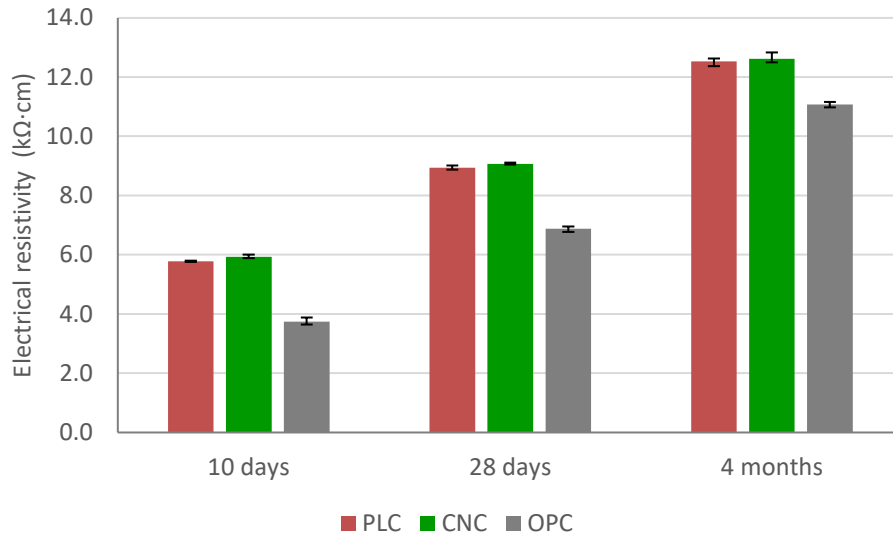
1179

1180　　　　　　　　　　Figure 37. Bulk electrical resistivity of the different mixtures.

1181
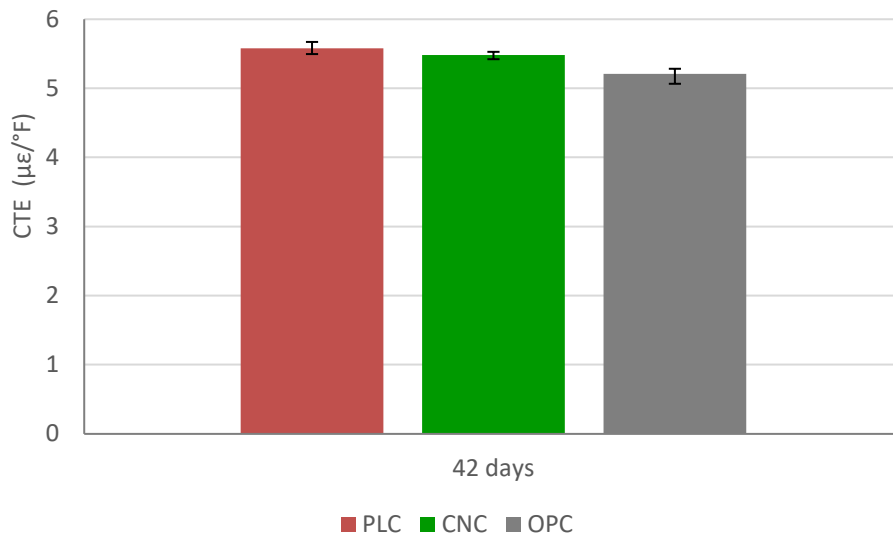
1182

1183　　　　　　　　　　　　Figure 38. CTE of the different mixtures.

1184
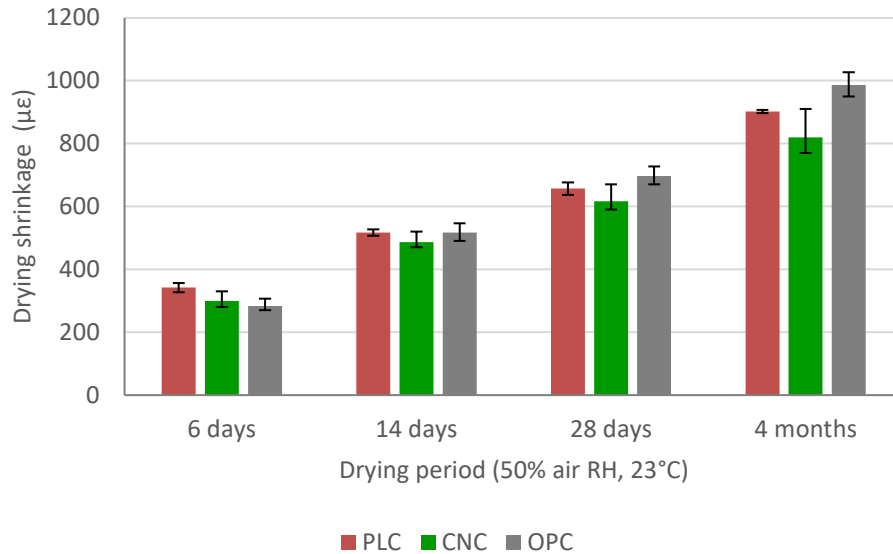
Figure 39. Drying shrinkage of the different mixtures.

5.5.4. Hygrothermal deformation of the slabs

One of the goals of the experiment is to evaluate the impact of the CNC addition on the moisture-related shrinkage and thermal deformations of the concrete. This evaluation was based on the strains measured with VWSGs in the two corresponding sets of slabs (CNC versus PLC sections). A secondary goal is to compare the mixture with Type IL cement versus the mixture with Type II/V cement (PLC versus OPC sections).

The strains measured with VWSGs in the three sections are presented in Figure 40 (ε_{MEAN}: mean strain, i.e. average of top and bottom of the slab) and Figure 41 (ε_{DIFF}: differential strain, i.e. top versus bottom of the slab). In all sections, a "field setting time" of 5 hours has been adopted as reference for strain calculation (ε is set to zero at the "field setting time"). The adoption of 5 hours is based on the setting time testing results presented in Table 9. The strain measured in the unrestrained shrinkage prisms is presented in Figure 42.

Note that there are two periods with missing data in Figure 40 and Figure 41: Aug-22 to Aug-30, and Sep-16 to Sep-30. In both cases, the problem was a failure in the data acquisition system electrical supply.

The average of all sensors per mixture type is shown In Figure 40 to Figure 42: the average of two pairs of VWSGs (located at each of the two instrumented corners in each section) in Figure 40 and Figure 41 and the average of three unrestrained shrinkage prisms per mixture type in Figure 42.

66

1206 Figure *43* shows an example of variability of strain measured within pairs of VWSGs. In this
1207 figure, the diurnal variations of the strain and temperature can be also observed.
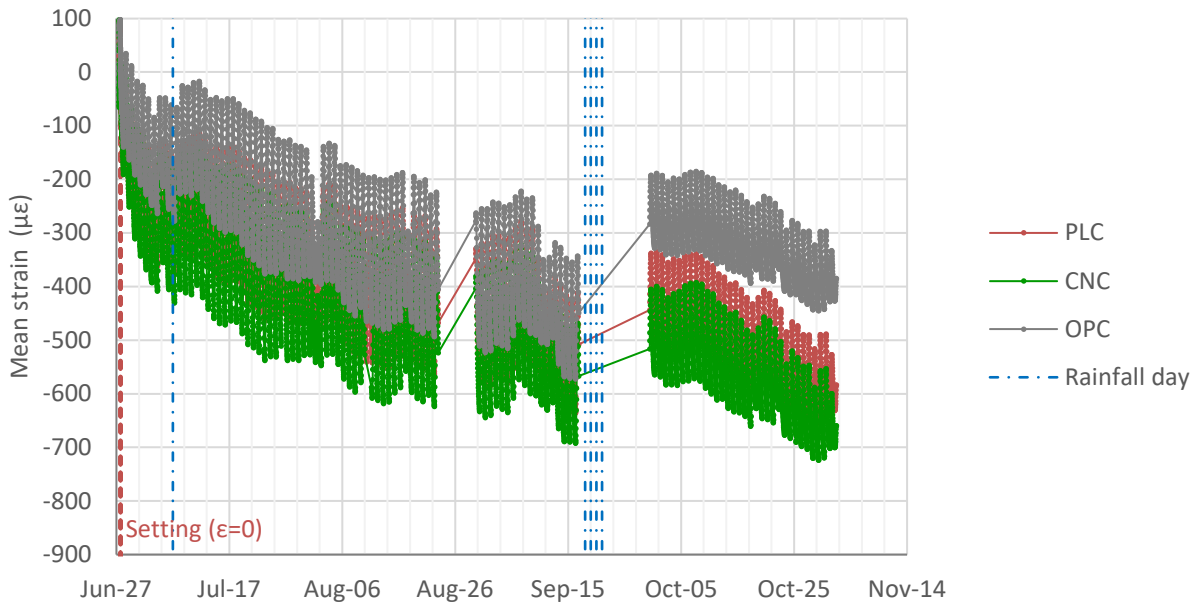
1208

1209 Figure 40. Mean strain measured in the slabs (average of top and bottom VWSGs; for each
1210 section, the average of two pairs of VWSGs is shown)

1211
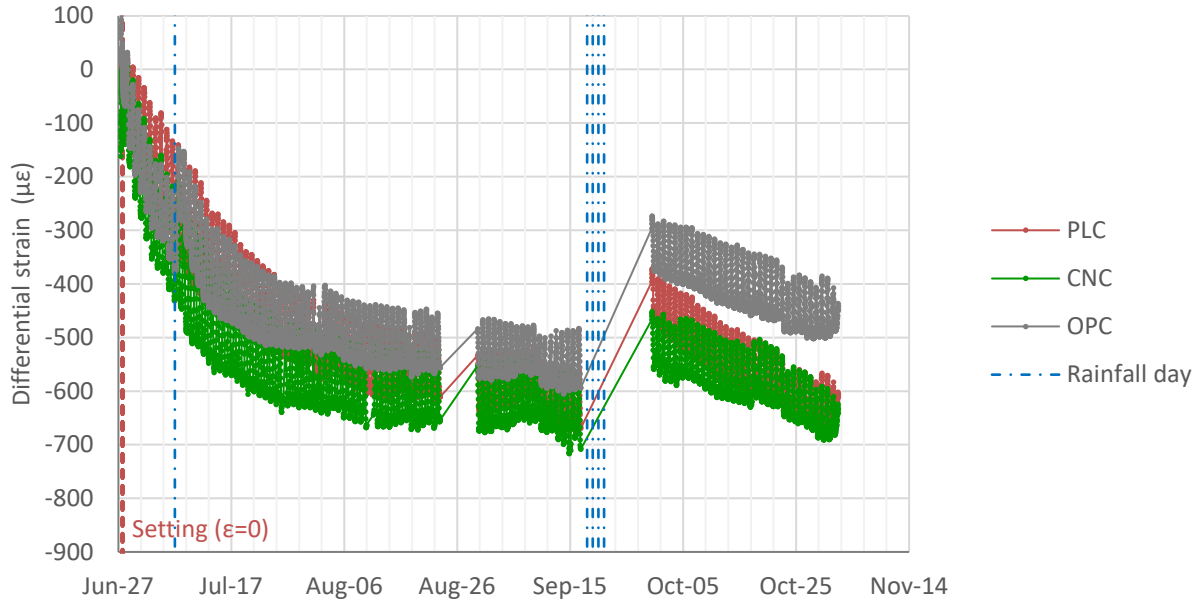
Figure 41. Differential strain measured in the slabs (difference between top and bottom VWSGs multiplied by H/D, where H is slab thickness [4 in.] and D is distance between VWSGs [2.4 in.]; for each section, the average of two pairs of VWSGs is shown)
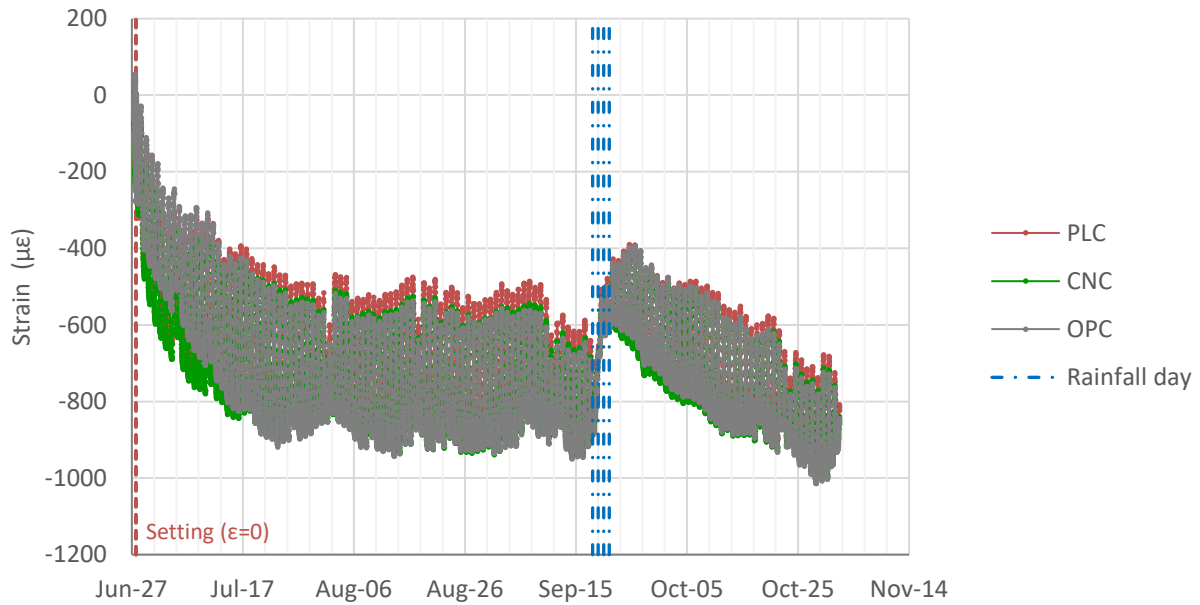
Figure 42. Strain measured in the unrestrained shrinkage prisms (for each mixture, the average of three unrestrained shrinkage prisms shown; one of the PLC prisms was regarded an outlier and discarded)

68
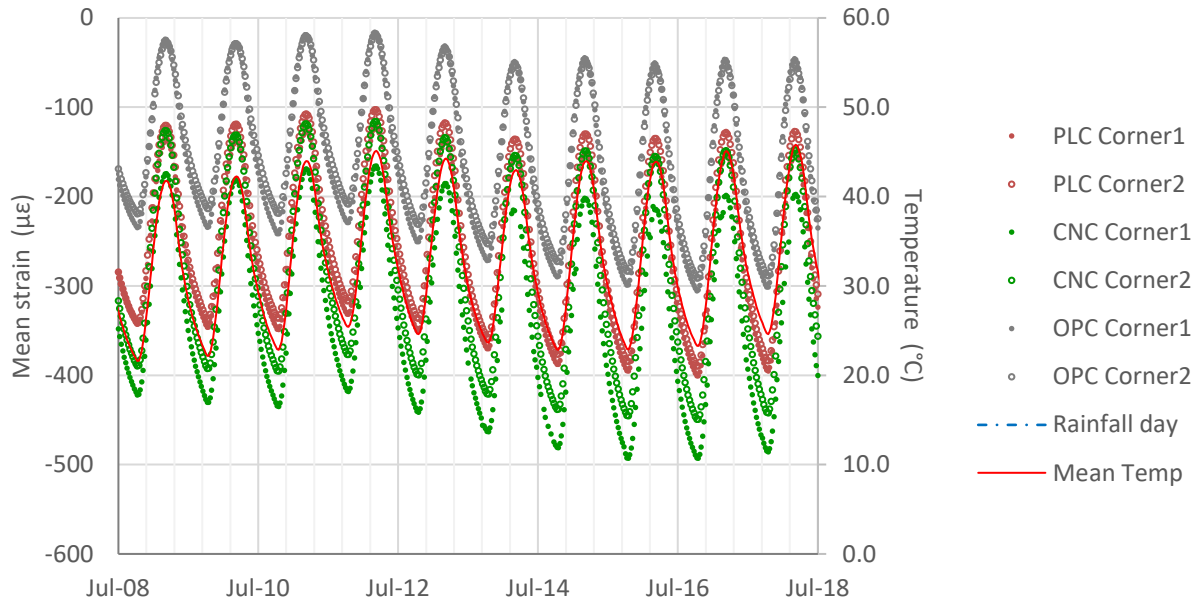
1222

1223   Figure 43. Example of diurnal variation of mean strain measured in the slabs (average of top and
1224   bottom VWSGs; Corner1 and Corner2 correspond to each of the two instrumented corners in
1225   each section; Mean Temp is the mean temperature of the slabs)

1226

1227   Based on the strains measured in the sections (Figure 40 and Figure 41) and in the unrestrained
1228   shrinkage prisms (Figure 42), it is evident that the CNC and PLC mixtures have similar
1229   hydrothermal deformations (moisture-related shrinkage and thermal strains).

1230   Further analysis of the strains measured in the sections and unrestrained shrinkage prisms was
1231   conducted to determine which part of the measured strain is related to the moisture-related
1232   shrinkage and which part is related to the thermal action. The strain data were fitted with the
1233   models shown in equations 11 and 12 below, following the methodology described in reference
1234   [104].

$$\Delta\varepsilon_{MEAN} = \Delta\varepsilon_{MEAN,Hyg} + \alpha \cdot CTE1(t) \cdot \Delta T_{MEAN} \qquad \text{(Eq. 11)}$$

1235   where: $\varepsilon_{MEAN,Hyg}$ is the component of ε_{MEAN} that is caused by the hygral action (Mean drying shrinkage
1236   shown in Figure 44)
1237 α is a coefficient that accounts for the restriction to slab expansion-contraction due to
1238   slab weight and slab interaction with its base; it can be assumed to be 1 for the
1239   VWSGs configuration used in this experiment
1240 $CTE1(t)$ is time-dependent equivalent CTE of the concrete slab in terms of mean expansion-
1241   contraction
1242 t is time
1243 T_{MEAN} is the mean slab temperature
1244

69

$$\Delta\varepsilon_{DIFF} = \Delta\varepsilon_{DIFF,Hyg} + \beta \cdot CTE2(t) \cdot \Delta ELTD \qquad \text{(Eq. 12)}$$

where: $\varepsilon_{DIFF,Hyg}$ is the component of ε_{DIFF} that is caused by the hygral action (Differential drying shrinkage shown in Figure 45)

β is a coefficient that accounts for the restriction to slab bending due to slab weight, slab interaction with its base, and transverse joint locking or lack of deployment; it can be assumed to be 1 for the VWSGs configuration used in this experiment

$CTE2(t)$ is time-dependent equivalent CTE of the concrete slab in terms of bending

t is time

$ELTD$ is the equivalent linear temperature difference in the slab (for a given temperature profile, the ELTD is the temperature difference between the top and bottom of the slab for the "equivalent linear temperature profile"; the "equivalent linear temperature profile" is the temperature profile that is linear versus depth and produces the same slab curvature produced by the actual vertical temperature profile)

The moisture-related shrinkage estimated in the sections, based on equations 11 and 12, is presented in Figure *44* (mean strain: average of top and bottom of the slab), Figure *45* (differential strain: top versus bottom of the slab), and Figure *46* (unrestrained shrinkage prisms). Note that the estimated moisture-related strain is referred to as "drying shrinkage" rather than "moisture-related shrinkage" as it is due to external drying and wetting of the concrete rather than internal desiccation. Internal desiccation and the consequent autogenous shrinkage are minimal in this experiment due to the relatively high water to cementitious materials ratio of the mixtures.
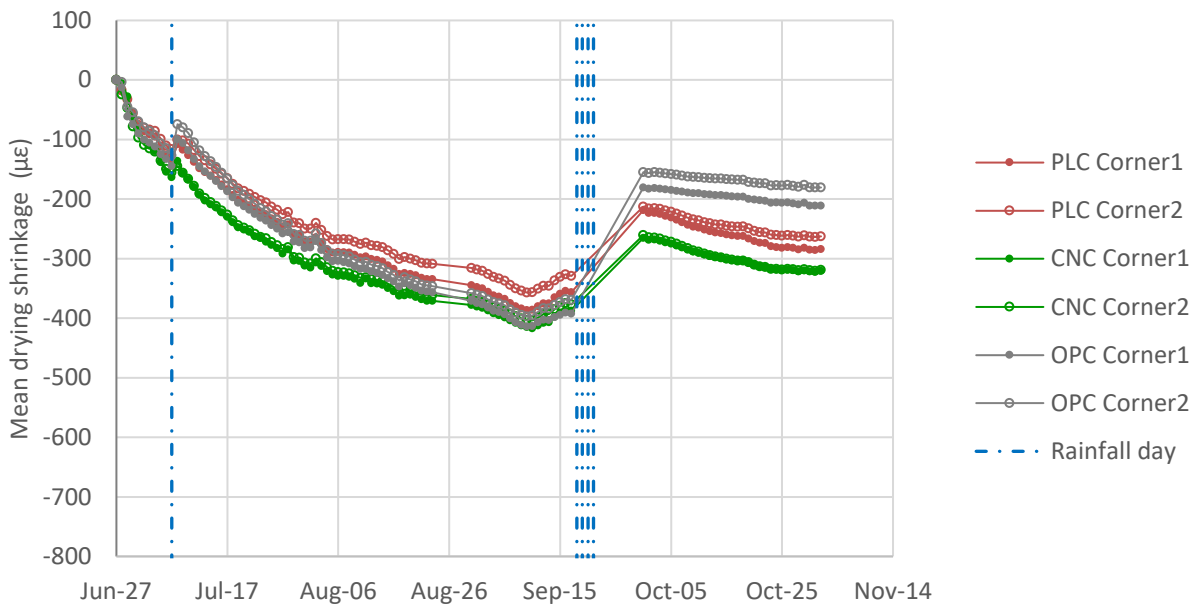
Figure 44. Mean drying shrinkage estimated in the slabs (Corner1 and Corner2 are each of the two instrumented corners in each section)
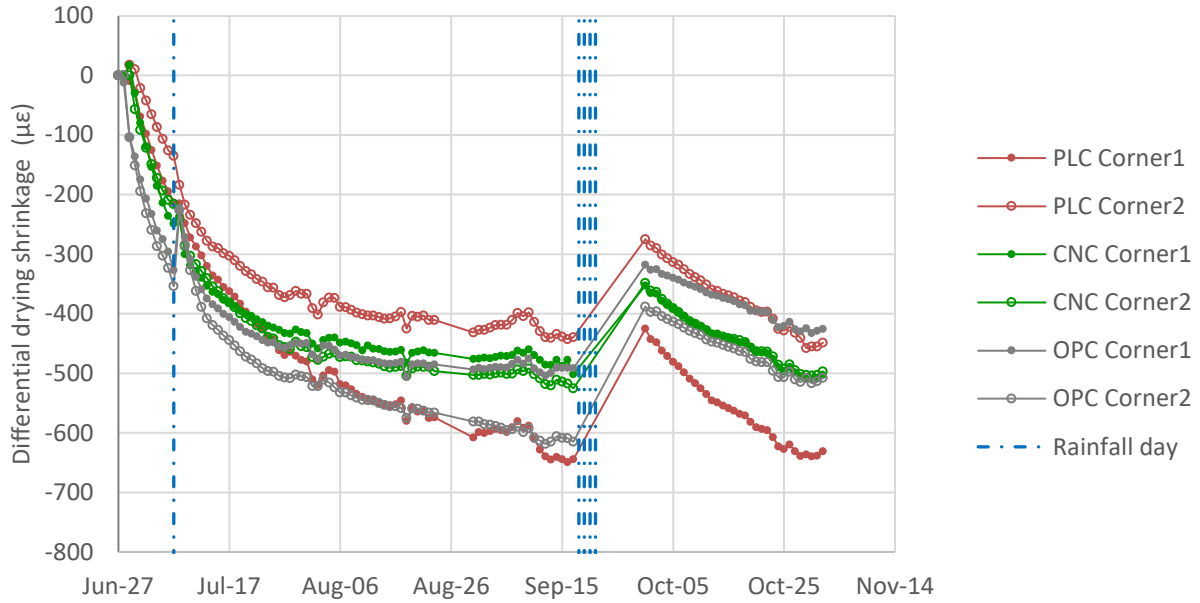
1268

1269   Figure 45. Differential drying shrinkage estimated in the slabs (Corner1 and Corner2 are each of
1270   the two instrumented corners in each section)

1271
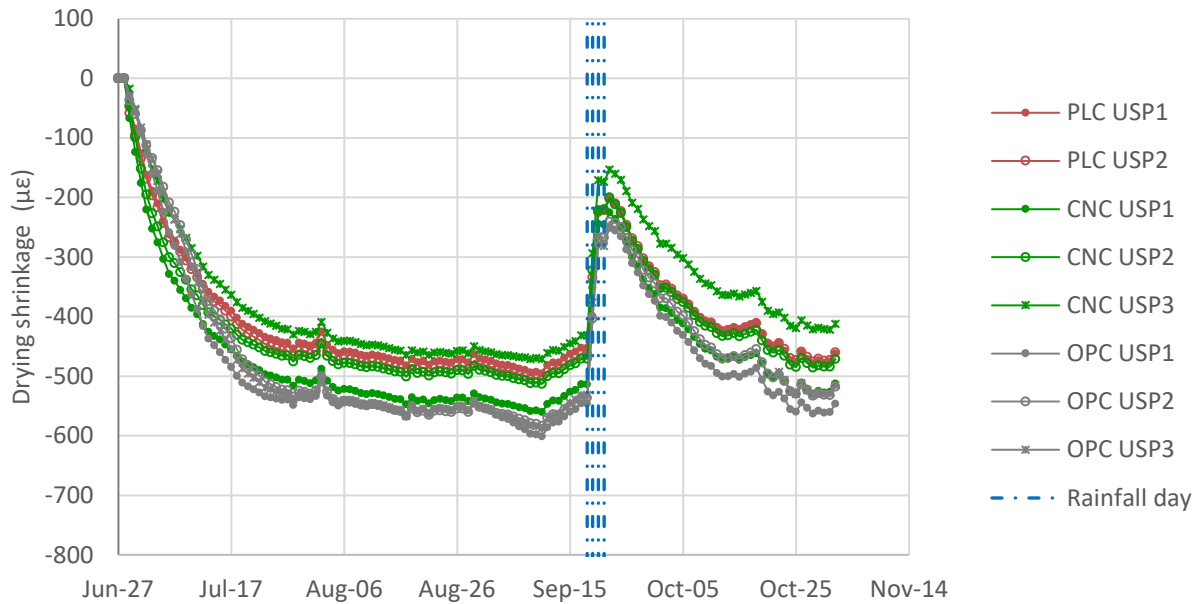
1272

1273   Figure 46. Drying shrinkage estimated in the unrestrained shrinkage prisms (USP1, USP2, and
1274   USP3 are the three prisms for each of the mixtures; PLC USP3 was regarded an outlier and
1275   discarded)

1276

71

1277 Based on the estimated drying shrinkage of the sections and the unrestrained shrinkage prisms,
1278 shown in Figure 44, Figure 45, and Figure 46, the CNC and PLC mixtures have similar
1279 performance. Also, these two mixtures present drying shrinkage similar to that of the OPC mixture.

1280 The thermal deformations of the CNC and PLC mixtures are similar to each other. As an example,
1281 the apparent CTE of the slabs in terms of expansion and contraction is shown in Figure *47*. In this
1282 figure, the increase in CTE as the concrete dries and the drop in CTE after rainfall are evident. In
1283 the CNC and PLC sections, because of drying, the apparent CTE of the slabs reached values up to
1284 40% higher than the CTE determined in the laboratory under saturated conditions (following
1285 AASHTO T 336); the CTE increase is somewhat smaller in the OPC section. Similar changes in
1286 CTE have been measured in other field experiments by UCPRC [104].

1287
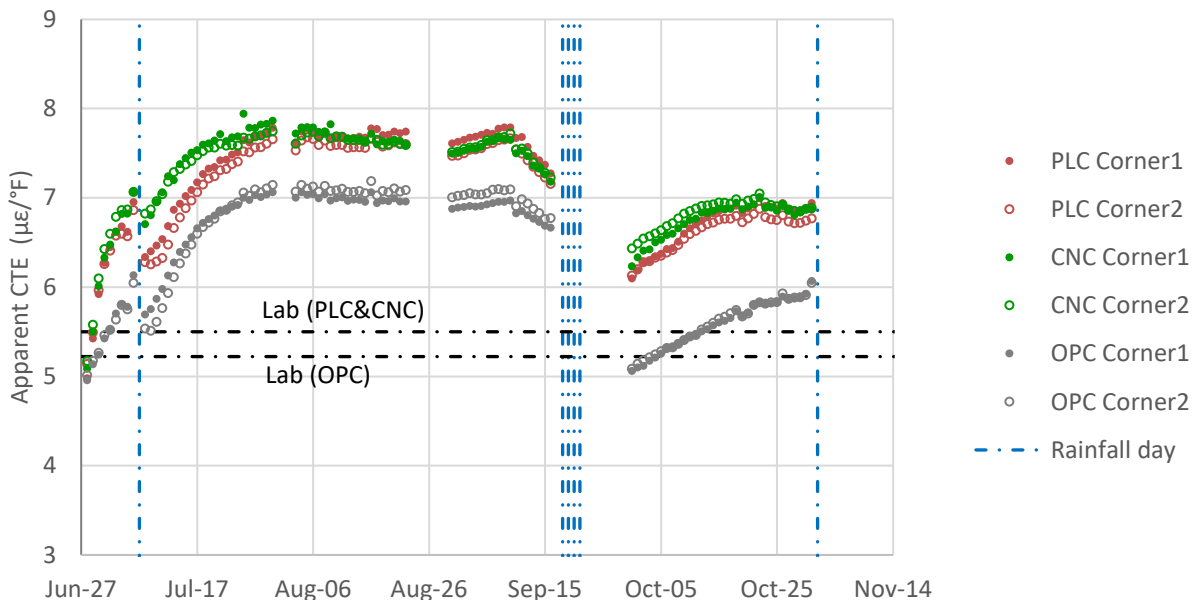
1288

1289   Figure 47. Apparent CTE of the slabs in terms of expansion-contraction (Corner1 and Corner2
1290   are each of the two instrumented corners in each section); for a given day, the apparent CTE can
1291   be defined as the ratio between changes in slab's horizonal strain and slab's mean temperature

1292 The RH measured at 0.8 inch depth in the sections can be also used to evaluate the effect of the
1293 CNC addition on RH. The measured RH data are presented in Figure *48*. While some CNC versus
1294 PLC differences are observed in this figure, the differences are within the sensor-to-sensor
1295 variability. Overall, the concrete internal RH was not affected much by the CNC addition. The RH
1296 measured in these two mixtures is somewhat different from the RH measured in the OPC mixture.
1297 Due to the dry and warm weather conditions of the summer, the RH in the OPC mixture dropped
1298 faster than in the CNC and PLC mixtures. This outcome might be related to a greater porosity of
1299 the OPC mixture compared to the other two mixtures, which needs to be confirmed.

72

1300   The diurnal variations of the concrete internal RH (variations within a day, mainly related to
1301   temperature changes) in the CNC and PLC mixtures are also similar to each other. Interestingly,
1302   the variations are somewhat higher for these two mixtures than for the OPC mixture (Figure 48
1303   and Figure 49). This outcome is believed to be the reason why the apparent CTE of the CNC and
1304   PLC mixtures increased upon drying somewhat more than the CTE of the OPC mixture (further
1305   investigation and explanation of this outcome is outside the scope of this report).

1306
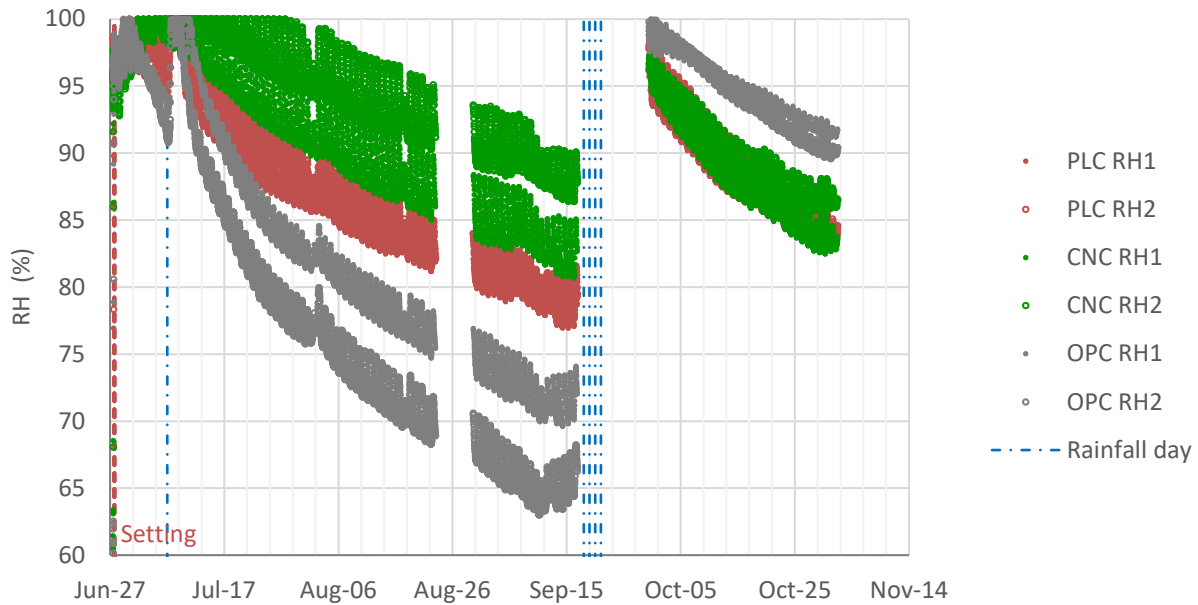
1307

1308   Figure 48. RH measured in the concrete, at 0.8 in. depth (RH1 and RH2 are each of the two RH
1309   sensors embedded in each of the sections)

1310
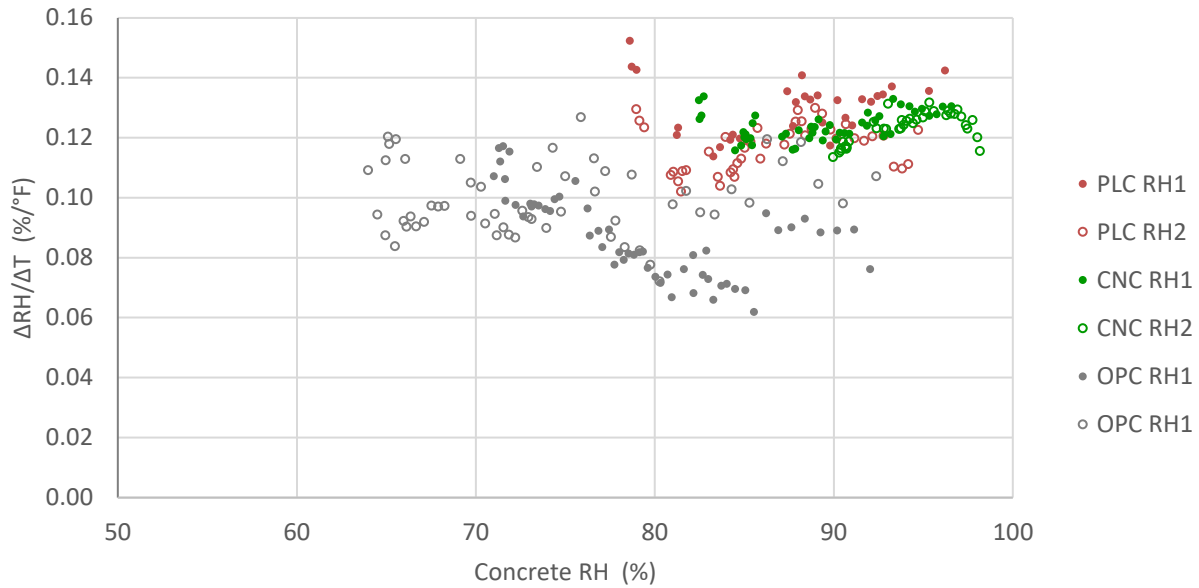
Figure 49. Diurnal variation of RH versus temperature (for a given day, the ratio ΔRH/ΔT indicates how much concrete internal RH changes versus temperature while the moisture of the concrete remains essentially constant)

5.6. Discussion of Test Sections Experimental Results

The experiment presented in this chapter of the report was designed to evaluate the effects of the addition of CNC on the constructability and properties of the portland-limestone cement concrete. A secondary goal of the experiment was to compare the constructability and properties of the portland-limestone cement concrete versus concrete made with Type II/V ordinary portland cement. The control mixture, made with Type II/V cement, represents a typical concrete paving mixture used in the Caltrans road network.

The experiment includes the construction and monitoring of a set of slabs and the testing of the mixtures sampled during the construction. Based on the collected experimental data, a number of conclusions can be drawn regarding mixtures constructability, including fresh concrete properties, hardened concrete mechanical properties, and concrete hygrothermal deformations (i.e., response under ambient environmental actions).

5.6.1. Effects of the CNC addition

The effect of the CNC addition can be established by comparing the initial properties, constructability, and several months of hydrothermal performance under the hot, dry environmental conditions of the test section location of the CNC and PLC mixtures. The only difference between the CNC and PLC mixtures is that the former includes 0.1% cellulose nanocrystals (CNC solids by weight of total cementitious materials).

74

1333 Based on the collected experimental data, no important differences were found between the CNC
1334 and PLC mixtures:

- 1335 Fresh concrete properties (slump, air content, and unit weight) were similar in the two
1336 mixtures.
- 1337 The setting time was similar for the two mixtures, and the same applies to the concrete
1338 temperature recorded during the setting time experiment, which indicates similar early-age
1339 heat of hydration release.
- 1340 Based on construction workers and Industry expert's observations, there were no
1341 consistency or workability differences between the two mixtures.
- 1342 Mechanical properties of the two mixtures, based on laboratory testing of the hardened
1343 concrete, were similar for all properties (strength, modulus of elasticity, electrical
1344 resistivity, CTE, and shrinkage), with differences being either approximately 10% or less
1345 (flexural and compressive strength) or not statistically significant at the 5% significance
1346 level (modulus of elasticity, electrical resistivity, CTE, and drying shrinkage).
- 1347 The hygrothermal responses of the slabs made with each of the two mixtures were very
1348 similar. The two groups of slabs presented similar drying shrinkage during the 4-month
1349 evaluation period and similar thermal deformations.

1350 Based on these results, it can be concluded that the CNC addition did not produce any significant
1351 effect on the fresh concrete properties, including constructability, and neither on the properties of
1352 the hardened-concrete.

1353 **5.6.2. Comparison of OPC and PLC**

1354 The effect of the substitution of the Type II/V ordinary portland cement by Type IL portland-
1355 limestone cement can be established by comparing the properties and performance of the PLC and
1356 OPC mixtures. The only difference between the PLC and OPC mixtures is that the former includes
1357 substituting Type IL instead of Type II/V cement. The cement content of both mixtures was the
1358 same.

1359 Based on the collected experimental data, some differences were found between the PLC and OPC
1360 mixtures:

- 1361 The slump of the OPC mixture was slightly higher than the slump of the PLC mixture (7.75
1362 versus 6.50 in.), with similar water content. This outcome suggests a higher water demand

75

1363   of the Type IL cement versus the Type II/V, for the same consistency. The other fresh
1364   concrete properties (air content and unit weight) were similar for the two mixtures.

1365   • The PLC mixture set faster than the OPC mixture. Initial and final setting times of the OPC
1366   mixture, based on penetrating resistance, were 4:05 and 5:25 hours, respectively. The
1367   setting times of the PLC mixture were approximately 15% shorter (3:25 and 4:30 hours for
1368   the initial and final set, respectively). The temperature recorded during the setting time
1369   experiment was slightly higher, up to 2°F (1°C) higher, in the PLC than in the OPC mixture.

1370   • The construction workers and industry experts present at the construction site indicated a
1371   "creamy" consistency of the PLC mixture compared to the OPC mixture, which would
1372   improve the constructability and reduce the segregation of the PLC mixture compared to
1373   the OPC.

1374   • The PLC mixture presented around 10-15% higher strength than the OPC mixture
1375   regardless of the testing age (between 10 days and 4 months). The PLC mixture also
1376   presented higher electrical resistivity than the OPC mixture (around 50% higher after 10
1377   days and around 15% higher after 4 months). On the contrary, the CTE of the PLC mixture
1378   was 0.7 $\mu\varepsilon$/°C higher than the CTE of the OPC mixture.

1379   • The PLC mixture presented 20% higher laboratory drying shrinkage (73°F (23°C), 50%
1380   air RH) than the OPC mixture in the short term (6 days drying) but 10% lower drying
1381   shrinkage after 4 months of drying.

1382   • The hygrothermal response of the slabs made with each of the two mixtures were similar
1383   to each other. The two groups of slabs presented similar drying shrinkage during the 4-
1384   month evaluation period and similar thermal deformations.

1385 Overall, the results indicate that PLC can be used interchangeably with OPC; however, the effect
1386 of differences in fineness of PLC and OPC should be noted. The mixtures with Type IL had better
1387 performance in terms of workability, mechanical, and durability properties than the mixture with
1388 Type II/V, mainly due to higher surface area of Type IL cement and synergistic behavior between
1389 the limestone and alumina. The mixtures with Type IL were observed to have higher water demand
1390 and somewhat higher CTE (0.7 $\mu\varepsilon$/°C) when compared to the mixture with Type II/V due to higher
1391 fineness of Type IL cement.

1392

76

6. CHAPTER 5: Conclusions

A comprehensive plan was undertaken to evaluate CNCs as a value-based additive for low-carbon footprint concrete. This project was aimed at evaluating the performance of mixtures with limestone and CNC to develop mixtures with a lower embodied carbon footprint. In addition, the project included the implementation of the use of CNC in a set of pilot slabs built on the research site of the University of California Pavement Research Center (UCPRC) in Davis, California.

OPC-LS-CNC mixtures were evaluated for various limestone additions ranging from 0 – 30% by weight and various CNC dosages ranging from 0 – 1% of CNC solids per volume of cementitious materials. The heat of hydration using isothermal calorimetry, B3B flexural strength, CH content, non-evaporable water content, porosity, pore connectivity, and bulk resistivity of the mixtures were determined. GHG emissions of the mixtures were calculated using the life cycle inventory (LCI) calculation tool.

The addition of CNCs to the OPC-LS mixtures resulted in slight retardation by approximately 2-3 hours, depending on the CNC dosage. When CNCs are added, there was an increase in heat release measured at seven days by about 2-3% for OPC-LS mixtures due to increased clinker hydration. The increase in the degree of hydration at early ages was due to the combined effect of LS and CNCs. When the degree of hydration at later ages (28 days) was determined by measuring non-evaporable water content, it was found that mixtures with CNCs at lower dosages up to 0.5% had a higher degree of hydration, which was mainly attributed to CNCs.

CNCs addition to OPC-LS mixtures did not have a significant impact on the porosity of the paste samples. B3B flexural strength of the OPC-LS-CNC mixtures measured at 28 days was within $\pm$15% of the flexural strength of the OPC-LS mixtures. Also, CNCs did not have a significant impact on the drying shrinkage strain of mortar samples. The drying shrinkage strain of the mortar mixtures with CNC was statistically similar or slightly higher (~5%) than mixtures without CNCs after 90 days of exposure to a drying environment.

The addition of CNCs to OPC-LS mixtures had an impact on pore connectivity (β). Lower dosages of CNC addition resulted in a decrease in pore connectivity by up to 29% and improved bulk resistivity by up to 38%. The addition of 20% LS and 0.2% CNC resulted in similar mechanical and transport properties to the conventional mixture; this resulted in the development of an OPC-LS-CNC mixture with 19.4% lower GHG emissions than 100% OPC mixture without compromising on the strength and transport properties.

The performance of OPC-SCM and PLC-SCM mixtures with CNC were evaluated. The 7-day heat of hydration, 28- and 56-day B3B flexural strength, 28- and 56-day porosity, 28- and 56-day pore connectivity, and 28- and 56-day bulk resistivity were determined. The addition of CNC to SCM mixtures resulted in slight retardation due to the CNC covering the clinker, primarily aluminate phase. The 7-day heat release of the SCM mixtures with CNCs were within $\pm$5% of the heat release

1429 of the mixtures without CNC. Overall porosity and B3B flexural strength did not vary significantly
1430 with the CNC dosage. Unlike what was observed for the plain and limestone mixtures, the CNC
1431 addition at low dosages resulted in an increase in pore connectivity and a decrease in bulk
1432 resistivity for the majority of the SCM mixtures. Additional research is needed to understand the
1433 role of the CNCs on the performance when SCMs are used. Specifically, research is needed to
1434 understand what surfaces the CNC are absorbed on. Work is underway to evaluate the long-term
1435 transport properties.

1436 The demonstration of the use of CNCs and PLCs was successfully done in field trials in California
1437 at the UC Davis Pavement Research Center. With the addition of CNCs, no significant difference
1438 in fresh concrete properties, including constructability, was observed. In addition, the compression
1439 and flexural strength of the mixtures with and without CNC were similar. CNCs addition had no
1440 statistically significant effect on the measured modulus of elasticity, electrical resistivity, and
1441 drying shrinkage. The hygrothermal responses of the slabs with and without CNC were very
1442 similar as well. The results indicated that PLC could be used alternative to OPC.

1443 Overall, in this project, comprehensive testing was done to evaluate CNCs as a value-based
1444 additive to mixtures with limestone to lower GHG emissions. Through this project, it was
1445 demonstrated that designing lower embodied carbon footprint mixtures with limestone and CNCs
1446 is possible without compromising on the mechanical and transport properties of concrete.

1447 **ACKNOWLEDGEMENTS**

7. References

1. Moon, R.J., et al., *Cellulose nanomaterials review: structure, properties and nanocomposites.* Chemical Society Reviews, 2011. **40**(7): p. 3941-3994.

2. Moon, R.J., G.T. Schueneman, and J. Simonsen, *Overview of cellulose nanomaterials, their capabilities and applications.* Jom, 2016. **68**(9): p. 2383-2394.

3. Fu, T., et al., *Cellulose nanomaterials as additives for cementitious materials*, in *Cellulose-Reinforced Nanofibre Composites*. 2017, Elsevier. p. 455-482.

4. Cuenca, E., et al., *Concept of ultra high durability concrete for improved durability in chemical environments: preliminary results.* 2019.

5. Aziz, M.A., M. Zubair, and M. Saleem, *Development and testing of cellulose nanocrystal-based concrete.* Case Studies in Construction Materials, 2021. **15**: p. e00761.

6. Cao, Y., *Nano-modification for high performance cement composites with cellulose nanocrystals and carbon nanotubes*. 2014: Purdue University.

7. Peters, S.J., et al., *Nanocellulose and microcellulose fibers for concrete.* Transportation Research Record, 2010. **2142**(1): p. 25-28.

8. Sun, X., et al., *Cellulose nanofibers as a modifier for rheology, curing and mechanical performance of oil well cement.* Scientific reports, 2016. **6**(1): p. 1-9.

9. da Costa Correia, V., et al., *Nanofibrillated cellulose and cellulosic pulp for reinforcement of the extruded cement based materials.* Construction and Building Materials, 2018. **160**: p. 376-384.

10. Haddad Kolour, H., et al., *An investigation on the effects of cellulose nanofibrils on the performance of cement paste and concrete.* Advances in Civil Engineering Materials, 2018. **7**(1): p. 15.

11. Lee, H.-J. and W. Kim, *Long-term durability evaluation of fiber-reinforced ECC using wood-based cellulose nanocrystals.* Construction and Building Materials, 2020. **238**: p. 117754.

12. Montes, F., et al., *Rheological impact of using cellulose nanocrystals (CNC) in cement pastes.* Construction and Building Materials, 2020. **235**: p. 117497.

13. Santos, R.F., et al., *Nanofibrillated cellulose and its applications in cement-based composites: A review.* Construction and Building Materials, 2021. **288**: p. 123122.

14. Cuenca, E., A. Mezzena, and L. Ferrara, *Synergy between crystalline admixtures and nano-constituents in enhancing autogenous healing capacity of cementitious composites under cracking and healing cycles in aggressive waters.* Construction and Building Materials, 2021. **266**: p. 121447.

15. Kamasamudram, K.S., W. Ashraf, and E.N. Landis, *Cellulose nanofibrils with and without nanosilica for the performance enhancement of Portland cement systems.* Construction and Building Materials, 2021. **285**: p. 121547.

16. Kamasamudram, K.S., et al., *Effects of ligno–and delignified–cellulose nanofibrils on the performance of cement-based materials.* Journal of Materials Research and Technology, 2021. **13**: p. 321-335.

17. Cao, Y., et al., *The influence of cellulose nanocrystal additions on the performance of cement paste.* Cement and Concrete Composites, 2015. **56**: p. 73-83.

18. Cao, Y., et al., *Performance-enhanced cementitious materials by cellulose nanocrystal additions.* Production and Applications of Cellulose Nanomaterials, 2013. **2**.

1494 19. Cao, Y., et al., *The relationship between cellulose nanocrystal dispersion and strength.* Construction and Building Materials, 2016. **119**: p. 71-79.
1496 20. Dousti, M.R., Y. Boluk, and V. Bindiganavile, *The effect of cellulose nanocrystal (CNC) particles on the porosity and strength development in oil well cement paste.* Construction and Building Materials, 2019. **205**: p. 456-462.
1499 21. Deze, E., et al., *Nanocellulose enriched mortars: Evaluation of nanocellulose properties affecting microstructure, strength and development of mixing protocols.* Materials Today: Proceedings, 2021.
1502 22. Haque, M.I., et al., *A comparative investigation on the effects of nanocellulose from bacteria and plant-based sources for cementitious composites.* Cement and Concrete Composites, 2022. **125**: p. 104316.
1505 23. Fu, T., et al., *The influence of cellulose nanocrystals on the hydration and flexural strength of Portland cement pastes.* Polymers, 2017. **9**(9): p. 424.
1507 24. Flores, J., M. Kamali, and A. Ghahremaninezhad, *An investigation into the properties and microstructure of cement mixtures modified with cellulose nanocrystal.* Materials, 2017. **10**(5): p. 498.
1510 25. Claramunt, J., et al., *Effect of nanocelluloses on the microstructure and mechanical performance of CAC cementitious matrices.* Cement and Concrete Research, 2019. **119**: p. 64-76.
1513 26. Cao, Y., et al., *The influence of cellulose nanocrystals on the microstructure of cement paste.* Cement and Concrete Composites, 2016. **74**: p. 164-173.
1515 27. Bu, Y., et al., *The influence of accelerated curing on the properties used in the prediction of chloride ingress in concrete using a Nernst–Planck approach.* Construction and Building Materials, 2014. **66**: p. 752-759.
1518 28. Bu, Y., R. Spragg, and W. Weiss, *Comparison of the pore volume in concrete as determined using ASTM C642 and vacuum saturation.* Advances in Civil Engineering Materials, 2014. **3**(1): p. 308-315.
1521 29. Becerril, A.P., *The Influence of Cellulose Nanocrystals on Performance and Transport Properties of Cementitious Materials and Gypsum.* 2020, Purdue University Graduate School.
1524 30. Barnat-Hunek, D., et al., *Effect of eco-friendly cellulose nanocrystals on physical properties of cement mortars.* Polymers, 2019. **11**(12): p. 2088.
1526 31. Washington, T., W.J. Weiss, and J. Youngblood, *Construction of full-scale concrete elements containing cellulose nanocrystals (CNCs) in bridge decks and pavements*, R.t.U.E.f.F.a. Communities, Editor. 2021.
1529 32. Ramanathan, S., et al., *Cellulose Nanocrystals as an Additive for Prestressed Box Girders* in *ASPIRE - The Concrete Bridge Magazine*. 2023 (In Press): www.aspirebridge.org.
1531 33. Lothenbach, B., K. Scrivener, and R. Hooton, *Supplementary cementitious materials.* Cement and concrete research, 2011. **41**(12): p. 1244-1256.
1533 34. Juenger, M.C. and R. Siddique, *Recent advances in understanding the role of supplementary cementitious materials in concrete.* Cement and Concrete Research, 2015. **78**: p. 71-80.
1536 35. Environment, U., et al., *Eco-efficient cements: Potential economically viable solutions for a low-CO2 cement-based materials industry.* Cement and Concrete Research, 2018. **114**: p. 2-26.

1539   36.   Hawkins, P., P.D. Tennis, and R.J. Detwiler, *The use of limestone in Portland cement: a*
1540   *state-of-the-art review*. 1996: Portland Cement Association.
1541   37.   Thomas, M.D. and R.D. Hooton, *The durability of concrete produced with portland-*
1542   *limestone cement: Canadian studies.* PCA R&D SN3142, Portland Cement Association,
1543   Skokie, IL, 2010: p. 28.
1544   38.   Tennis, P., M. Thomas, and W. Weiss, *State-of-the-Art Report on Use of Limestone in*
1545   *Cements at Levels of up to 15%.* PCA R&D SN3148, Portland Cement Association, Skokie,
1546   IL, 2011.
1547   39.   Barrett, T.J., *Performance of portland limestone cements: Cements designed to be more*
1548   *sustainable that include up to 15% limestone addition.* 2013, Purdue University.
1549   40.   Hooton, R. and M. Thomas, *Sulfate resistance of mortar and concrete produced with*
1550   *portland-limestone cement and supplementary cementing materials*, in *Recommendation*
1551   *for ASTM C595/AASHTO M 240, PCA R&D SN3285a*. 2016, Portland Cement
1552   Association.
1553   41.   Bharadwaj, K., et al., *CALTRANS: Impact of the Use of Portland-Limestone Cement on*
1554   *Concrete Performance as Plain or Reinforced Material - Final Report.* 2021.
1555   42.   Bharadwaj, K., et al., *Predicting pore volume, compressive strength, pore connectivity, and*
1556   *formation factor in cementitious pastes containing fly ash.* Cement and Concrete
1557   Composites, 2021: p. 104113.
1558   43.   Bentz, D.P., et al., *Limestone fillers conserve cement; Part 1: an analysis based on Powers'*
1559   *model.* Concrete international, 2009. **31**(11): p. 41-46.
1560   44.   Berodier, E. and K. Scrivener, *Understanding the Filler Effect on the Nucleation and*
1561   *Growth of C-S-H.* Journal of the American Ceramic Society, 2014. **97**(12): p. 3764-3773.
1562   45.   Zajac, M., et al., *Influence of limestone and anhydrite on the hydration of Portland*
1563   *cements.* Cement and Concrete Composites, 2014. **46**: p. 99-108.
1564   46.   Ramanathan, S., M. Croly, and P. Suraneni, *Comparison of the effects that supplementary*
1565   *cementitious materials replacement levels have on cementitious paste properties.* Cement
1566   and Concrete Composites, 2020. **112**: p. 103678.
1567   47.   Association, P.C., *Roadmap to Carbon Neutrality*. 2021.
1568   48.   Bharadwaj, K., *Towards the Development of Performance-Based Concrete Mixtures Made*
1569   *with Modern Cementitious Materials Using Thermodynamic Modeling*, in *Civil*
1570   *Engineering*. 2022, Oregon State University: Corvallis, OR. p. 327.
1571   49.   Bharadwaj, K., et al., *Predicting Pore Volume, Compressive Strength, Pore Connectivity,*
1572   *and Formation Factor in Cementitious Pastes Containing Fly Ash.* Cement and Concrete
1573   Composites, 2021. **122**: p. 104113.
1574   50.   Bharadwaj, K., et al., *Toward the Prediction of Pore Volumes and Freeze-Thaw*
1575   *Performance of Concrete Using Thermodynamic Modelling.* Cement and Concrete
1576   Research, 2019. **124**: p. 105820.
1577   51.   Bharadwaj, K., B.O. Isgor, and J.W. Weiss, *Pozzolanic reactivity of SCMs from a*
1578   *thermodynamic perspective.* ACI Materials Journal, 2022. **In Review**.
1579   52.   Bharadwaj, K., B.O. Isgor, and J.W. Weiss, *A Simplified Approach to determine the*
1580   *Pozzolanic Reactivity of Commercial Supplementary Cementitious Materials.* Concrete
1581   International, 2022. **44**(1): p. 27-32.
1582   53.   Choudhary, A., et al., *Pozzolanic Reactivity Test of Supplementary Cementitious*
1583   *Materials.* ACI Mater J, 2022. **119**(2): p. 255-268.

1584 54.   Glosser, D., et al., *Investigation of Reactivity of Fly Ash and Its Effect on Mixture*
1585   *Properties.* ACI Materials Journal, 2019. **116**(4): p. 193-200.
1586 55.   Glosser, D., O.B. Isgor, and W.J. Weiss, *Non-Equilibrium Thermodynamic Modeling*
1587   *Framework for Ordinary Portland Cement/Supplementary Cementitious Material Systems.*
1588   ACI Materials Journal, 2020. **117**(6): p. 111-123.
1589 56.   Lothenbach, B. and M. Zajac, *Application of thermodynamic modelling to hydrated*
1590   *cements.* Cement and Concrete Research, 2019. **123**.
1591 57.   Kulik, D.A., et al., *GEM-Selektor geochemical modeling package: revised algorithm and*
1592   *GEMS3K numerical kernel for coupled simulation codes.* Computational Geosciences,
1593   2013. **17**(1): p. 1-24.
1594 58.   Wagner, T., et al., *Gem-Selektor geochemical modeling package: TSolmod library and*
1595   *data interface for multicomponent phase models.* Canadian Mineralogist, 2012. **50**(5): p.
1596   1173-1195.
1597 59.   Lothenbach, B., et al., *Cemdata 18: A chemical thermodynamic database for hydrated*
1598   *Portland cements and alkali-activated materials.* Cement and Concrete Research, 2019.
1599   **115**: p. 472-506.
1600 60.   Lothenbach, B., et al., *Thermodynamic modelling of the effect of temperature on the*
1601   *hydration and porosity of Portland cement.* Cement and Concrete Research, 2008. **38**(1):
1602   p. 1-18.
1603 61.   Lothenbach, B. and F. Winnefeld, *Thermodynamic modelling of the hydration of Portland*
1604   *cement.* Cement and Concrete Research, 2006. **36**(2): p. 209-226.
1605 62.   Lothenbach, B., et al., *Effect of temperature on the pore solution, microstructure and*
1606   *hydration products of Portland cement pastes.* Cement and Concrete Research, 2007.
1607   **37**(4): p. 483-491.
1608 63.   Myers, R.J., S.A. Bernal, and J.L. Provis, *A thermodynamic model for C-(N-) ASH gel:*
1609   *CNASH_ss. Derivation and validation.* Cement and Concrete Research, 2014. **66**: p. 27-
1610   47.
1611 64.   Myers, R.J., et al., *Thermodynamic modelling of alkali-activated slag cements.* Applied
1612   Geochemistry, 2015. **61**: p. 233-247.
1613 65.   Lothenbach, B., K. Scrivener, and R.D. Hooton, *Supplementary cementitious materials.*
1614   Cement and Concrete Research, 2011. **41**(12): p. 1244-1256.
1615 66.   Zajac, M., et al., *Impact of microstructure on the performance of composite cements: Why*
1616   *higher total porosity can result in higher strength.* Cement and Concrete Composites, 2018.
1617   **90**: p. 178-192.
1618 67.   Azad, V.J., et al., *Interpreting the pore structure of hydrating cement phases through a*
1619   *synergistic use of the Powers-Brownyard model, hydration kinetics, and thermodynamic*
1620   *calculations.* Advances in Civil Engineering Materials, 2017. **6**(1): p. 1-16.
1621 68.   Glosser, D., et al., *An extension of the Powers-Brownyard model to pastes containing SCM.*
1622   ACI Materials Journal, 2019. **116**(5): p. 205-216.
1623 69.   Bharadwaj, K., et al., *A New Mixture Proportioning Method for Performance-Based*
1624   *Concrete.* ACI Materials Journal, 2022. **119**(2): p. 207-220.
1625 70.   Bharadwaj, K., et al., *CALTRANS: Impact of the Use of Portland-Limestone Cement on*
1626   *Concrete Performance as Plain or Reinforced Material - Final Report.* 2021, Oregon State
1627   University: Corvallis. p. 320.

1628 71.   Isgor, B., et al., *Development of a performance-based mixture proportioning procedure for*
1629 *concrete incorporating off-spec fly ash*. 2020, Energy Power Research Institute (EPRI):
1630 Palo Alto, CA. p. 78.
1631 72.   Ramanathan, S., et al., *Reducing GHG Emission Using Cellulose Nanocrystals, OPC, and*
1632 *Limestone.* ACI Materials Journal, 2023. **120**(1): p. 205-217.
1633 73.   Han, D. and R.D. Ferron, *Effect of mixing method on microstructure and rheology of*
1634 *cement paste.* Construction and Building Materials, 2015. **93**: p. 278-288.
1635 74.   Oguz, O., et al., *Poly (lactide)/cellulose nanocrystal nanocomposites by high-shear mixing.*
1636 Polymer Engineering & Science, 2021. **61**(4): p. 1028-1040.
1637 75.   Barger, G.S., *A Fusion Method for the X-Ray Fluorescence Analysis of Portland Cements,*
1638 *Clinker and Raw Materials Utilizing Cerium (IV) Oxide in Lithium Borate Fluxes.*
1639 Advances in X-ray Analysis, 1985. **29**: p. 581-585.
1640 76.   Tsui Chang, M., *The Evaluation of Cementitious Pore Solution Composition and Electrical*
1641 *Resistivity Using X-ray Fluorescence (XRF).* 2017, Oregon State University.
1642 77.   Castro, J., I.D.l. Varga, and J. Weiss, *Using isothermal calorimetry to assess the water*
1643 *absorbed by fine LWA during mixing.* Journal of materials in civil engineering, 2012. **24**(8):
1644 p. 996-1005.
1645 78.   Zaw, M., *Automated Chemical Acidification Testing of Cementitious Materials*. 2021,
1646 Oregon State University.
1647 79.   Fu, T. and W.J. Weiss, *The Ball-on-Three-Ball (B3B) Test–Application to Cement Paste*
1648 *and Mortar.* Advances in Civil Engineering Materials, 2020. **9**(1): p. 128-142.
1649 80.   Börger, A., P. Supancic, and R. Danzer, *The ball on three balls test for strength testing of*
1650 *brittle discs: stress distribution in the disc.* Journal of the European Ceramic Society, 2002.
1651 **22**(9-10): p. 1425-1436.
1652 81.   Kim, T. and J. Olek, *Effects of sample preparation and interpretation of thermogravimetric*
1653 *curves on calcium hydroxide in hydrated pastes and mortars.* Transportation research
1654 record, 2012. **2290**(1): p. 10-18.
1655 82.   AASHTO, *AASHTO TP 119—Standard Method of Test for Electrical Resistivity of a*
1656 *Concrete Cylinder Tested in a Uniaxial Resistance Test*, in *AASHTO, Washington, DC*.
1657 2021.
1658 83.   Spragg, R., et al., *Factors that influence electrical resistivity measurements in cementitious*
1659 *systems.* Transportation research record, 2013. **2342**(1): p. 90-98.
1660 84.   Coyle, A.T., et al., *Activation energy of conduction for use in temperature corrections on*
1661 *electrical measurements of concrete.* Advances in Civil Engineering Materials, 2019. **8**(1):
1662 p. 158-170.
1663 85.   AASHTO, *AASHTO TP 135—Standard Method of Test for Determining the Total Pore*
1664 *Volume in Hardened Concrete Using Vacuum Saturation*, in *AASHTO, Washington, DC*.
1665 2020.
1666 86.   Barrett, E.P., L.G. Joyner, and P.P. Halenda, *The Determination of Pore Volume and Area*
1667 *Distributions in Porous Substances. I. Computations from Nitrogen Isotherms.* Journal of
1668 the American Chemical Society, 1951. **73**: p. 373-380.
1669 87.   Rajabipour, F. and W.J. Weiss, *Electrical conductivity of drying cement paste.* Materials
1670 and Structures, 2007. **40**: p. 1143-1160.
1671 88.   Leao, T.P. and M. Tuller, *Relating soil specific surface area, water film thickness, and*
1672 *water vapor adsorption.* Water Resources Research, 2014. **50**(7873-7885).

1673 89. Parrot, L.J. and D.C. Killoh, *Prediction of cement hydration.* British Ceramic Proceedings,
1674 1984. **35**: p. 41-53.
1675 90. Glosser, D., et al., *Estimating reaction kinetics of cementitious pastes containing fly ash.*
1676 Cement and Concrete Composites, 2020. **112**: p. 103655.
1677 91. Palacios, M., et al., *Effect of PCs superplasticizers on the rheological properties and*
1678 *hydration process of slag-blended cement pastes.* Journal of Materials Science, 2009.
1679 **44**(10): p. 2714-2723.
1680 92. Lerch, W., *The influence of gypsum on the hydration and properties of Portland cement*
1681 *pastes.* 2008.
1682 93. Niemuth, M.D., *Effect of fly ash on the optimum sulfate of Portland Cement.* 2012: Purdue
1683 University.
1684 94. Ramanathan, S., *Reactivity of Supplementary Cementitious Materials in Model Systems*
1685 *and Cementitious Pastes.* 2021, University of Miami.
1686 95. Valadez-Carranza, Y., et al., *Report - Working Group for Advancement of Cellulose Nano-*
1687 *Materials Use in Cement-Based Materials.* 2022, US Endowment.
1688 96. Haddad Kolour, H., W. Ashraf, and E.N. Landis, *Hydration and early age properties of*
1689 *cement pastes modified with cellulose nanofibrils.* Transportation Research Record, 2021.
1690 **2675**(9): p. 38-46.
1691 97. Matschei, T., B. Lothenbach, and F.P. Glasser, *The role of calcium carbonate in cement*
1692 *hydration.* Cement and concrete research, 2007. **37**(4): p. 551-558.
1693 98. Bharadwaj, K., O. Isgor, and W. Weiss, *Supplementary Cementitious Materials in Portland*
1694 *Limestone Cements.* ACI Materials Journal, 2022. **119**(2).
1695 99. Matschei, T., et al. *Relationships of Cement Paste Mineralogy to Porosity and Mechanical*
1696 *Properties.* in *International Conference on Modelling of Heterogeneous Materials with*
1697 *Applications in Construction and Biomedical Engineering.* 2007.
1698 100. Hisseine, O.A., et al., *Nanocellulose for improved concrete performance: A macro-to-*
1699 *micro investigation for disclosing the effects of cellulose filaments on strength of cement*
1700 *systems.* Construction and Building Materials, 2019. **206**: p. 84-96.
1701 101. Miller, S.A., et al., *Carbon dioxide reduction potential in the global cement industry by*
1702 *2050.* Cement and Concrete Research, 2018. **114**: p. 115-124.
1703 102. Bradford, K. and F. Lolli, *CONOMIC AND ENVIRONMENTAL IMPACT OF*
1704 *NANOCELLULOSE ADDITIVES IN PORTLAND CEMENT*, in *18th International*
1705 *Conference on Non-conventional Materials and Technologies (NOCMAT 2022).* 2022.
1706 103. Nassiri, S., et al., *Comparison of unique effects of two contrasting types of cellulose*
1707 *nanomaterials on setting time, rheology, and compressive strength of cement paste.*
1708 Cement and Concrete Composites, 2021. **123**: p. 104201.
1709 104. Mateos, A., et al., *Structural Response of Concrete Pavement Slabs under Hygrothermal*
1710 *Actions.* Construction and Building Materials, 2020. **243**.

1711

8. Appendix

8.1. CNC Amounts

Forest management helps reduce hazardous fuels and improves forest health. It is estimated that about 25 tons of biomass per thin-from-below prescription is obtained per acre from the forest management; this translates to about 12.5 bone dry tons per acre. CNC suspension yield from bone dry mass (without needles and bark) is estimated to be about 12.5% i.e., 1.5-ton CNC suspension per acre.

Assuming that a freeway lane width is 12 feet and the cement content used in concrete pavements is 525 lb/yd^3, Table 10 gives an estimated acres of forest management that will result in CNC suspension that can be used in constructing a lane mile of concrete pavement for different CNC dosages and pavement thicknesses.

Table 10. Acres of forest management biomass that can be used in one lane mile construction of a freeway for different CNC dosages in concrete and different pavement thicknesses

Unit: acres/lane mile	CNC dosage (% CNC solids volume by volume of binder)		
Pavement thickness (in.)	0.2	0.5	1.0
8	2.5	6.4	12.7
10	3.2	7.9	15.9
12	3.8	9.5	19.1
15	4.8	11.9	23.8

To put the CNC amounts used in terms of cubic yard of concrete, for CNC dosages of 0.2, 0.5, and 1.0% CNC solids volume per binder volume, it was calculated that 4.9, 12.2, and 24.4 lbs. of CNC suspension, respectively, is required for one cubic yard of concrete.

1733 ## 8.2. Mill Certificates

1734 The following are the mill certificates of the OPC, PLC, and Slag used for the field trials.

CEMEX	4200 E Jurupa St. Suite 312 Ontario, CA 91761 Telephone (909) 974-5469 FAX (909) 974-5525		CEMENT MILL TEST REPORT	

Cemex Identified as: Date: 6/17/2022

Plant: Cemex Construction Materials Pacific LLC

Location: Victorville, CA — Prod dates: Beginning: 6/3/2022 / Ending: 6/9/2022 — Ref. No 44729

STANDARD CHEMICAL REQUIREMENTS (ASTM C114)	ASTM C150 / AASHTO M 85 SPECIFICATIONS	TYPE I	TYPE II	TYPE V	TEST RESULTS
Silicon Dioxide (SiO_2), %	Minimum	----	----	----	20.3
Aluminum Oxide (Al_2O_3), %	Maximum	----	6.0	----	4.1
Ferric Oxide (Fe_2O_3), %	Maximum	----	6.0	----	3.9
Calcium Oxide (CaO), %		----	----	----	62.4
Magnesium Oxide (MgO), %	Maximum	6.0	6.0	6.0	4.9
Sulfur Trioxide (SO_3), % **	Maximum	3.0	3.0	2.3	3.1
Loss on Ignition (LOI), %	Maximum	3.5	3.5	3.5	2.6
Insoluble Residue, %	Maximum	1.5	1.5	1.5	1.07
Sodium Oxide (Na_2O), %		----	----	----	0.19
Potassium Oxide (K_2O), %		----	----	----	0.41
Equivalent Alkalies ($Na_2O+.658K_2O$), %	Maximum	0.60	0.60	0.60	0.46
CO_2(%)		----	----	----	1.7
Limestone (%)	Maximum	5.0	5.0	5.0	3.4
$CaCO_3$ in limestone	Minimum	70.0	70.0	70.0	74.7
Inorganic addition	Maximum	5.0	5.0	5.0	2.1
Tricalcium Silicate (C3S), %	Maximum	----	----	----	54
Dicalcium Silicate (C2S), %		----	----	----	16
Tricalcium Aluminate (C3A), %	Maximum	----	8	5	4
Tetracalcium Aluminoferrite (C4AF), %		----	----	----	11
Heat Index (C3S + 4.75C3A)	Maximum		100		73
(C4AF + 2C3A) or (C4AF + C2F), %	Maximum	----	----	25	19
PHYSICAL REQUIREMENTS					
Heat of Hydration (ASTM C1702)	Informational data only				
7 days, kj/kg (cal/g)	Most recent value				301(72.4)
(ASTM C204) Blaine Fineness, cm²/gm	Minimum	2600	2600	2600	4184
(ASTM C430) -325 Mesh, %		----	----	----	98
(ASTM C191) Time of Setting (Vicat)					
Initial Set, minutes	Minimum / Maximum	45 / 375	45 / 375	45 / 375	108
Final Set, minutes		---	---	---	266
(ASTM C451) False Set, %	Minimum	50	50	50	89
(ASTM C185) Air Content, %	Maximum	12	12	12	6.1
(ASTM C151) Autoclave Expansion, %	Maximum	0.80	0.80	0.80	0.01
(ASTM C87) Normal Consistency, %		----	----	----	26
(ASTM C1038) Expansion in Water %	Maximum	0.020	0.020	0.020	0.008
(ASTM C109) Compressive Strength, psi (MPa)					
1 Day		----	----	----	2140(14.8)
3 Day	Minimum	1740(12.0)	1450(10.0)	1160(8.0)	3670(25.3)
7 Day		2760(19.0)	2470(17.0)	2180(15.0)	4600(31.7)
28 Day (strength for Ref. No. 44701)	Minimum			3050(21.0)	5850(40.3)

** The performance of CEMEX Type II, Type V has proven to be improved with sulfur trioxide levels in excess of the 2.3% limit for Type V. Note D in ASTM C150 allows for additional sulfate, provided expansion as measured by ASTM C1038 does not exceed 0.020%.

CEMEX hereby certifies that this cement meets or exceeds the chemical and physical Specifications of:
ASTM C150-21 Type I, Type II, and Type V Low Alkali portland cements
ASTM C1157-20 Type GU Hydraulic Cement
AASHTO M 85-20 Type I, Type II, and Type V Low Alkali portland cements
CalTrans, Section 90-2.01 T II Modified and Type V (2006)
CalTrans, Section 90-1.02B (2) (2010-2020)
Arizona DOT Standard Specification 1006-2.01 Hydraulic Cement
Nevada DOT Specification 701.03.01
C465 qualification data will be made available upon request

By: _____
Quality Control Manager
CEMEX - Victorville Cement Plant
16888 North "E" St., 'Victorville, CA 92394

1735

CEMEX

4200 E Jurupa St
Suit 312
Ontario, Ca 91764
Telephone (909) 974-5469
Fax (909) 974-5525

**CEMENT
MILL
TEST
REPORT**

Cement Identified as:

Plant: CEMEX Construction Materials Pacific LLC **TYPE IL (15)** Date: 10/30/2021
Location: Victorville, Ca
Production Dates:

Beginning: **October 20, 2021**
Ending: **October 25, 2021**

STANDARD CHEMICAL REQUIREMENTS (ASTM C114)	TEST RESULTS		ASTM C595 Spec.	Type IL
Sulfur Trioxide (SO3), % **	3.6		Maximum	3.0
Loss on Ignition (LOI), %	5.6		Maximum	10
CO_2, %	5.0			
Limestone, %	14		Min. - Max.	5 - 15
$CaCO_3$ in Limestone, %	85		Minimum	70
PHYSICAL REQUIREMENTS				
(ASTM C 204) Blaine Fineness, cm^2/gm	5470			----
(ASTM C 188) Density	3.06			----
(ASTM C 430) -325 Mesh, %	97.5			----
(ASTM C 191) Time of Setting (Vicat)				
Initial Set, minutes	135		Min. - Max.	45 - 420
Final Set, minutes	315			----
(ASTM C 185) Air Content, %	8		Maximum	12
(ASTM C 151) Autoclave Expansion, %	0.01		Contraction	0.2
			Expansion	0.8
(ASTM C 109) Compressive Strength, psi (MPa)	psi	MPa		
1 Day	2650	18.3		
3 Day	3970	27.4	Minimum	1890 (13.0)
7 Day	4790	33.0	Minimum	2900 (20.0)
28 Day	5820	40.1	Minimum	3620 (25.0)

CEMEX hereby certifies that this cement meets or
exceeds the chemical and physical Specifications of:

ASTM C595 - 19 for Type IL Cement

James W Martin

James Martin
Quality Control Manager
CEMEX - Victorville Cement Plant

1736

87

Slag Cement Test Report

CTC ID: 607	
Slag Source: Rizhao	Cemex Technical Center
Vessel: Monthly sample- Redwood City	6725 78th St, Riverview, FL, 33578
Sample Date: April 2022	Phone: (813) 671-2266
Report Date: 5/27/2022	Fax: (813) 677-7597
Sample Log CTC ID: 2022-227	

Specifications: ASTM C 989 Grades 100 & 120

Chemical and Physical Requirements	Test Result	Specifications
Sulfur Trioxide (SO_3) (ASTM C114), %	2.46	---
Sulfide Sulfur (S) (ASTM C114), %	0.32	2.5 Max
Chloride (Cl) (ASTM C114), %	0.013	---
Aluminum Oxide (Al_2O_3) (ASTM C114), %	17.5	---
Blaine Fineness (ASTM C204), m^2/kg	478	---
Fineness Retained - 45 Micron (ASTM C430), %	0.3	20 Max
Specific Gravity (ASTM C188)	2.91	---
Air Content (ASTM C185), %	3	12 Max
Mortar Expansion (ASTM C1038) 14-day ,%	0.018	0.020 Max
Total Equivalent Alkalies ($Na_2O+0.685 K_2O$), (ASTM C114), %	0.45	---

Slag Activity Index (ASTM C109)		Grade 100	Grade 120
7 Day - Individual, %	119	---	---
7 Day - Average of last 5, %	108	---	---
28 Day - Individual, %	133	90 Min	110 Min
28 Day - Average of last 5, %	123	95 Min	115 Min

Compressive Strength (ASTM C109)		Specifications
7 Day - Reference Cement, psi	4126	---
28 Day - Reference Cement, psi	5397	5,000 Min
7 Day Slag and Cement Reference, psi	4906	---
28 Day Slag and Cement Reference, psi	7164	---

Reference Cement (ASTM C114 & C150)		Specifications
Cement Type	Type I/II	Type I-Type II
Total Equivalent Alkalies ($Na_2O+0.685 K_2O$), %	0.79	0.6 Min/ 0.9 Max

This GGBFS meets requirements of ASTM C 989-18a and AASHTO M 302-19

- ☐ Grade 100 ASTM C989
- ☐ Grade 100 AASHTO M302
- ☑ Grade 120 ASTM C989
- ☑ Grade 120 AASHTO M302

Chemical testing completed by: YR

Physical testing completed by: YR

Jose M. Dominguez
Director at Cemex Technical Center USA

1737

FULL 6(c)(i)